AD-A066 991 IOWA INST OF HYDRAULIC RESEARCH IOWA CITY F/G 8/12
EFFECTS OF ICE COVERS ON ALLUVIAL CHANNEL FLOW AND SEDIMENT TRA--ETC(U)
FEB 79 W W SAYRE, G B SONG

UNCLASSIFIED IIHR-218 NI

1 OF 2
AD A066991

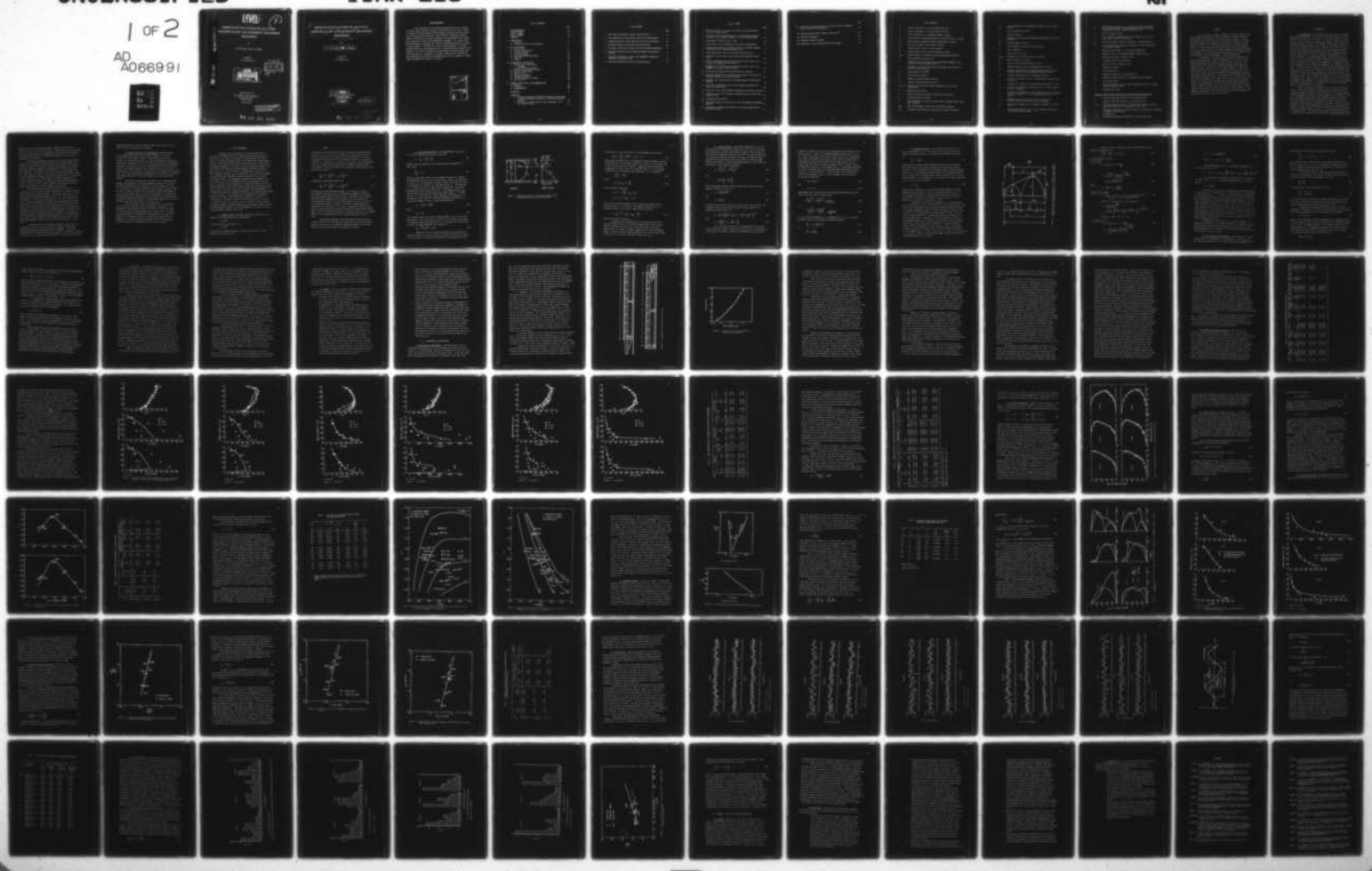

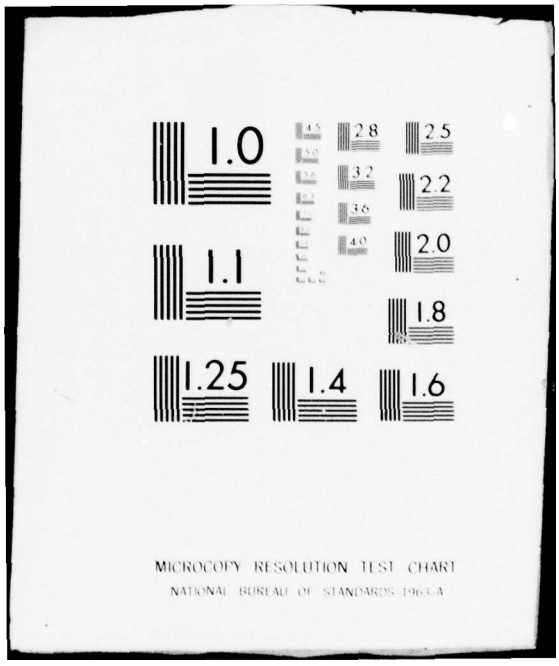
1.0
1.1
1.25
1.4
1.6
2.8
3.2
3.6
4.0
2.5
2.2
2.0
1.8
MICROCOPY RESOLUTION TEST CHART
NATIONAL BUREAU OF STANDARDS 1963-A

EFFECTS OF ICE COVERS ON ALLUVIAL CHANNEL FLOW AND SEDIMENT TRANSPORT PROCESSES

by

W. W. Sayre and G. B. Song

Prepared for

U.S. Geological Survey

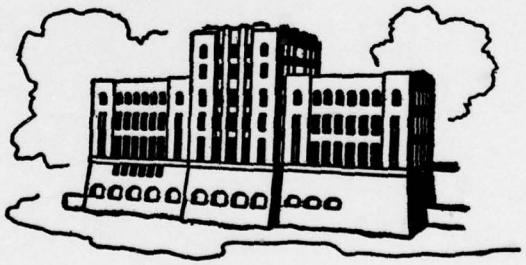

IIHR Report No. 218

Iowa Institute of Hydraulic Research
The University of Iowa
Iowa City, Iowa

February 1979

(6)

EFFECTS OF ICE COVERS ON ALLUVIAL CHANNEL FLOW AND SEDIMENT TRANSPORT PROCESSES

by

(10) W. W. Sayre and G. B. Song

Prepared for

U.S. Geological Survey

(14) IIHR Report No. 218

Iowa Institute of Hydraulic Research

The University of Iowa

Iowa City, Iowa

(11) February 1979

(12) 109 p.

ACKNOWLEDGEMENTS

This investigation was partially supported by the U.S. Geological Survey, Water Resources Division, through the office of John F. Ficke, in connection with the National Stream Quality Accounting Network program. E.R. Slattery, Research Assistant, Iowa Institute of Hydraulic Research (IIHR), contributed to the early planning of the experiment and the design and calibration of some of the experimental equipment. S.Y. Liong, IIHR, Research Assistant, performed the velocity and suspended-sediment concentration measurements. Professor J.R. Glover provided guidance in solving problems related to instrumentation and to computerized data acquisition and reduction. D.C. Harris coordinated and supervised the supporting shop and technical services. Professor J.F. Kennedy, IIHR Director, reviewed the final manuscript and contributed illuminating advice and insights at various stages throughout the course of the study.

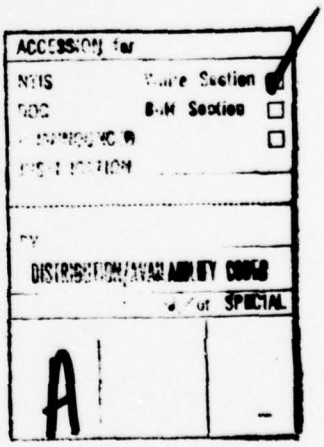

TABLE OF CONTENTS

LIST OF TABLES

LIST OF FIGURES

LIST OF SYMBOLS

a^+	Positive amplitude of alluvial-channel bed form
a^-	Negative amplitude of alluvial-channel bed form
C	Local concentration of suspended sediment, in mg/ℓ
C_a	Concentration of suspended sediment at reference level η_a, in mg/ℓ
C_s	Depth-averaged suspended sediment concentration, in mg/ℓ
C_t	Mean total sediment concentration, in mg/ℓ
d	Average depth of flow in a cross section
$\bar{d}$	Average depth of flow in working section of flume
D_{50}	Median diameter of sediment particles composing bed material
f	Darcy-Weisbach friction factor
f'	Component of friction factor due to sand-grain roughness, also called the flat-bed friction factor
f"	Component of friction factor due to form drag, also called the bed-form friction factor
F	Froude number, $F = \bar{U}/\sqrt{gY_1}$
g	Acceleration of gravity
H	Height of alluvial-channel bed form
L	Length of alluvial-channel bed form
m_2, m_3	Second and third central moments, defined by (63) and (64), respectively
n	Manning friction factor
N	Number of discrete bed forms included in a bed profile
P	Wetted perimeter of channel
q	Water discharge, by volume, per unit width of channel, also called unit discharge
q_{sb}	Bed load discharge, by mass, per unit width of channel
q_{ss}	Suspended load discharge, by mass, per unit width of channel

q_{st}	Total bed-material load discharge, by mass, per unit width of channel
Q	Water discharge, by volume
r	Hydraulic radius
r_b	Hydraulic radius of bed (determined using sidewall correction procedure)
$\mathbb{R}$	Reynolds number, $\mathbb{R} = \bar{U}Y_1/\nu$
S	Slope (channel, friction, or water surface)
T	Water temperature
u	Local velocity of flow
u_{max}	Maximum local velocity of flow in a vertical
u_*	Shear velocity, $u_* = \sqrt{\tau_o/\rho}$
U	Cross-sectional average velocity of flow
$\bar{U}$	Average velocity of flow in working section of flume
U_c	Critical cross-sectional average velocity of flow at which sediment particles of a designated size begin to move
w_p	Terminal settling velocity of sediment particles
x	Distance in direction of flow, tilted downward from horizontal at slope S
y	Distance above channel bed, measured perpendicularly to x axis
y_i	Distance from boundary, lower boundary if i=1, upper boundary if i=2; see figure 1
Y_i	Distance from boundary to point of maximum velocity in vertical, from lower boundary if i=1, from upper boundary if i=2; see figure 1
z_i	Exponent in (31) and (35) for vertical distribution of suspended sediment concentration, $z_i = w_p/\beta_i\kappa_i u_{*_i}$
Z_j	Characteristic dimension, e.g. height or length, of j-th bed form
β	Proportionality factor in $\varepsilon_s = \beta\varepsilon_{mo}$, sometimes identified as the turbulent Schmidt number

β_i	Proportionality factor in $z_i = w_p/\beta_i \kappa_i u_{*i}$, where z_i determined from suspended sediment concentration profiles and k_i and u_{*i} from velocity profiles; theoretically equal to β
γ	Specific weight of water
ε_i	Local turbulent momentum transfer coefficient, ε_{mo}, i=1 if in lower layer, i=2 if in upper layer
ε_{mo}	Turbulent momentum transfer coefficient, or eddy diffusivity
ε_s	Local turbulent mass transfer coefficient, or mass diffusivity, for suspended sediment
η	Dimensionless distance, $\eta = y/d$, above channel bed
η_a	Reference level for suspended sediment concentration C_a
θ	Skewness coefficient, defined in (62)
κ	von Karman turbulence coefficient
μ	Mean value of Z_j, defined in (60)
ν	Kinematic viscosity
ρ	Fluid mass density
σ	Standard deviation of Z_j, defined in (61)
σ_g	Geometric standard deviation of sediment particle diameters
τ	Local shear stress
τ_c	Critical bed shear stress at which sediment particles of a designated size begin to move
τ_0	Boundary shear stress

Selected frequently-used subscripts and other secondary nomenclature

F	Subscript denoting reference to a free-surface flow
I	Subscript denoting reference to an ice-covered flow
i=1, 2	Subscript denoting reference to either lower layer or bed (i=1), and either upper layer or simulated ice cover (i=2)
j	Subscript identifying a discrete bed form in a bed profile containing a sequence of N bed forms
$(\bar{})$	Average value
$(\hat{})$	Estimated as opposed to a measured or a theoretical value

ABSTRACT

Ice covers cause a number of changes in alluvial channel flows by approximately doubling the wetted perimeter and thereby producing a redistribution of the boundary and internal shear stresses. A series of flume experiments was conducted to investigate the effects of simulated ice covers on the following characteristics of alluvial channel flows: (1) depth versus discharge and friction factor relationships; (2) velocity distribution; (3) suspended sediment concentration profiles and discharge; (4) total bed-material discharge; and (5) characteristics of bed forms and their relationship to bed friction factors.

In comparison to free-surface flows with the same unit discharge and energy slope, flows with simulated ice covers were found to have substantially larger depths and lower average velocities. Due mainly to the lower velocities, sediment discharges were found to be sharply reduced. The flow in an ice-covered channel is divided by a plane of zero shear stress (locus of maximum velocities) into a lower and an upper layer, each with average velocities approximately equal to the overall average velocity. To the extent that the shear-stress and velocity distributions in the lower layer of an ice-covered flow are the same as in a free surface flow with the same mean velocity, and depth equal to the thickness of the lower layer, relationships developed for flows in alluvial channels with a free surface can be used for predicting certain features of flows in ice-covered alluvial channels. This applies in particular to bed friction factors, sediment discharge, and apparently also to bed-form characteristics.

I. INTRODUCTION

A. Background. At the higher latitudes in Earth's northern and southern hemispheres, the surfaces of most natural bodies of water undergo an annual period of freezing. In alluvial channels, the presence of an ice cover radically alters many features of the water- and sediment-transport processes. The dynamics of this type of system are none too well understood even for the simpler case of flow in an ice-free alluvial channel, mainly because it is the interaction between the flow and the channel bed that determines the configuration of the bed and consequently its hydraulic roughness and the depth of flow. Thus in contrast to a rigid-boundary channel, wherein only the water surface is a free surface, an alluvial channel has two free surfaces. In an ice-covered alluvial channel, this complexity is compounded further by the variability of the hydraulic roughness of the underside of the ice cover. The under surface is typically very smooth during formation and growth of the ice cover when temperatures are cold, but becomes rippled following the onset of higher temperatures and melting from below, and becomes very rough after candling and break-up of the cover occur (Ashton and Kennedy 1972). Thus not only the presence of an ice cover, but also any change in the roughness of its underside is expected to cause changes in the bed configuration of the channel and in the flow and sediment transport characteristics of the stream.

Some of the qualitative effects of a stationary, floating ice cover on the flow and sediment transport regimes can be inferred from elementary physical reasoning. The addition of a solid upper boundary surface approximately doubles the wetted perimeter of the channel. Barring a compensating reduction in the hydraulic roughness of the bed, the total boundary shear and consequently the depth of flow will be increased, and the average velocity will be reduced. Because the total boundary shear must be divided between the upper and lower surfaces, a reduction in shear stress at the bed is to be expected unless the depth is roughly doubled. The reduction in velocity and bed shear stress is in turn expected to reduce both the bed and the suspended sediment loads.

Changes in the internal distributions of turbulent shear stress and velocity are apt to be even more drastic. The redistribution of turbulent shear stress will affect the turbulent mass diffusivity and consequently the vertical distribution of suspended and probably also the ratio of suspended load to bed load.

Quantitative prediction of the ice-cover effects would require knowledge of the magnitudes and distributions of the new boundary and internal turbulent shear stresses, which in turn depend on the relative degrees of hydraulic roughness of the underside of the ice cover and the channel bed. The principal difficulty lies in the freedom of the bed configuration to adjust to the new shear stress distribution, which in turn is modified by changes in the bed configuration. In the parlance of system dynamics, the stream contains an internal feedback loop. Progress toward development of a quantitative model for predicting the effects of an ice cover on alluvial channel flow processes requires a better understanding of how this feedback loop operates.

The river-morphology literature contains very little information on ice-cover effects that could serve as a guide in developing a quantitative predictive model. In addition, the accuracy of the limited amount of sediment-transport data for ice-covered streams that is available, is open to question because of: (1) the reduced reliability of sampling equipment and methods when operating under freezing conditions; and (2) insufficient knowledge concerning the interaction between the ice cover and the flow to interpret fully the measurements and design an efficient and reliable sampling program. Heretofore, these problems have been investigated little, both because of the many difficulties entailed in obtaining sediment transport and related measurements under freezing conditions, and a general consensus that flow discharges and sediment transport rates are much reduced when ice covers exist.

The motivation for the research described in this report is an outgrowth of the U.S. Geological Survey's charge to develop the National Stream Quality Accounting Network (NASQUAN). To meet the NASQUAN objective of describing the water quality of the Nation's streams and rivers on a systematic and continuing basis, winter data acquisition

and interpretation activities in parts of the country with a freezing climate need to be upgraded and expanded.

B. Purpose and Scope of Investigation. The main purpose of this investigation was to obtain basic information on how ice covers affect the sediment-transport characteristics of alluvial streams. As outlined in section I-A, these characteristics include the mean velocity and depth of flow, the velocity distribution, the hydraulic roughness of the bed and ice cover, the magnitude and vertical distribution of the suspended sediment load, and either the bed or the total sediment load. The various ice-cover effects are investigated and analyzed with a view toward formulating recommendations that would help to improve field sampling and data collection programs for ice-covered alluvial channels.

The project activities have included: (1) a one-day USGS-IIHR Workshop on Measurement of Suspended Sediment Transport in Ice-Covered Alluvial Streams held at The University of Iowa on November 25, 1975; (2) a field-trip to the Upper Iowa River near Dorchester, Iowa on January 20, 1976, to observe a USGS flow and sediment discharge measurement in an ice-covered stream; and (3) a series of experiments in a laboratory flume wherein detailed comparisons were made between the characteristics of alluvial-channel flow processes occurring under simulated ice covers, and those occurring in equivalent free surface flows.

Aside from brief reviews in the Appendices, this report is restricted to the laboratory-flume experimental investigation. The experimental investigation addresses the effects of smooth and rough ice covers on the following characteristics of the flows: (1) depth versus discharge and friction-factor relationships; (2) velocity distribution; (3) suspended sediment concentration distributions and discharge; (4) total bed-material discharge; and (5) characteristics of bed forms and their relationship to bed friction factors.

II. BASIC HYPOTHESES

Throughout this investigation, flows occurring under an ice cover are compared insofar as possible with equivalent free-surface flows. The concept of equivalent ice-covered and free-surface flows as used herein embodies pairs of two-dimensional uniform flows, one with a free surface and the other with an ice cover, for which the unit water discharge, q, the slope, S, and the fluid and sediment properties are all the same, but the mean depth, d, hydraulic radius, r, mean velocity, U, friction factor, f (or Manning's n), and the unit total sediment discharge, q_{st}, are different. The ice cover is assumed to be stationary and floating so that the pressure at the ice-water interface is equal to the atmospheric pressure plus the weight of an ice column of unit area and height equal to the thickness of the ice cover. In nature, this corresponds to a comparison between the state of affairs which would exist prior to and for some time following the formation of an ice cover in a long reach of channel with steep banks (i.e., no appreciable increase in channel width due to the increased depth caused by the ice cover). For both flows q_{st} is assumed to be a dependent variable, and longer term effects due to changes in the imposed sediment load, or changes in slope or flow distribution due to shifts in meander patterns, for example, are not considered. Other phenomena relating to sediment transport which are not considered include ice jams and the uptake and transport of bottom sediments by clusters of frazil ice and dislodged chunks of anchor ice.

A. Depth of Flow. The Chezy resistance equation for a uniform flow in a wide channel may be expressed as

$$q = C\, d\sqrt{rs} \tag{1}$$

in which the Chezy coefficient, C, is

$$C = \frac{1}{n}\, r^{1/6} \tag{2}$$

according to the Manning formula (in metric units), where n is the Manning friction factor, and

$$C = \sqrt{8g/f} \tag{3}$$

according to the Darcy-Weisbach formula, where f is the Darcy-Weisbach friction factor, and g is the acceleration of gravity. Using the subscript I to denote an ice-covered flow, and the subscript F to denote an equivalent free-surface flow, the hydraulic radii for the respective flows are $r_I = d/2$ and $r_F = d$. Since $q_I = q_F$ and $S_I = S_F$ for equivalent flows, the foregoing relationships can be combined to give the ratio of the depth of the ice-covered flow to the depth of the equivalent free-surface flow, which is

$$\frac{d_I}{d_F} = 2^{0.4} \left(\frac{n_I}{n_F}\right)^{0.6} = 1.32 \left(\frac{n_I}{n_F}\right)^{0.6} \tag{4}$$

according to the Manning formula, and

$$\frac{d_I}{d_F} = 2^{1/3} \left(\frac{f_I}{f_F}\right)^{1/3} = 1.26 \left(\frac{f_I}{f_F}\right)^{1/3} \tag{5}$$

according to the Darcy-Weisbach formula. In (4) and (5) n_I and f_I are composite friction factors, reflecting the roughness of both the bed and the under surface of the ice cover. Equations 4 and 5 indicate that unless the composite friction factors for an ice-covered flow are substantially smaller than the bed friction factors for an equivalent free-surface flow, the depth of flow will be significantly increased by the formation of an ice cover. Assuming the same bed roughness for ice-covered and free-surface conditions, Carey's (1966) measurements in the St. Croix River, Wisconsin, indicated values of n_I/n_F ranging from 0.73 to 1.06 which would result in d_I/d_F ranging from 1.09 to 1.37.

Discussion pertaining to how the composite friction factors n_I and f_I are related to the friction factors for the bed and the undersurface of the ice cover is deferred, pending discussion of the effect of an ice cover on the vertical distribution of velocity.

B. Velocity Distribution. The Karman-Prandtl velocity defect law for turbulent flow written in the form

$$u_i - u_{max} = \frac{u_{*i}}{\kappa_i} \ln \frac{y_i}{Y_i} \tag{6}$$

together with the equation for the linear vertical distribution of shear stress

$$\frac{d\tau_i}{dy_i} = -\gamma S \tag{7}$$

provide an appropriate model for the internal structure of a uniform two-dimensional flow in an ice-covered channel. Most of the quantities in (6) and (7) are represented in figure 1, which illustrates the vertical distribution of velocity, u_i, and shear stress τ_i. The subscript $i = 1, 2$ denote the lower or upper layer, respectively. Previously undefined quantities in (6) and (7) are: the maximum velocity, u_{max}, which occurs at the interface between two layers, where $\tau_i = 0$; the distance, y_i, from the lower or upper boundary; the thickness, Y_i, of the lower or upper layer; the von Karman turbulence coefficient, κ_i; the specific weight of water, γ; and the shear velocity

$$u_{*_i} = \sqrt{\tau_{0i}/\rho} = \sqrt{gY_iS} \tag{8}$$

where

$$\tau_{0i} = \gamma Y_i S \tag{9}$$

is the shear stress at the lower or upper boundary, and ρ is the fluid mass density. Also, from figure 1 and (9) it is clear that the average or composite boundary shear stress for an ice-covered flow, taking both the lower and upper boundaries into account, is

$$\tau_{0I} = \frac{\tau_{01} + \tau_{02}}{2} = \gamma dS/2 \tag{10}$$

Equations 6 and 7 can both be obtained from the x-direction Reynolds' equation for steady, uniform turbulent flow between two parallel plates that are oriented horizontally in the transverse direction

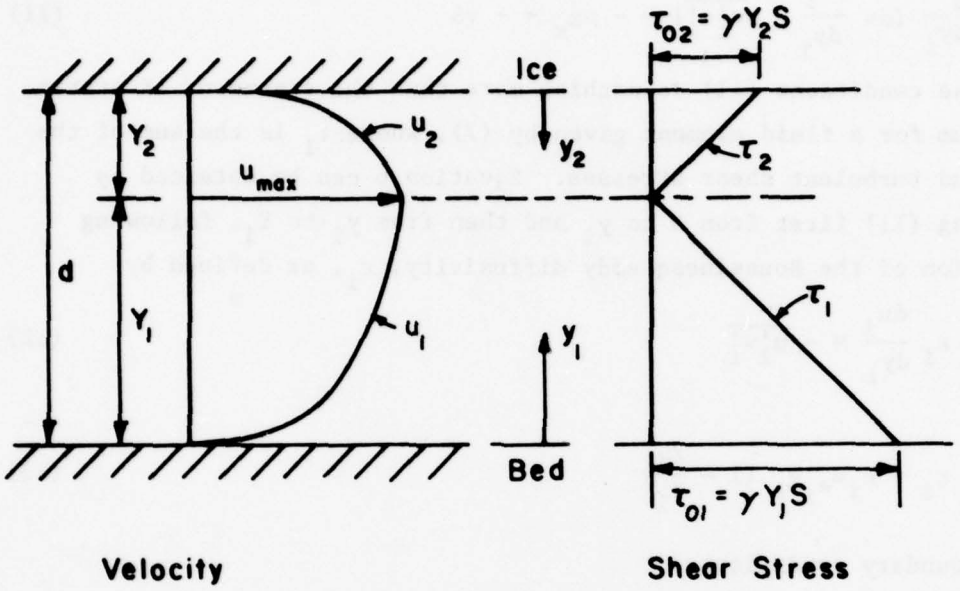

Figure 1.- Definition sketch for velocity and shear stress distributions in an ice-covered channel.

and parallel to the x axis which is tilted downward at the slope S,

$$\frac{d}{dy_i}\left(\rho\nu \frac{du_i}{dy_i} - \rho\overline{u_i'v_i'}\right) = -\rho g_x = -\gamma S \tag{11}$$

Under these conditions (11) is nothing more than the statement of static equilibrium for a fluid element given by (7), where τ_i is the sum of the viscous and turbulent shear stresses. Equation 6 can be obtained by integrating (11) first from 0 to y_i and then from y_i to Y_i, following introduction of the Boussinesq eddy diffusivity, ε_i, as defined by

$$\varepsilon_i \frac{du_i}{dy_i} = -\overline{u_i'v_i'} \tag{12}$$

where

$$\varepsilon_i = \kappa_i u_{*_i} y_i \left(1 - \frac{y_i}{Y_i}\right) \tag{13}$$

and the boundary conditions

$$y_i = 0: \quad \rho\nu \frac{du_i}{dy_i} = \tau_{0i} = \gamma Y_i S$$

$$y_i = Y_i: \; u_i = u_{max}, \quad \tau_i = 0$$

Also, in the second integration of (11), the viscous shear stress is neglected since $\nu << \varepsilon_i$ except in the immediate vicinity of $y_i = 0$. The mean velocity in the lower or upper layer is given by

$$U_i = \frac{1}{Y_i} \int_0^{Y_i} u_i dy_i = u_{max} - \frac{u_{*_i}}{\kappa_i} \tag{14}$$

which can be used to evaluate κ_i.

Essentially the same model for the internal flow structure was used by Hancu (1967), as reported by Uzuner (1975), and by Larsen (1969) to describe the flow in an ice-covered channel, and also by Ismail (1952) in a study of sediment suspension in a closed rectangular channel. Clearly the model applies equally well to a free surface flow, in which case $Y_1 = d$, the total depth of flow, and $Y_2 = 0$.

C. Friction Factors. The relative magnitudes of the friction factors for the bed and the underside of the ice cover are important because they influence the division of shear stress between the lower and upper boundaries, which in turn fixes the relative magnitudes of Y_1 and Y_2 and the vertical position of u_{max}. The Manning (metric system) and Darcy-Weisbach friction factors for the lower and upper surfaces are related to the bulk flow characteristics in the lower and upper layers by the respective equations

$$n_i = \frac{Y_i^{2/3} S^{1/2}}{U_i} = \frac{Y_i^{5/3} S^{1/2}}{q_i} \tag{15}$$

and

$$f_i = 8gS \frac{Y_i}{U_i^2} = 8gS \frac{Y_i^3}{q_i^2} \tag{16}$$

The corresponding composite friction factors for a wide ice-covered channel, for which $r = d/2$, are

$$n_I = \frac{(d/2)^{2/3} S^{1/2}}{U} \tag{17}$$

and

$$f_I = 4gS \frac{d}{U^2} \tag{18}$$

In terms of the friction factors for the upper and lower surfaces, the composite friction factors given by Hancu's (1967) equations, as reported by Uzuner (1975), are

$$n_I = (\tfrac{1}{2})^{2/3} \left[n_1^2 (\frac{U_1}{U})^2 (\frac{d}{Y_1})^{1/3} + n_2^2 (\frac{U_2}{U})^2 (\frac{d}{Y_2})^{1/3} \right]^{1/2} \tag{19}$$

and

$$f_I = \frac{1}{2} \left[(\frac{U_1}{U})^2 f_1 + (\frac{U_2}{U})^2 f_2 \right] \tag{20}$$

One of the main questions to be investigated in the present study involves the extent to which bed friction factors, characteristics of bed forms, and sediment-transport relationships in an ice-covered

channel are equivalent to those in a free-surface flow with depth Y_1 and mean velocity U_1. This is a reasonable hypothesis insofar as $y_i = Y_i$ is a plane of zero shear stress like the water surface in a free-surface flow. The relationships of Y_1 and U_1 to the velocity and shear-stress distributions and bed friction factor in the lower layer of an ice-covered flow then would be exactly the same as those of d and U to the corresponding features of a free surface flow. It is therefore important to be able to estimate Y_1/d, the fractional depth where maximum velocity occurs, in an ice-covered flow. If the friction factors for both surfaces can be estimated, and q, S, and d are known, this can be done by solving the equations

$$Y_1/d + Y_2/d = 1 \tag{21}$$

and

$$q_1 + q_2 = q \tag{22}$$

simultaneously by trial and error following the substitution of either (15) or (16) into (22) to obtain either

$$\frac{(Y_1/d)^{5/3}}{n_1} + \frac{(Y_2/d)^{5/3}}{n_2} = \frac{q}{d^{5/3}\, S^{1/2}} \tag{23}$$

or

$$\frac{(Y_1/d)^{3/2}}{f_1^{1/2}} + \frac{(Y_2/d)^{3/2}}{f_2^{1/2}} = \frac{q}{\sqrt{8gS}\, d^{3/2}} \tag{24}$$

If, as a first approximation, it is assumed that $U_1 = U_2 = U$, the same procedure results in the simpler approximate equations

$$\frac{Y_1}{d} \approx \left[1 + \left(\frac{n_2}{n_1}\right)^{3/2}\right]^{-1} \tag{25}$$

or

$$\frac{Y_1}{d} \approx \frac{f_1}{f_1 + f_2} \tag{26}$$

D. Suspended Sediment. For a steady, uniform flow in an ice-covered channel, as for a free-surface flow, the vertical distribution of suspended sediment is governed by the Schmidt-O'Brien equation

$$w_p C + \varepsilon_s \frac{dC}{dy} = 0 \tag{27}$$

which expresses a balance between downward transport due to gravitational settling and net upward transport due to turbulent diffusion. In (27), C is the concentration of suspended sediment (usually expressed in mg/ℓ), w_p is the terminal settling velocity of the sediment particles, and ε_s is the vertical turbulent mass transfer coefficient for the suspended sediment. It is assumed that ε_s is related to the eddy diffusivity $\varepsilon_{mo} = \varepsilon_i$ in (13) by the relation

$$\varepsilon_s = \beta \varepsilon_{mo} \tag{28}$$

where β is the reciprocal of the turbulent Schmidt number. For fine sediment particles ($w_p/\kappa u_* \leq 0.5$), it is usually accepted that $\beta \approx 1$. For larger particles there is conflicting evidence (e.g., Jobson and Sayre, 1970) as to whether β is smaller or larger than one, or even whether it is constant over the depth of flow.

The model for the vertical distribution of ε_s adopted herein for a flow with an ice cover is an extension of the one developed by Ismail (1952) in an experimental investigation of suspended sediment transport in a closed rectangular conduit. A definition sketch is shown in figure 2, where $\eta = y/d$ is the normalized elevation above the bed. Near the lower and upper boundaries ε_s follows the parabolic distribution usually associated with a logarithmic velocity distribution. However, in the mid-depth region, ε_s is assumed to be distributed linearly between the vertices of the lower and upper parabolas. The model depicted in figure 2 differs from Ismail's in two respects. First, the one shown in figure 2 allows for different upper- and lower-boundary roughnesses so that symmetry about $\eta = 0.50$ is not required. Second, the constant value of ε_s adopted by Ismail for the mid-depth region is twelve percent less than maximum value at the vertices.

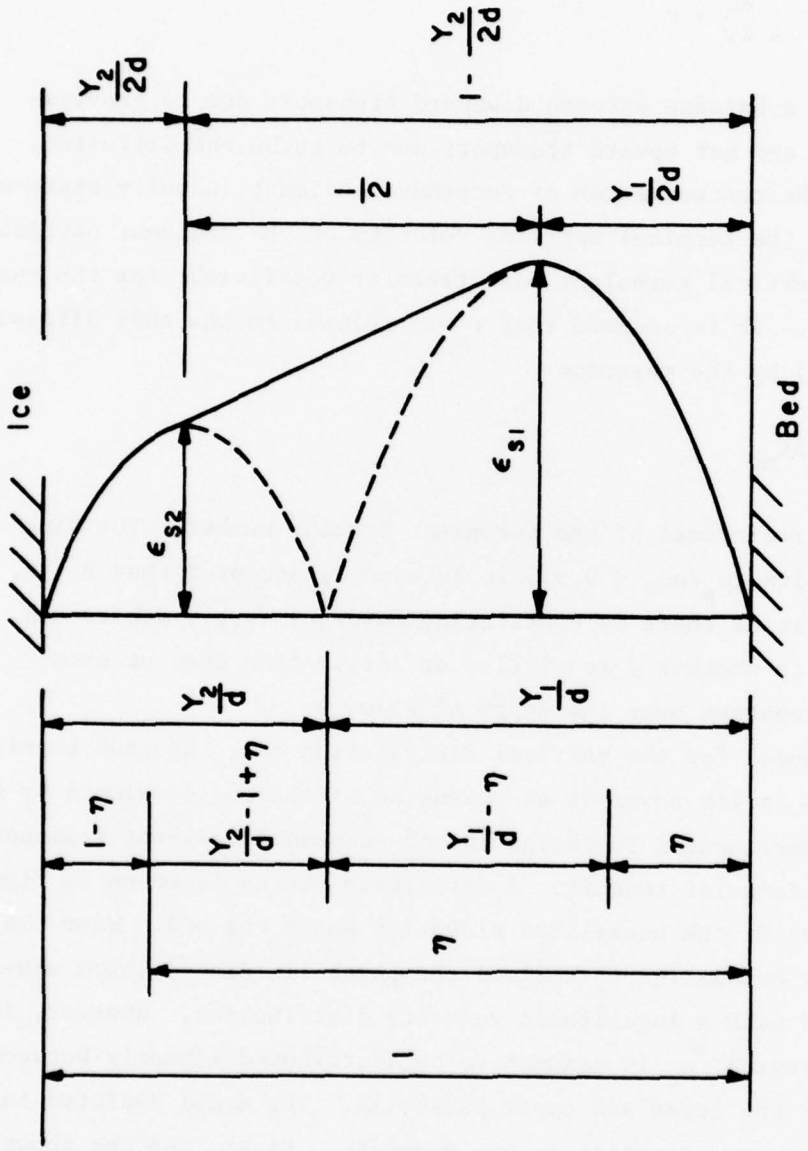

Figure 2.- Definition sketch for distribution of turbulent mass transfer coefficient for suspended sediment in an ice-covered channel.

The flow field is divided into three layers wherein ε_s and C, obtained by integrating (27)

$$\int_{C_a}^{C} \frac{dC}{C} = \ln[\frac{C}{C_a}] = -w_p d \int_{\eta_a}^{\eta} \frac{1}{\varepsilon_s} d\eta \tag{29}$$

are distributed as follows:

$0 \leq \eta \leq Y_1/2d$:

$$\varepsilon_s = \beta_1 \kappa_1 u_{*_1} d\eta \ (1 - \frac{\eta}{Y_1/d}) \tag{30}$$

$$C = C_a \left[\frac{Y_1/d-\eta}{\eta} \frac{\eta_a}{Y_1/d-\eta_a}\right]^{\frac{w_p}{\beta_1 \kappa_1 u_{*_1}}}$$

$$= C(Y_1/2d) \left[\frac{Y_1/d-\eta}{\eta}\right]^{z_1} \tag{31}$$

where

$$\eta_a = Y_1/2d, \ z_1 = \frac{w_p}{\beta_1 \kappa_1 u_{*_1}}$$

$Y_1/2d \leq \eta \leq 1 - Y_2/2d$:

$$\varepsilon_s = \underbrace{2(\varepsilon_{s2} - \varepsilon_{s1})}_{a}\eta + \underbrace{\varepsilon_{s1} - 2(\varepsilon_{s2} - \varepsilon_{s1})Y_1/2d}_{b} = a\eta + b \tag{32}$$

where $\varepsilon_{s1} = \beta_1 \kappa_1 u_{*_1} Y_1/4$, $\varepsilon_{s2} = \beta_2 \kappa_2 u_{*_2} Y_2/4$

$$C = C_a \left[\frac{a\eta + b}{a\eta_a + b}\right]^{\frac{-w_p d}{a}}$$

$$= C(Y_1/2d) \left[\frac{2(\varepsilon_{s2} - \varepsilon_{s1})(\eta - Y_1/2d)}{\varepsilon_{s1}} + 1\right]^{-\frac{w_p d}{2(\varepsilon_{s2}-\varepsilon_{s1})}} \tag{33}$$

where $\eta_a = Y_1/2d \rightarrow a\eta_a + b = \varepsilon_{s1}$

$1 - Y_2/2d \leq \eta \leq 1$:

$$\varepsilon_s = \beta_2 \kappa_2 u_{*_2} d(1-\eta) \ (1 - \frac{1-\eta}{Y_2/d}) \tag{34}$$

$$C = C_a \left[\frac{1 - \eta}{Y_2/d-1+\eta} \frac{Y_2/d-1+\eta_a}{1-\eta_a}\right]^{\frac{w_p}{\beta_2 \kappa_2 u_{*_2}}}$$

$$= C(1 - Y_2/d)\ [\frac{1-\eta}{Y_2/d-1+\eta}]^{z_2} \tag{35}$$

where $\eta_a = 1 - Y_2/d$, $z_2 = \frac{w_p}{\beta_2 \kappa_2 u_{*_2}}$

The depth-averaged value of ε_s, obtained by integrating ε_s over the three layers, is

$$\bar{\varepsilon}_s = \int_0^1 \varepsilon_s d\eta = \beta_1 \kappa_1 u_{*_1} Y_1 (\frac{Y_1}{12d} + \frac{1}{16}) + \beta_2 \kappa_2 u_{*_2} Y_2 (\frac{Y_2}{12d} + \frac{1}{16}) \tag{36}$$

For a free-surface flow, (30) and (31), with $Y_1 = d$, apply over the whole range $0 < \eta < 1$. The depth-averaged value of ε_s for this case is

$$\bar{\varepsilon}_s = \beta \kappa u_* d/6 \tag{37}$$

Equations 31, 33, and 35 all express the vertical distribution of C relative to the concentration C_a, often determined by measurement, at some reference level η_a. Lack of a reliable method for predicting C_a corresponding to a given set of flow and sediment characteristics is one of the weaknesses in current sediment transport theories. Einstein (1950) attempted to relate C_a at a distance of two particle diameters above the bed to the theoretical bed-load discharge and velocity at the outer edge of the viscous sublayer. Willis and Kennedy (1977) have proposed relating C_a to the theoretical average local maximum sediment flux, the concentration in the bed, and the probability that the local bed elevation equals or exceeds the elevation above the mean bed level, y_m, at which the maximum flux occurs.

Using Ismail's (1952) model for ε_s, Shen and Harden (1978) predicted profiles with lower suspended sediment concentrations for ice-covered than for free-surface flows, especially in the upper region. They attributed this to a reduction in the vertical mixing capacity due to the presence of the ice cover.

E. Total Bed-Material Discharge. When computed for a particular channel, unit discharges of total bed-material load, q_{st}, and bed load, q_{sb}, predicted by most of the currently-used formulas, can be

approximated by a generalized relationship of the type

$$\left.\begin{matrix} q_{st} \\ q_{sb} \end{matrix}\right\} \propto (U - U_c)^m (\tau_0 - \tau_c)^n \tag{38}$$

The exponents m and n have different values (usually between 0 and about 3, but with m+n ≈ 2 to 3) in the different formulas, and U_c and τ_c, if included, represent the critical mean velocity and bed shear stress at which particles begin to move.

For the equivalent ice-covered and free-surface flows as defined at the beginning of this chapter the mean velocity in the ice-covered flow will be reduced according to the ratio

$$\frac{U_I}{U_F} = \frac{d_F}{d_I} \tag{39}$$

and the bed shear stress according to the ratio

$$\frac{\tau_{01}{}_I}{\tau_{0_F}} = \left(\frac{Y_1}{d}\right)_I \frac{d_I}{d_F} \tag{40}$$

With typical values for both ratios ranging between about 0.7 and 0.9, it is clear from (38) that bed-material and bed-load transport rates can be greatly reduced by the presence of an ice cover.

Fundamental work-energy considerations lead to the same conclusion. The equation of motion for steady uniform flow, integrated over the cross-sectional area, can be reduced to the statement

$$\gamma QS = U \overline{\tau_0} P \tag{41}$$

where the left-hand side represents the mean rate of energy dissipation per unit length of channel, and the right-hand side represents the mean rate of work to overcome resistance at the boundary, denoted by the wetted perimeter, P. Considering equivalent ice-covered and free-surface flows, the left-hand side is the same for both cases. However the right-hand side for the free-surface flow is

$$RHS_F = U_F \overline{\tau_{0F}} P_F \tag{42}$$

where the wetted perimeter, P_F, consists of the bed (including submerged banks), whereas for the ice-covered flow it is

$$RHS_I = U_I \overline{\tau_{01}} P_1 + U_1 \overline{\tau_{02}} P_2 \tag{43}$$

where the work is divided between the wetted perimeter of the bed, $P_1 \approx P_F$, and the wetted perimeter of the ice cover, P_2. Since the two right-hand sides have the same value, it is clear that the energy dissipated by the bed forces must be significantly less in the ice-covered flow. The fraction of the total work expended in overcoming bed resistance is equal to $\tau_{01} P_1/(\tau_{01} P_1 + \tau_{02} P_2)$, which reduces to Y_1/d for a wide rectangular channel where $P_1 = P_2$, $\overline{\tau_{01}} = \gamma Y_1 S$, and $\overline{\tau_{02}} = \gamma Y_2 S$.

It is reasonable to assume that q_{sb} and the entrainment of bed material into suspension are associated only with that fraction of the work that is exerted in overcoming bed resistance. It follows that both q_{sb} and the suspended sediment unit discharge

$$q_{ss} = \int_{0+}^{d} uC \, dy \tag{44}$$

must be significantly reduced by the presence of an ice cover. With respect to (44), one would not expect the increase in d, due to the ice cover, to be sufficient to offset the reduction in C, due to the decreased capacity of the flow to entrain sediment from the bed and maintain it in suspension.

The foregoing conclusions concerning the reduction in bed-material transport due to the presence of an ice cover are consistent with observations on a number of rivers in Canada reported by Tywoniuk and Fowler (1972). They found both flow and suspended sediment transport to be usually much lower and less variable during the ice-cover periods, with roughly 10 percent of the total annual suspended sediment discharge transported by the 20 percent of the total annual flow occurring during the approximately 5-month ice-cover period. Observations which contradicted this trend were obtained mainly in break-up periods, during which concentrations and discharges may be relatively high.

F. Bed Forms. In a given sand bed channel, characterized by a given slope, width, and distribution of bed-material particle sizes, the bed forms progress through an orderly spectrum of configurations, from ripples to dunes to flat bed to antidunes to chutes and pools as the water and sediment discharges are increased. The heights and lengths of these bed forms are responsive to changes in the flow conditions, and in turn the resulting bed configuration largely determines the hydraulic roughness, thereby significantly influencing the depth and velocity of flow. The way in which the presence of an ice cover affects the bed forms is not clear from presently available bed-form predictors, all of which have been developed for free-surface flows.

Vanoni (1974) developed a set of charts, each for a different range of bed-material sizes, which consist of graphs of the Froude number, $\mathbb{F} = U/\sqrt{gd}$, versus the ratio of depth to median grain diameter, d/D_{50}, on which the data group into zones corresponding to different types of bed forms. In general the bed forms progress toward the upper end of the bed-form spectrum from ripples to dunes to transition to flat bed to antidunes to chutes and pools as $\mathbb{F}$ or d/D_{50} increases. In using the charts for ice-covered channels, it is not entirely clear whether d or Y_1 is the more appropriate length scale for the flow in $\mathbb{F}$ and d/D_{50}, or even whether the same length scale should be used in both parameters. In particular, the physical significance of $\mathbb{F}$ is not clear for an ice-covered flow. If $\mathbb{F}$ is interpreted as $\sqrt{8S/f}$ where $f = f_1$, then it appears reasonable to use Y_1. If Y_1 is used in both $\mathbf{F}$ and d/D_{50}, formation of an ice cover will cause both $\mathbf{F}$ and Y_1/D_{50} to decrease below their corresponding values for an equivalent free-surface flow, indicating a regression toward the lower end of the bed-form spectrum. If d_1 is used in both parameters, $\mathbf{F}$ will decrease but d/D_{50} will increase, although probably not by enough to offset the decrease in $\mathbf{F}$, so an indication of regression toward the lower end of the bed-form spectrum is still likely. However, if Y_1 is used in $\mathbf{F}$ and d_1 in d/D_{50}, progression toward the upper end of the spectrum would be indicated in some cases.

Simons and Richardson (1966) presented a graphical relationship of stream power, $\tau_0 U$, versus median particle fall diameter wherein, for

any given fall diameter, the progression toward the upper end of the bed-form spectrum is always in the direction of increasing stream power. In light of the discussion on work-energy considerations in the last section it seems clear that only that part of the stream power that is associated with the bed (i.e., gY_1SU) should be considered when using the relationship for ice-covered flows. Because the stream power associated with the bed is always less for an ice-covered flow than for an equivalent free-surface flow, regression toward the lower end of the bed-form spectrum accompanying formation of an ice cover would invariably be predicted by the Simons-Richardson relationship.

Willis and Kennedy (1977) presented graphical relationships wherein the ratios of indicators, obtained by spectral analysis, of mean length, L, and mean height, H, of bed forms to depth are shown to increase with $\mathbb{F}^2$ in the sub-transition range of the bed-form spectrum. In applying these relationships to ice-covered flows, it is again uncertain whether Y_1 or d_I is the more appropriate length scale to represent the flow. Calculations using typical values of d_I/d_F and Y_1/d_F show that the relationships would predict a reduction in both length and height of bed forms accompanying formation of an ice cover for all combinations of Y_1 and d_I in $\mathbb{F}^2$ and (L or H)/d, except when d_I is used in the former and Y_1 in the latter. However there is considerable variation in the results predicted using the other three combinations.

Grigg (1970) reported data for free-surface flows with ripples and dunes, indicating that both L and σ_y (standard deviation of bed elevation, which is roughly proportional to H) increase with stream power. For a given grain size, the data also indicate a fairly consistent tendency for L/σ_y to increase with stream power. Considering only that portion of the stream power that is expended in overcoming bed resistance, one would expect from these trends that formation of an ice cover would invariably cause a reduction in the size of the bed forms, but possibly cause the hydraulic roughness of the bed to increase due to a reduction in L/H.

Alam and Kennedy (1969), in an investigation of friction factors for flow in sand bed channels, used dimensional analysis together with flume and river data obtained by several investigators to develop

a chart wherein the bed-form friction factor, f", is represented as a function of $U/\sqrt{gD_{50}}$ and r_b/D_{50}, where r_b is the hydraulic radius associated with the bed. Replacing f" by f_1'' and r_b by Y_1 for flows with ice covers, the chart indicates that in most cases f_1'' would be larger than f" for an equivalent free-surface flow. The increase in friction factor could be due to a reduction in L/H even through there is a decrease in both L and H.

G. Summary. For easy reference, the main items introduced in this chapter that pertain to the effects of an ice cover on alluvial channel flow and transport phenomena are summarized as follows:

1. Equivalent ice-covered and free-surface flows are considered to be uniform two-dimensional flows which have the same unit water discharge, slope, and temperature.
2. In comparison to a free-surface flow, the depth of an ice-covered flow is increased due to the drag on the underside of the ice cover. The amount of increase, which depends on the composite roughness of the ice cover and bed relative to the bed roughness for the equivalent free-surface flow, is typically 10 to 40 percent. There is a corresponding reduction in velocity.
3. Flows with ice covers are characterized by lower and upper layers of respective thicknesses Y_1 and Y_2, with the locus of maximum velocity and zero shear stress at the interface between the two layers. For linear shear stress distributions in both layers, the thicknesses of the lower and upper layers are proportional to the relative magnitudes of the shear stresses at the lower and upper boundaries, and the velocity distribution in both layers can be represented by the Karman-Prandtl logarithmic velocity defect law. It follows that the velocity and shear stress distribution in the lower layer, and possibly the sediment-transport and bed-form characteristics to a considerable extent also, should be the same as in a free-surface flow with depth Y_1 and mean velocity U_1.

4. The two-layer model can also be extended to estimate the vertical distribution of suspended sediment in an ice-covered flow. It is assumed that the vertical turbulent mass transfer coefficient for suspended sediment is distributed parabolically like the eddy diffusivity in the regions near the lower and upper boundaries but that it is linearly distributed between the vertices of the two parabolas in the mid-depth region.
5. From generalized sediment transport relationships and also from elementary work-energy considerations, it is seen that both the total bed-material discharge and the bed-load discharge can be greatly reduced by the presence of an ice cover. This results from the reduction in both mean velocity and bed shear stress due to the ice cover.
6. From a consideration of currently available relationships for predicting the type, characteristic dimensions, and hydraulic roughness of alluvial channel bed forms, it appears likely that an ice cover causes a change in bed-form characteristics similar to that which would occur in a free surface flow if the flow discharge were reduced, or if the discharge were held constant and the depth increased. For flows in the ripple and dune regimes a reduction in bed-form size, and possibly an increase in bed roughness due to decreasing bed-form length-to-height ratio, is expected. This is consistent with the hypothesis that bed friction factors, bed-form characteristics, and sediment-transport properties of an ice-covered alluvial channel are equivalent to those in a free-surface flow with depth Y_1 and mean velocity U_1.

III. EXPERIMENTAL INVESTIGATION

A. Description of Experiments. The main purpose of the experimental investigation was to obtain comparisons between the characteristics of alluvial-channel flows with a simulated ice cover and equivalent (same discharge and slope) free-surface flows. To this end, three sets of experiments were performed in a laboratory flume with a sand

bed. Each set consisted of three runs, one with a free surface, and one each with a smooth and a rough simulated ice cover. The slope and discharge were supposed to be the same for the three runs in each set; however, for reasons to be explained later, equality of discharge was achieved in only one set. Data obtained during each run included measurements of discharge, water-surface elevations and slope, water temperature, several longitudinal bed profiles, and concentration of the total sediment load. Velocity and suspended sediment concentration profiles were obtained for all runs in two of the sets. The experimental equipment and procedures are described in the next two sections.

1. Equipment. The principal experimental facility was a recirculating flume with a glass-walled working section measuring 27.4 m in length, 0.914 m in width, and 0.45 m in depth. An elevation view of the flume is shown in figure 3. The power to recirculate the water-sediment mixture was provided by two 7.5-horsepower variable speed motor-pump units located under the downstream end of the flume, each discharging into separate 10-inch spiral weld return pipes terminating at a transition to the flume inlet. Discharge could be measured at side-contracted orifices in each return pipe. The flume was supported by a central pivot and four synchronized motor-driven cam jacks so that the slope could be changed without interrupting operation of the flume. Flume slope could be measured by means of a dial gage and a point gage at the downstream end of the flume for measuring vertical deflection from the horizontal position. Steel rails for the instrument carriage, mounted atop the flume walls, provided a reference frame for elevation relative to a plane tilted at the flume slope.

The bed was composed of quartz foundry sand with a median diameter, D_{50}, of 0.25 mm and a geometric standard deviation, σ_g, of 1.41. A plot of the sieve-diameter distribution for the sand is shown in figure 4. The same flume and sand were used in experimental investigations reported by Onishi et al. (1972), Jain (1971), Annambholta (1969), and Squarer (1968).

A smooth ice cover was simulated by 1.27-cm thick, 0.91 m by 1.22 m painted plywood panels, connected by hinges, so that they constituted a nonrigid floating cover extending over almost the entire length of the 27.4-m-long working section. Each panel was reinforced to prevent warping.

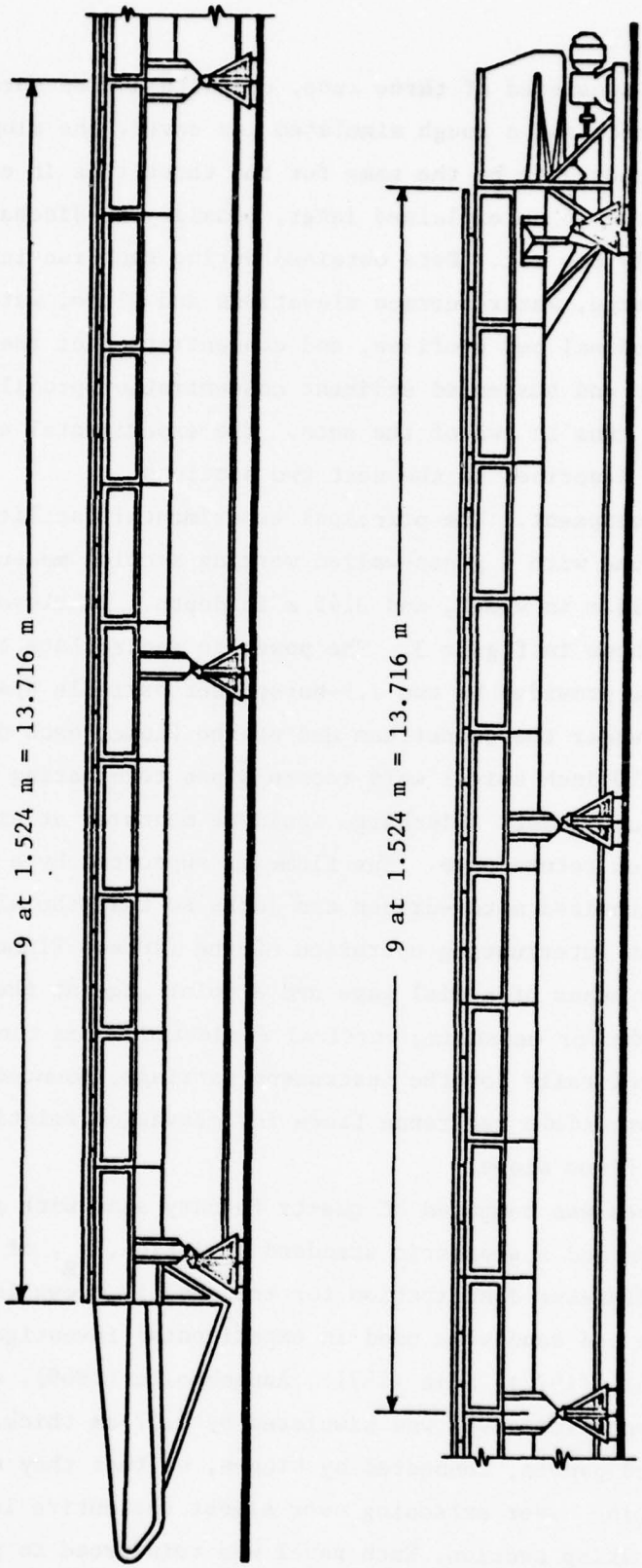

Figure 3. Longitudinal elevation view of flume.

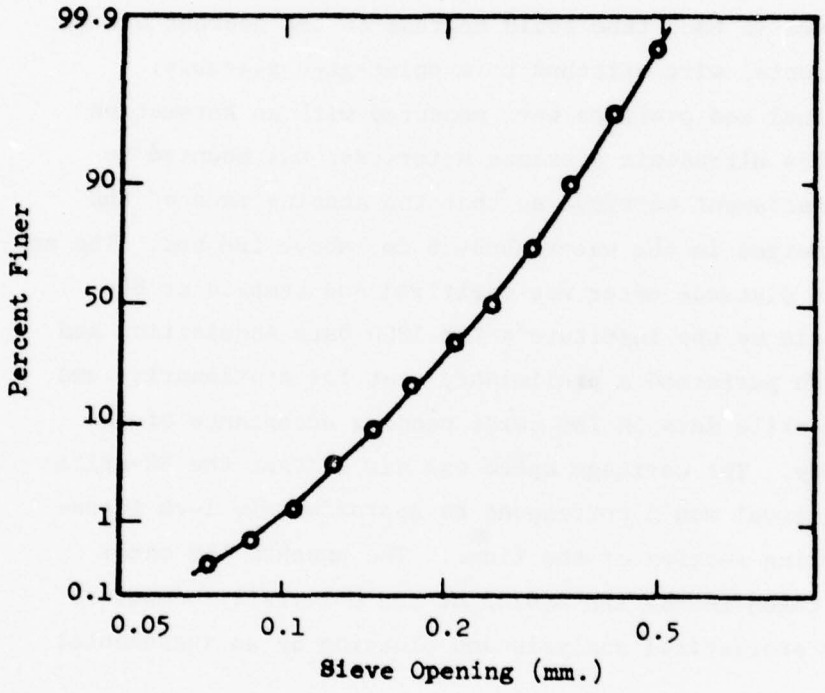

Figure 4. Distribution of sieve diameters of sand used in experiments.

To simulate a rough ice cover, 0.64-cm thick by 2.54-cm wide continuous masonite strips, extending across the width of the panels, were tacked to the bottom surface of the panels at intervals of 15.24 cm.

Water surface elevations and slopes were measured by means of piezometers consisting of perforated, gauze-wrapped copper tubes, buried in the sand and extending across the flume at 3.048-m intervals along the working section of the flume. The piezometers were connected by flexible plastic tubing to a bank of glass manometer tubes, where the water level in each tube could be read to the nearest 0.3 mm by means of a horizontal wire attached to a point-gage assembly.

Longitudinal bed profiles were measured with an Automation Industries Model 1054 ultrasonic distance meter that was mounted to the motor-driven instrument carriage so that the sensing face of the transducer was submerged in the water about 8 cm. above the bed. The analog output from the distance meter was digitized and sampled at 80-millisecond intervals by the Institute's IBM 1800 Data Acquisition and Control System which performed a preliminary test for stationarity and then punched the profile data on IBM cards pending acceptance of the data as satisfactory. The carriage speed was set so that the 80-millisecond sampling interval would correspond to approximately 1-cm intervals along the working section of the flume. The punched IBM cards were subsequently taken to the IBM 360/65 at the University Computer Center for further statistical analysis and plotting by an incremental plotter.

Samples for determining total sediment load concentrations were obtained by withdrawing a representative water-sediment mixture through a vertical slot sampler, consisting of two parallel sheet metal plates connected to a hose and pump, at the downstream end of the flume. This device sampled a 1-cm wide vertical slice extending over the entire depth of flow at the centerline. Samples were pumped into a 0.65-m^3 collecting tank at such a rate that the mean entrance velocity into the slot equalled the depth-averaged flow velocity in the flume. Makeup water was added during sampling to maintain a constant volume of water in the flume system. Following collection and sufficient time for

the sediment to settle, the water was decanted and the sediment was carefully flushed into a beaker for subsequent drying and weighing.

Velocity profiles were measured by means of a 6.3-mm outside-diameter Prandtl Pitot tube mounted to a point-gage assembly and connected to a dual pressure-transducer system. The dynamic and static pressures were transmitted by water columns to two ± 1 kPa capacity Model PM5-TC Statham pressure transducers. The outputs of the transducers were amplified by noninverting high-gain chopper amplifiers and fed sequentially through a difference amplifier and voltage-to-frequency converter to an electronic counter for display. Sensitivity balancing of the transducer outputs by the difference amplifier reduced errors due to temperature fluctuations and vibrations. The system was capable of accurately measuring velocities down to about 3 cm/sec. Calibration was performed by placing the Pitot tube in the center of a submerged jet just downstream from a flow nozzle, the discharge of which had been determined by weighing the flow accumulated over a measured time interval.

Samples for determining suspended sediment concentration profiles were siphoned through a sampling nozzle, attached to a point-gage assembly, into 400-ml beakers. The intake end of the sampling nozzle was shaped into a rectangle, 3.2 mm high and 11.1 mm wide. For each sample, the outlet elevation of the siphon tube was fixed so that the entrance velocity into the sampling nozzle would be equal to the local flow velocity which had just been measured at the sampling point. After weighing the total samples and allowing the sediment to settle, the excess water was decanted and the sediment and remaining water were transferred to evaporation dishes for oven-drying and weighing. Samples were weighed to the nearest milligram with a Sartorius electronic precision balance.

2. Experimental procedures. Three sets of three runs each were conducted, constituting a total of nine runs. They were designated by two alphabetic characters: the first (A,B, or C) in reference to the slope, S, and unit discharge, q, for the set; and the second (F, S, or R) to denote flow with a free surface (F), a smooth simulated ice

cover (S), or a rough simulated ice cover (R). Thus Run BR, for example, means a run with slope and discharge set B, and a rough simulated ice cover.

The original intent was for the three runs in each set to have equivalent flow conditions in the sense that they all be characterized by the same slope and discharge. Unfortunately it was discovered following sets A and B that equality of discharge in these sets had not been achieved. In set C, the condition causing the unequal discharges was corrected, so that the discharges as well as the slopes were the same. The difference in the discharges for the three runs in sets A and B occurred because only one of the two pumps in the parallel return-flow pipe system was operated during these runs because it was considered that at low discharges, the discharge could be measured more accurately and there would be less deposition of sediment in the pipe with this mode of operation. However, since there are no shutoff valves in the system - discharge control is achieved entirely by regulating pump speed - a portion of the flow could be recirculated from the headbox of the flume back through the other pipe instead of through the flume. To the extent that this occurred, the discharge in the flume was less than that indicated by the orifice and manometer unit for the pipe with the operating pump. Comparison of discharges computed by integrating the measured velocity profiles over the flow cross section in the flume and those indicated by the orifice and manometer unit showed that the backflow through the second pipe was negligible in the runs with a free surface, but significant in the runs with a simulated ice cover due to the added resistance to flow through the flume. Consequently the discharges reported for sets A and B are the ones which were computed by integrating the measured velocities over the flow cross section.

The experimental procedures were somewhat different for the free-surface runs and the runs with the simulated ice covers. The free-surface run was always the first of a set. Before starting the run, the sand bed was leveled over the length and width of the flume with the aid of a screed that was mounted to the instrument carriage. Next, with the flume slope horizontal, enough water was added to the flume to

bring the depth to an estimated 0.100 m. Then the flume slope was set at the estimated value for uniform flow, and the flow was started at the desired discharge. From time to time the water surface slope was checked by reading the water-surface elevations on the manometer bank, and the flume slope was adjusted as necessary to make it equal to the water-surface slope. Discharge would also be checked and any necessary adjustments made at these times. This procedure of successive adjustments was continued as the bed-form configuration came into equilibrium with the flow conditions. After the water-surface slope had remained equal to the flume slope for a period of several hours, usually overnight, and the flow depths at several points along the glass walls had been checked with a tape measure to see if the flow depth was approximately 0.10 m along the entire length of the flume, the flow was stopped and the bed profile along the centerline was measured with the ultrasonic distance meter. The output from the IBM 1800 Data Acquisition and Control System was reviewed for nonstationarity, i.e. any consistently rising or falling trend along the flume in the bed elevation with respect to the mean bed elevation. If a visual scan indicated stationarity of the data, the slope, discharge and average depth were recorded and the bed profile data, stored on disk by the computer, were punched on IBM cards; otherwise the flow was started again, and the process was repeated after a few more hours. If the centerline data passed the stationarity test, bed profiles were obtained along two additional sailing lines, one quarter of the flume width to the left of and to the right of the centerline. The flow was then started again and five or six total sediment load samples were obtained, taking care to add sufficient makeup water to maintain uniform flow at the proper depth and slope. Then three sets of velocity and suspended sediment concentration profiles were obtained at about mid-length along the working section, one each at the centerline and one-quarter flume width to the left and right of the centerline. Velocity measurements were obtained at twelve to fifteen points in the vertical, and suspended sediment samples at five points. The flow was then stopped again and a second set of three longitudinal bed profiles was obtained, along the centerline and along the left and right sailing lines. Water temperature was measured with a

mercury thermometer at intervals throughout the run. This completed the procedure for a free-surface run.

Except for the differences noted below, the procedures for the runs with the simulated ice covers were the same. In these runs, the flume slope was maintained constant at the value determined for the corresponding free surface run, i.e. the first run of the set. The bed was not leveled and screeded before installing the simulated ice cover and starting the flow at the beginning of the run. During the first part of the run, the amount of water in the flume was increased and adjusted by successive trials until the piezometric slope became and remained equal to the flume slope. Before obtaining the longitudinal bed profiles and after stopping the flow, the panels simulating the ice cover had to be removed. This was done with care to minimize disturbance to the bed forms. The panels were replaced before obtaining the total sediment load samples and velocity and the suspended sediment concentration profiles. Then the panels had to be removed once more before obtaining the final set of bed profiles.

In set C the procedures were varied somewhat from those outlined above. Both pumps in the flume recirculating system were operated which eliminated the problem of backflow through the second pipe. Also, no velocity and suspended-sediment concentration profiles were obtained, and bed profiles were taken only along the centerline.

B. Summary of Experimental Results. The bulk flow and sediment-transport characteristics for each run are listed in table 1. All quantities listed are averages obtained in one or more of the following ways: averages of measurements taken at various times throughout the runs, averages of measurements obtained at the centerline and at the left and right quarter points across the flume, averages along the length of the working section, and averages over the depth of flow. The unit discharge, q, was determined from the average of the centerline and the left and right quarter-point velocity profiles for the series A and B runs, and from the orifice-meter discharge measurements for the series C runs. The mean depth, $\bar{d}$, was determined by subtracting the mean bed elevation from the mean water-surface elevation, where the former was

Table 1. BULK FLOW AND SEDIMENT TRANSPORT CHARACTERISTICS

Run	Unit discharge q m^2/sec	Mean depth $\bar{d}$ m	Mean velocity $\bar{U}$ m/sec	Slope S	Temperature T °C	Kinematic viscosity $\nu \times 10^6$ m^2/sec	Mean total sed. conc. C_t mg/ℓ	Unit total sed. disch. q_{st} kg/m-sec	Mean susp. sed. conc. C_s mg/ℓ	Unit susp. load disch. q_{ss} kg/m-sec
(1)	(2)	(3)	(4)	(5)	(6)	(7)	(8)	(9)	(10)	(11)
AF	0.0397	0.106	0.375	0.00180	16.7	1.10	103	0.00409	58	0.0023
AS	0.0355	0.118	0.301	0.00180	16.9	1.09	24.8	0.000880	49	0.0017
AR	0.0332	0.121	0.274	0.00180	20.5	0.994	11.2	0.000372	27	0.00090
BF	0.0552	0.102	0.541	0.00208	19.3	1.02	252	0.0139	540	0.030
BS	0.0392	0.122	0.321	0.00204	19.7	1.01	121	0.00474	42	0.0016
BR	0.0428	0.148	0.289	0.00211	18.2	1.05	125	0.00535	35	0.0015
CF	0.0497	0.107	0.464	0.00198	15.0	1.14	127	0.00631	-	-
CS	0.0495	0.133	0.372	0.00187	16.2	1.11	20.5	0.00101	-	-
CR	0.0495	0.162	0.306	0.00194	15.6	1.12	4.2	0.000208	-	-

determined from the bed profiles along the centerline and the left and right sailing lines, and the latter from the piezometer readings along the working section of the flume. The mean velocity, $\bar{U}$, is equal to $q/\bar{d}$. The slope, S, is the flume slope which in turn was set to equal the water-surface slopes indicated by the piezometers. The temperature, T, and mean total sediment concentration, C_t, are averages of measurements and samples taken several times during the course of the runs. The unit total sediment discharge, q_{st} is equal to qC_t multiplied by the appropriate conversion factor ($\frac{kg}{mg}\frac{\ell}{m^3} = 10^{-3}$).

The bed configuration consisted of ripples for all runs. A statistical analysis of the bed forms is presented in section III-h.

Data showing the vertical distributions of velocity, u, suspended sediment concentration, C, and the suspended sediment flux uC, for the A and B series of runs, are presented in figure 5, (a) through (f). The curves, which are based on the average of the three measurements taken at the centerline and the right and left quarter points, were drawn with some smoothing.

Various quantities determined from the velocity profiles are listed in table 2. The reference depths and velocities, d and U, for the profiles in figure 5, are averages for the three verticals at which the profiles were measured. The values of d and U, which are listed in table 2, are in general not equal to the mean values, $\bar{d}$ and $\bar{U}$, for the entire working section listed in table 1.

For both the velocity and concentration data in figure 5, departures from the mean profile appear to be more systematic than random. For the velocity data, the tendency for departures to be greater near the bed is likely due to variations in the positions of the Pitot tube relative to the bed forms. For the suspended sediment concentration data, there is a fairly consistent tendency for the concentrations measured at the left and right one-quarter points to be fairly close to each other, but for the concentrations measured at the centerline to be either significantly higher or lower - more often higher in the free-surface runs, and lower in the runs with the simulated ice cover. This could be due to the existence of secondary circulation cells, wherein an upward velocity component would tend to increase the local concentration

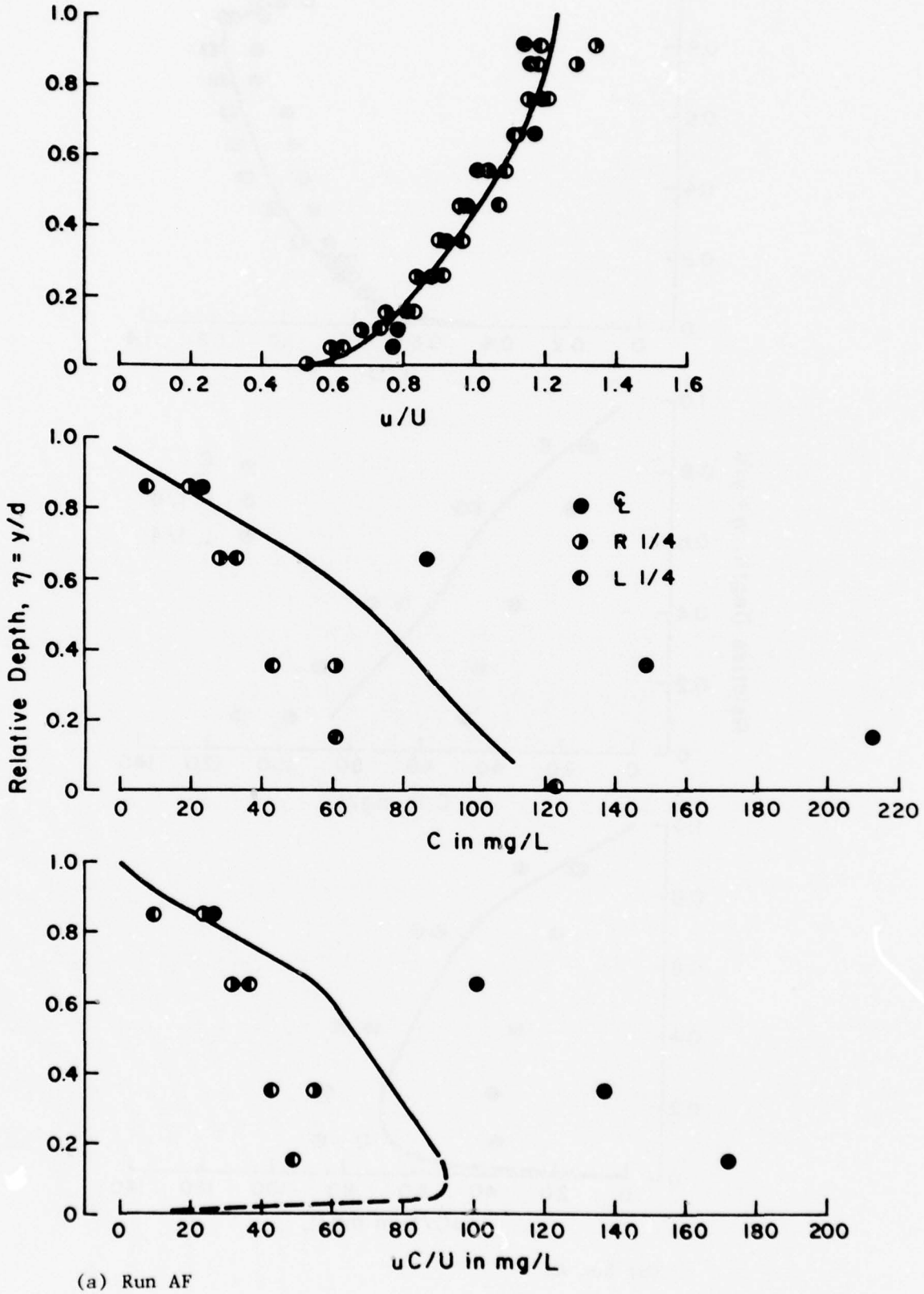

(a) Run AF

Figure 5. Vertical distributions of measured velocity, suspended sediment concentration, and suspended sediment flux.

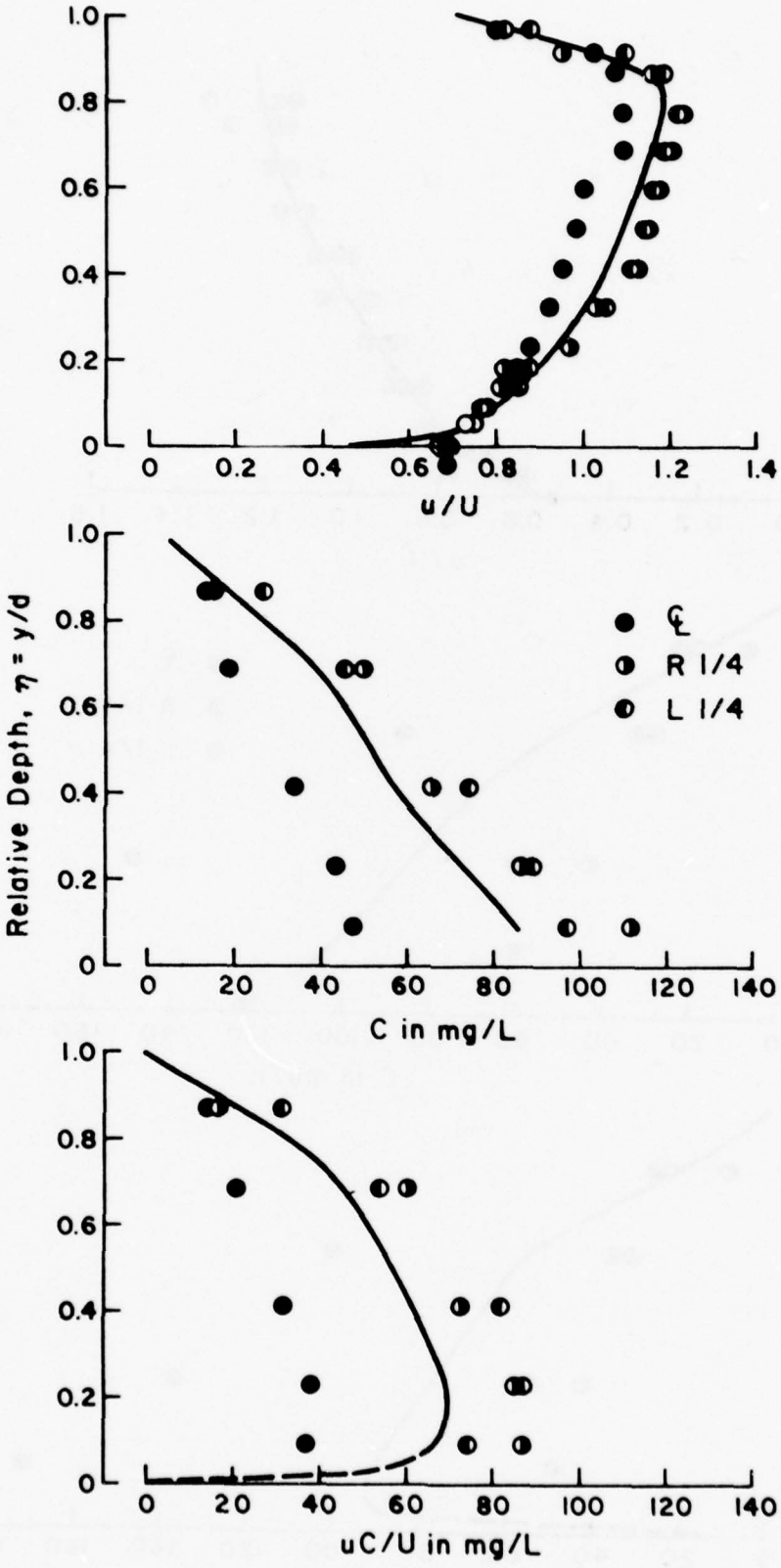

(b) Run AS

Figure 5. (continued).

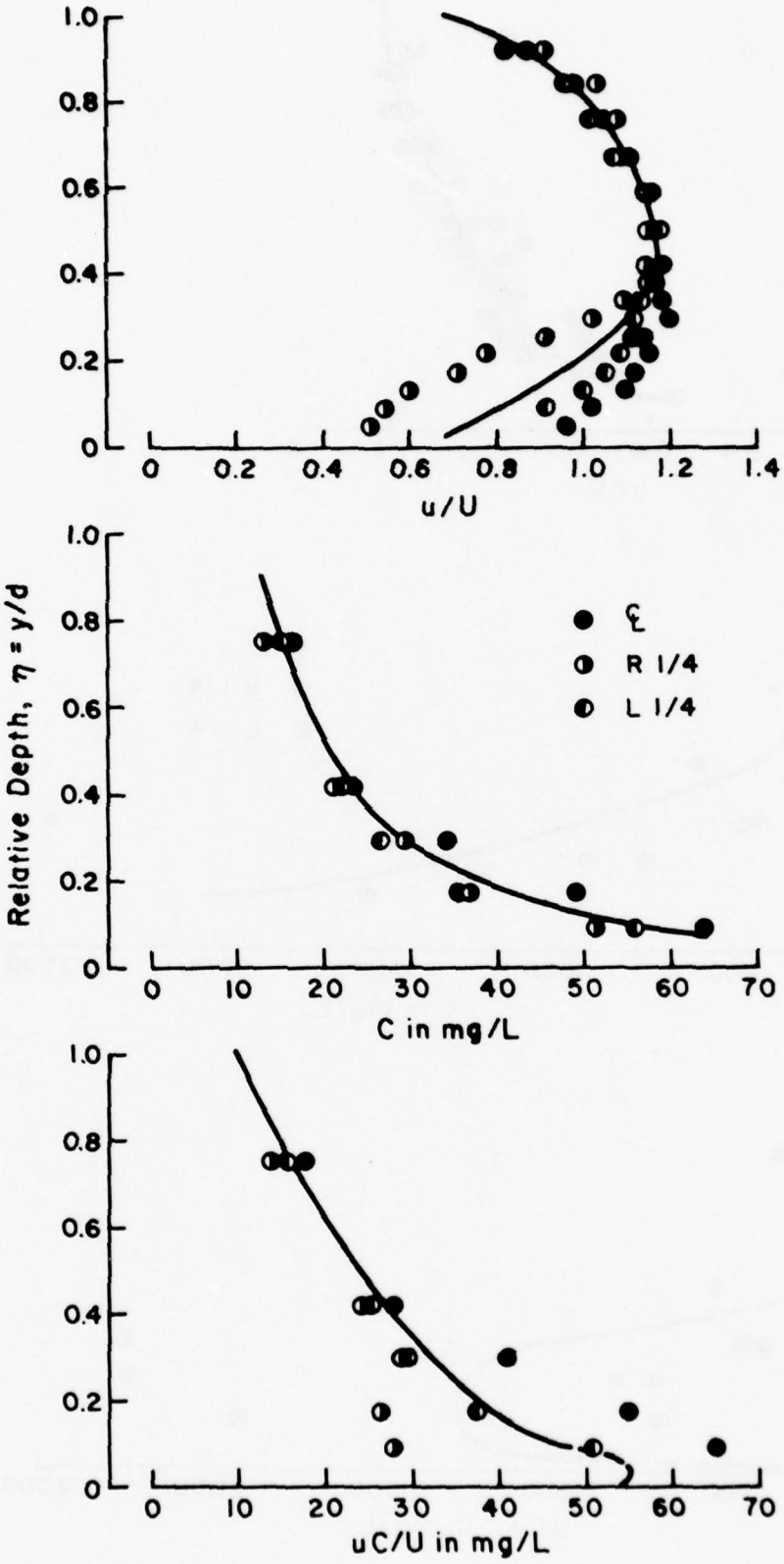

(c) Run AR

Figure 5. (continued).

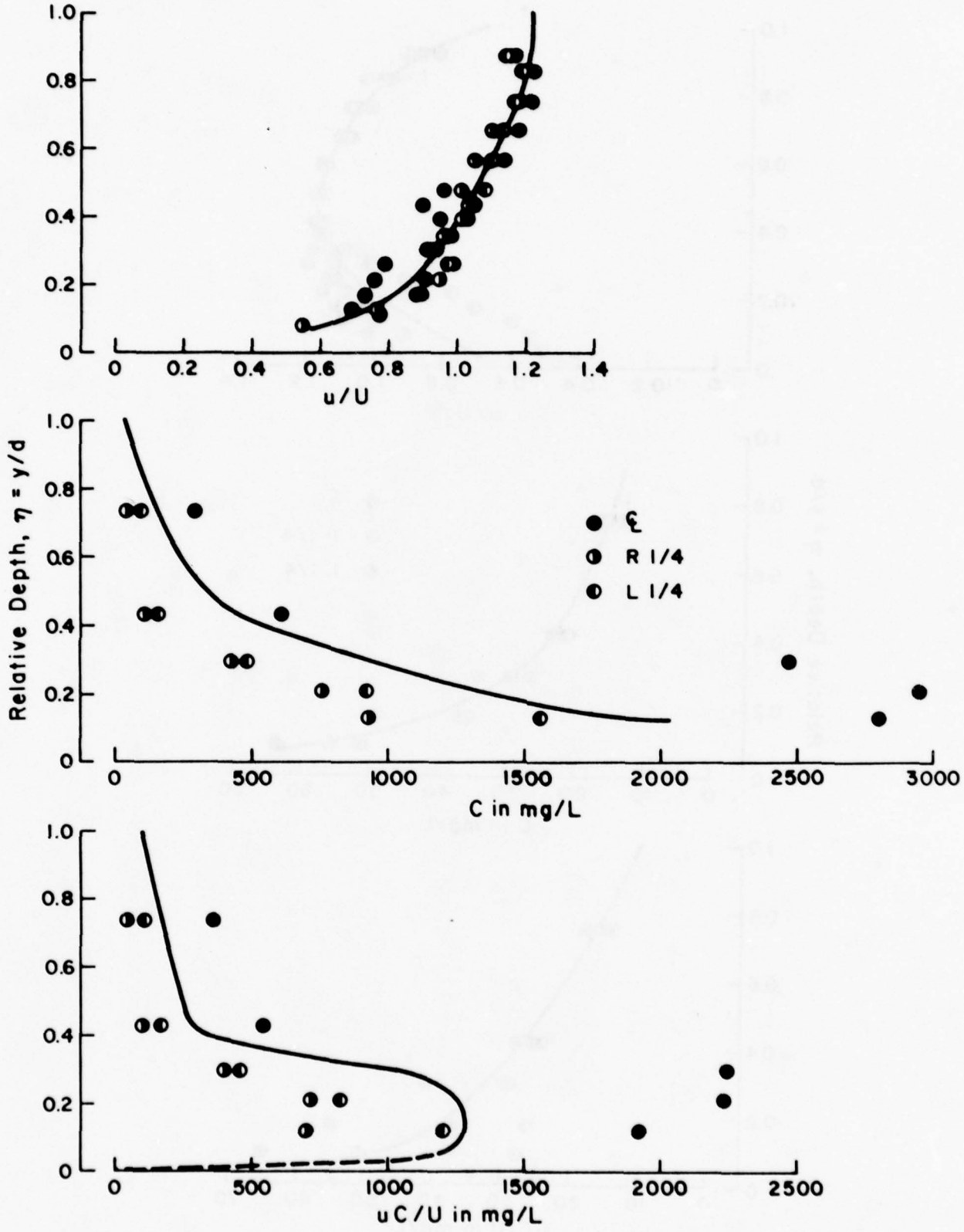

(d) Run BF

Figure 5. (continued).

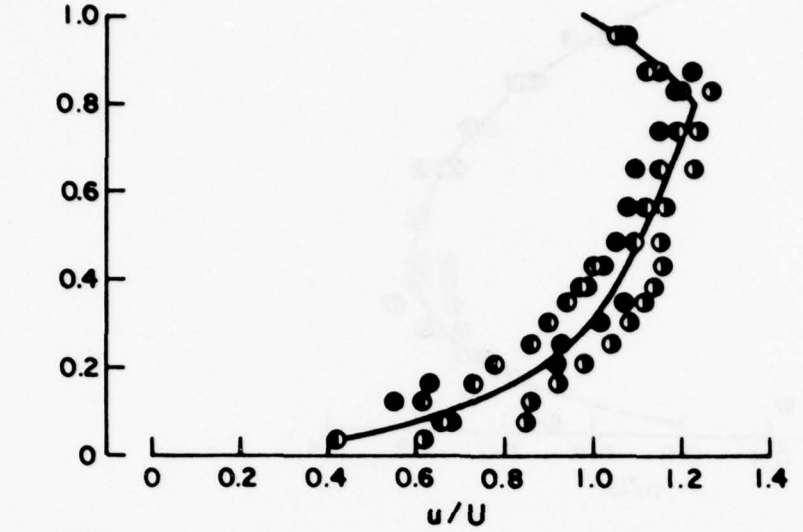

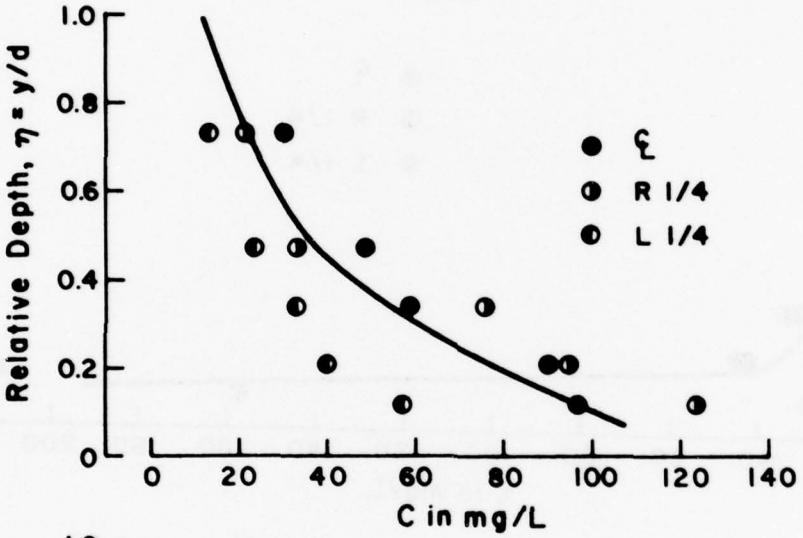

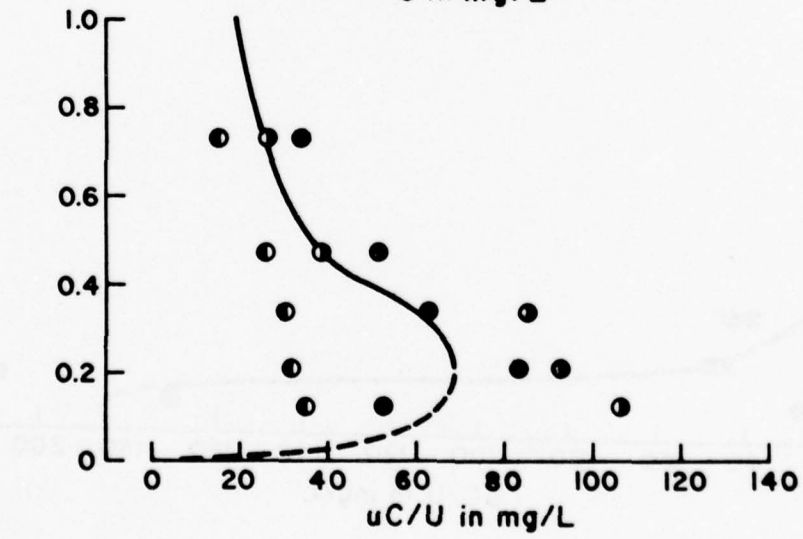

(e) Run BS

Figure 5. (continued).

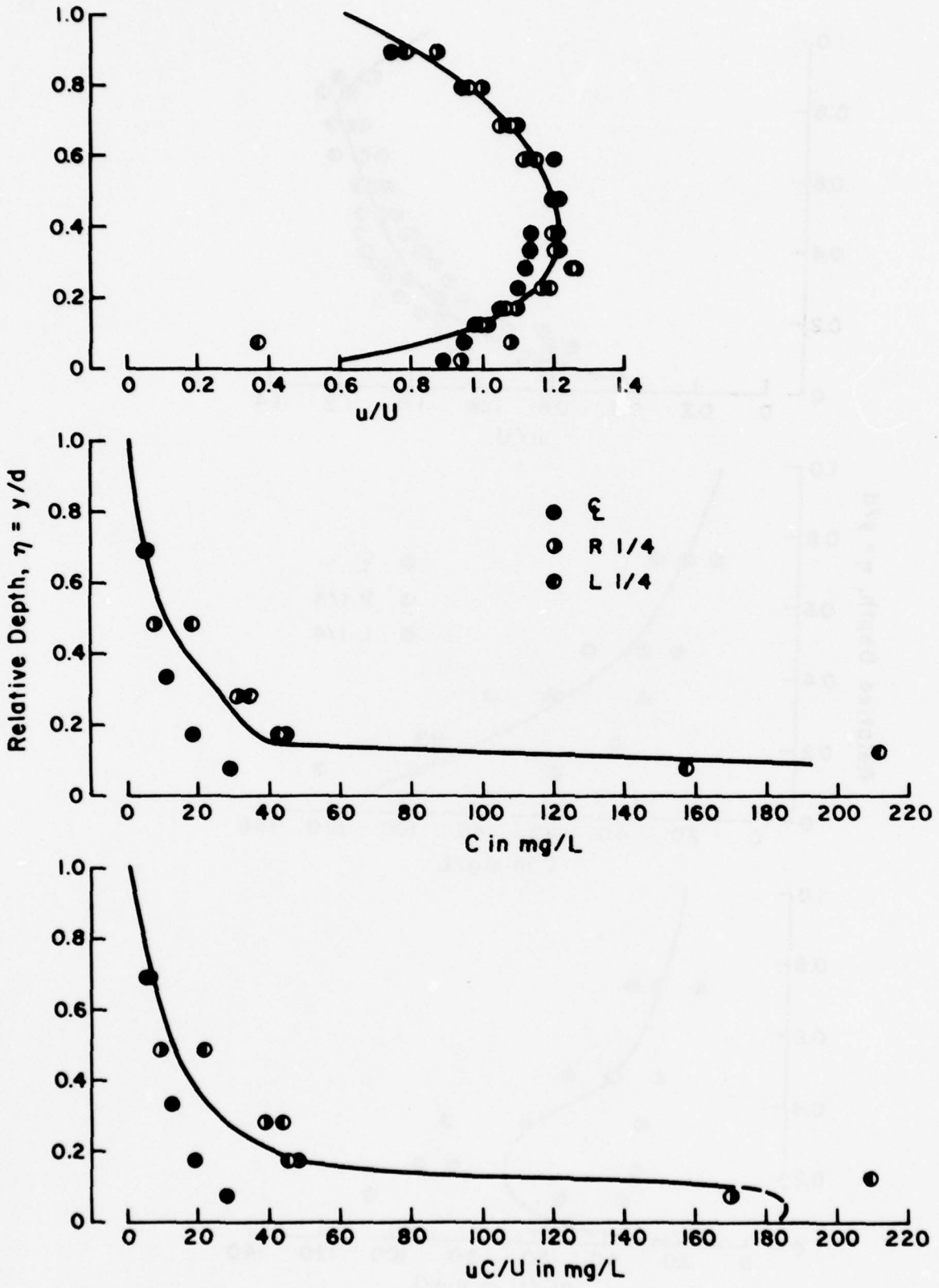

(f) Run BR

Figure 5. (continued).

Table 2. FLOW CHARACTERISTICS DETERMINED FROM VELOCITY MEASUREMENTS

Run	Composite				Lower Layer				Upper Layer			
	q m^2/sec	d m	U m/sec	$\frac{u_{max}}{U}$	$\frac{Y_1}{d}$	$\frac{U_1}{U}$	u_{*_1} m/sec	κ_1	$\frac{Y_2}{d}$	$\frac{U_2}{U}$	u_{*_2} m/sec	κ_2
(1)	(2)	(3)	(4)	(5)	(6)	(7)	(8)	(9)	(10)	(11)	(12)	(13)
AF	0.0397	0.100	0.397	1.23	1	1	0.0420	0.46	0	-	-	-
AS	0.0355	0.110	0.323	1.18	0.80	0.995	0.0394	0.65	0.20	1.020	0.0197	0.38
AR	0.0332	0.121	0.274	1.17	0.45	0.975	0.0310	0.58	0.55	1.020	0.0343	0.83
BF	0.0552	0.114	0.484	1.22	1	1	0.0482	0.45	0	-	-	-
BS	0.0392	0.114	0.343	1.23	0.80	0.975	0.0427	0.49	0.20	1.100	0.0214	0.48
BR	0.0428	0.146	0.293	1.23	0.40	1.025	0.0348	0.58	0.60	0.983	0.0426	0.59

and a downward component to decrease it. This tendency is not evident in the velocity data. In keeping with the above observations, it is to be expected that velocities would be relatively more responsive to local stimuli such as the location of a bed form with respect to the Pitot tube, whereas the local concentrations would depend to a greater extent on the integrated effects of mass transfer phenomena which have occurred for some distance upstream.

The mean suspended sediment concentrations, C_s, listed in column 10 of table 1 were computed by integrating the average sediment-flux distribution (uC/U vs η) curves in figure 5, over the depth of flow. The unit suspended load discharge, q_{ss}, is equal to qC_s multiplied by the appropriate conversion factor. No satisfactory explanation is at hand as to why the C_s values exceed the C_t values in Runs AS, AR and BF. Overall, the C_t values are considered to be more reliable than the C_s values. However, the variability of individual C_t values from the average values listed in table 1 for the A and B series of runs (ranging up to ± 50% and more) was much greater than the variability for the C series. This suggests that an unstable condition due to the recirculation back through the second return flow pipe may have existed at the downstream end of the flume near the slot sampler and affected the total-sediment concentration samples.

The quantities listed in columns 5 through 13 of table 2 were determined in the process of fitting (6) to the velocity-distribution data in figure 5. They will be discussed in the next section.

Average velocities, shear velocities, and Manning and Darcy-Weisbach friction factors for the composite channel, and for the lower and upper layers are listed in table 3. They were computed from the bulk flow characteristics in table 1, using the Y_1/d, Y_2/d, U_1/U, and U_2/U values in table 2 that were determined from the velocity measurements. It is assumed that these ratios remained constant along the length of the working section. Values of the composite shear velocity were computed from the equation

$$u_{*_I} = \sqrt{\frac{\tau_{01}+\tau_{02}}{2\rho}} = \sqrt{gdS/2} \qquad (45)$$

Table 3. AVERAGE VELOCITIES, SHEAR VELOCITIES, AND FRICTION FACTORS

Run	Composite				Lower Layer				Upper Layer			
	$\bar{U}$	u_{*_I}	n_I	f_I	U_1	u_{*_1}	n_1	f_1	U_2	u_{*_2}	n_2	f_2
		m/sec				m/sec				m/sec		
(1)	(2)	(3)	(4)	(5)	(6)	(7)	(8)	(9)	(10)	(11)	(12)	(13)
AF	-	-	-	-	0.375	0.0433	0.0253	0.106	-	-	-	-
AS	0.301	0.0323	0.0214	0.0920	0.299	0.0408	0.0294	0.149	0.307	0.0204	0.0114	0.0354
AR	0.274	0.0327	0.0239	0.114	0.267	0.0310	0.0228	0.108	0.279	0.0343	0.0249	0.120
BF	-	-	-	-	0.541	0.0456	0.0184	0.0569	-	-	-	-
BS	0.321	0.0349	0.0218	0.0948	0.313	0.0442	0.0306	0.159	0.353	0.0221	0.0108	0.0313
BR	0.289	0.0391	0.0280	0.0147	0.296	0.0350	0.0236	0.112	0.284	0.0429	0.0322	0.0182
CF	-	-	-	-	0.464	0.0456	0.0216	0.0772	-	-	-	-
CS[1]	0.372	0.0349	0.0191	0.0705	0.372	0.0442	0.0261	0.113	0.372	0.0221	0.0104	0.0282
CR[2]	0.306	0.0392	0.0269	0.0132	0.306	0.0351	0.0232	0.105	0.306	0.0430	0.0304	0.158

[1]Assume $Y_1/d = 0.80$, $Y_2/d = 0.20$, $U_1 = U_2 = \bar{U}$

[2]Assume $Y_1/d = 0.40$, $Y_2/d = 0.60$, $U_1 = U_2 = \bar{U}$

and values of n_I, f_I, u_{*1}, and u_{*2}, n_1 and n_2, and f_1 and f_2, according to (17), (18), (8), (15), and (16) respectively. These results will be discussed in the sections on bed friction factors and depth of flow.

C. Velocity Distribution. Using the relative depth, $\eta = y/d$, where y is measured from the bed, instead of y_1 and y_2 as defined in figure 1, as independent variables, the velocity distribution according to (6) becomes

$$0 \leq \eta \leq Y_1/d: \qquad u_1 - u_{max} = \frac{u_{*1}}{\kappa_1} \ln[\eta\, d/Y_1]$$
$$Y_1/d \leq \eta \leq 1: \qquad u_2 - u_{max} = \frac{u_{*2}}{\kappa_2} \ln[(1-\eta)d/Y_2] \tag{46}$$

Figure 6 shows (46) fitted to the average velocity profile data for each run. The fitting was accomplished in the following manner. After first averaging the velocities measured at corresponding distances below the upper surface in the verticals at the centerline and the left and right quarter points, the average velocities were plotted as a function of $\eta = y/d$, and smooth curves were drawn by eye through the plotted points. In the averaging, velocities for points below the local bed level were assigned a value of zero. Values of Y_1/d and u_{max} were then read from the curves, and values of U, U_1, and U_2 were computed by numerically integrating the curves. Values of u_{*1} were then computed by (8), with $Y_i = d\ (Y_i/d)$ and d as the average depth for the three verticals. Finally, values of κ_1 and κ_2 were computed by (14), completing the information needed for computing and plotting the curves in figure 6.

The values of the various parameters determined during the fitting process are listed in columns 5 through 13 of table 2. These results show: (1) that Y_i/d appears to depend primarily on the roughness of the ice cover, and to be relatively insensitive to q, implying that the bed roughness, given a particular ice cover, may also be relatively insensitive to q; (2) that the ratio u_{max}/U remains relatively constant for different combinations of upper and lower boundary roughnesses and flow conditions; and (3) that the mean velocities in the lower and upper layers, U_1 and U_2, are quite close to the overall mean velocity $\bar{U}$. In

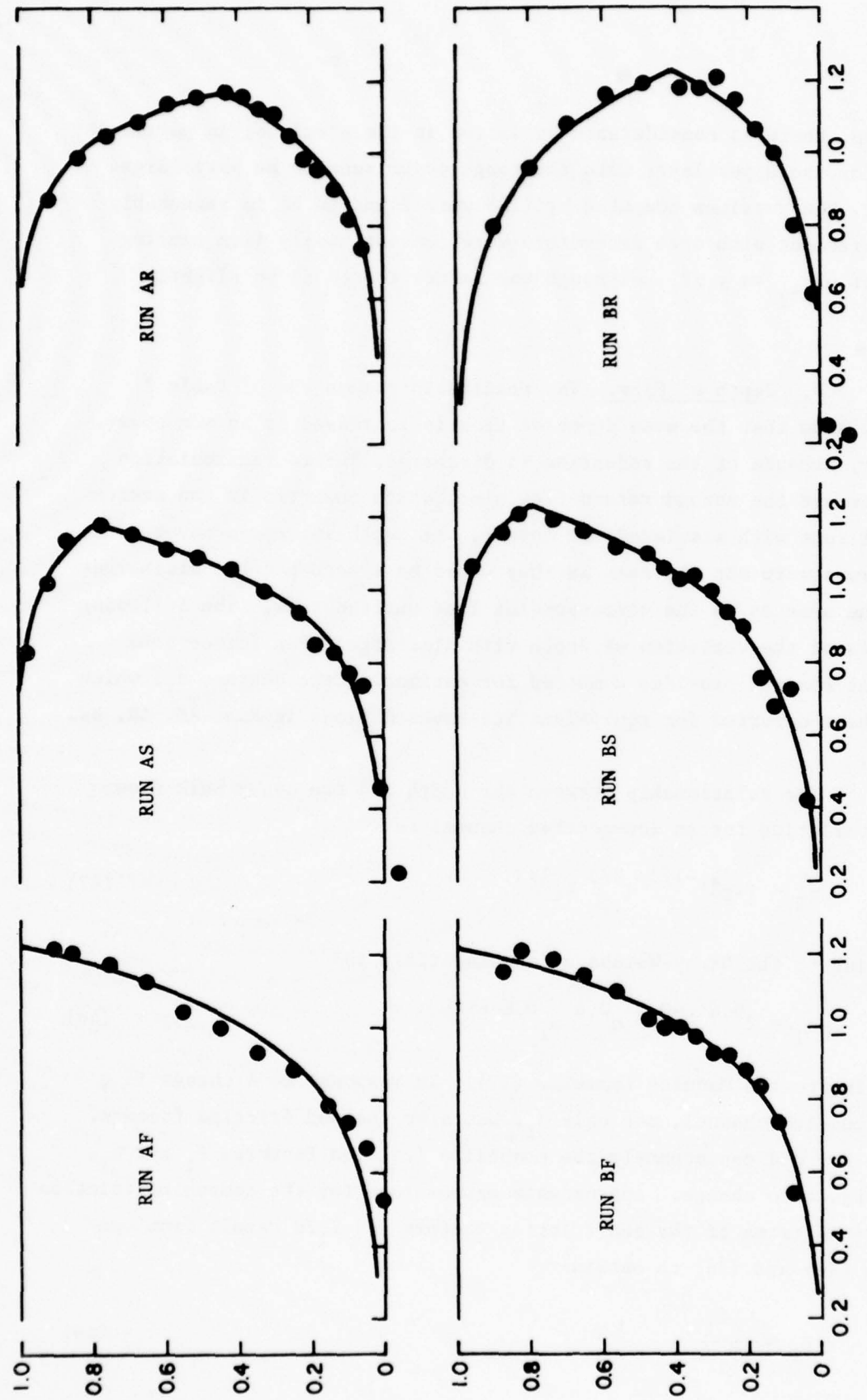

Figure 6. Graph showing (46) fitted to velocity distribution data.

addition, there is considerable variation in the κ values; in particular those for the upper layer with the rough cover seem to be very large. However, the κ values computed by (13) were found to be in reasonably good agreement with ones determined more conventionally from semilog plots of u/u_{*_i} vs y_i/Y_i, although the latter tended to be slightly lower.

D. Depth of Flow. The results in column 3 of table 1 clearly show that the mean depth of flow is increased by an ice cover. However, because of the reduction in discharge, due to recirculation back through the second return-flow pipe, which occurred in the series A and B runs with simulated ice covers, the depth increases observed in these runs were not the same as they would have been had the discharges been the same as in the corresponding free-surface runs. The following analysis of the variation of depth with discharge in an ice-covered alluvial channel provides a method for estimating the depths, $\hat{d}_I$, which would have occurred for equivalent ice-covered flows in Runs AS, AR, BS, and BR.

The relationship between the depth and the other bulk flow characteristics for an ice-covered channel is

$$d_I = (4gS)^{-1/3} q^{2/3} f_I^{1/3} \tag{47}$$

according to the Darcy-Weisbach formula, (18), and

$$d_I = 2^{0.4} S^{-0.3} q^{0.6} n_I^{0.6} \tag{48}$$

according to the Manning formula, (17). In response to a change in q in a sand-bed channel, not only d_I, but also the bed friction factors, f_1 and n_1, and consequently the composite friction factors, f_I and n_I, are subject to change. Approximate expressions for the composite friction factors in terms of the bed-friction factors and Y_1/d result from combining (20) and (26) to obtain

$$f_I = \frac{f_1}{2Y_1/d} \tag{49}$$

and (19) and (25) to obtain

$$n_I = (2Y_1/d)^{-2/3} n_1 \tag{50}$$

Finally, in keeping with the hypothesis that flow in the lower layer resembles a free-surface flow with depth Y_1 and mean velocity U_1, the experimentally-determined values of f_1 and n_1 are plotted in figure 7 as functions of unit discharge in the lower layer

$$q_1 = U_1 Y_1 \approx \frac{Y_1}{d} q \tag{51}$$

It should be noted that the experimental conditions for the data in figure 7 are restricted to a narrow range of slopes (0.0018 to 0.0021) and a single set of bed material characteristics. In using (49), (50), and (51) it is also implied that $U_1 = U_2 = \bar{U}$, and that Y_1/d is independent of q. The data in table 2 appear to indicate that both of these conditions are satisfied, at least approximately.

Estimated values of the depth, $\hat{d}_I/d_F$, for ice-covered flows that are equivalent to the free-surface flows in Runs AF, BF, and CF are listed in table 4. The values of $\hat{d}_I$ in columns 7 and 9 were computed by (47) and (48), using the q and S values in columns 2 and 3, and the f_1 and n_1 values from figure 7 in (49) and (50) to obtain the f_I and n_I values. The small differences between the estimates based on the Darcy Weisbach and Manning formulas are not considered to be significant. The d_I values in column (5) represent the experimentally observed depths. They should be compared directly with the $\hat{d}_I$ estimates in columns 7 and 9 only for the C series of runs wherein the discharge remained constant. Such comparison indicates quite good agreement between the observed d_I values and the $\hat{d}_I$ estimates for Runs CS and CR. Differences between d_I and $\hat{d}_I$ for the A and B series of runs are of course due mainly to the recirculation-related discharge reductions in the experiments.

E. Bed Friction Factors. The hypothesis that the flow in the lower layer of an ice-covered flow is like that in a free-surface flow of

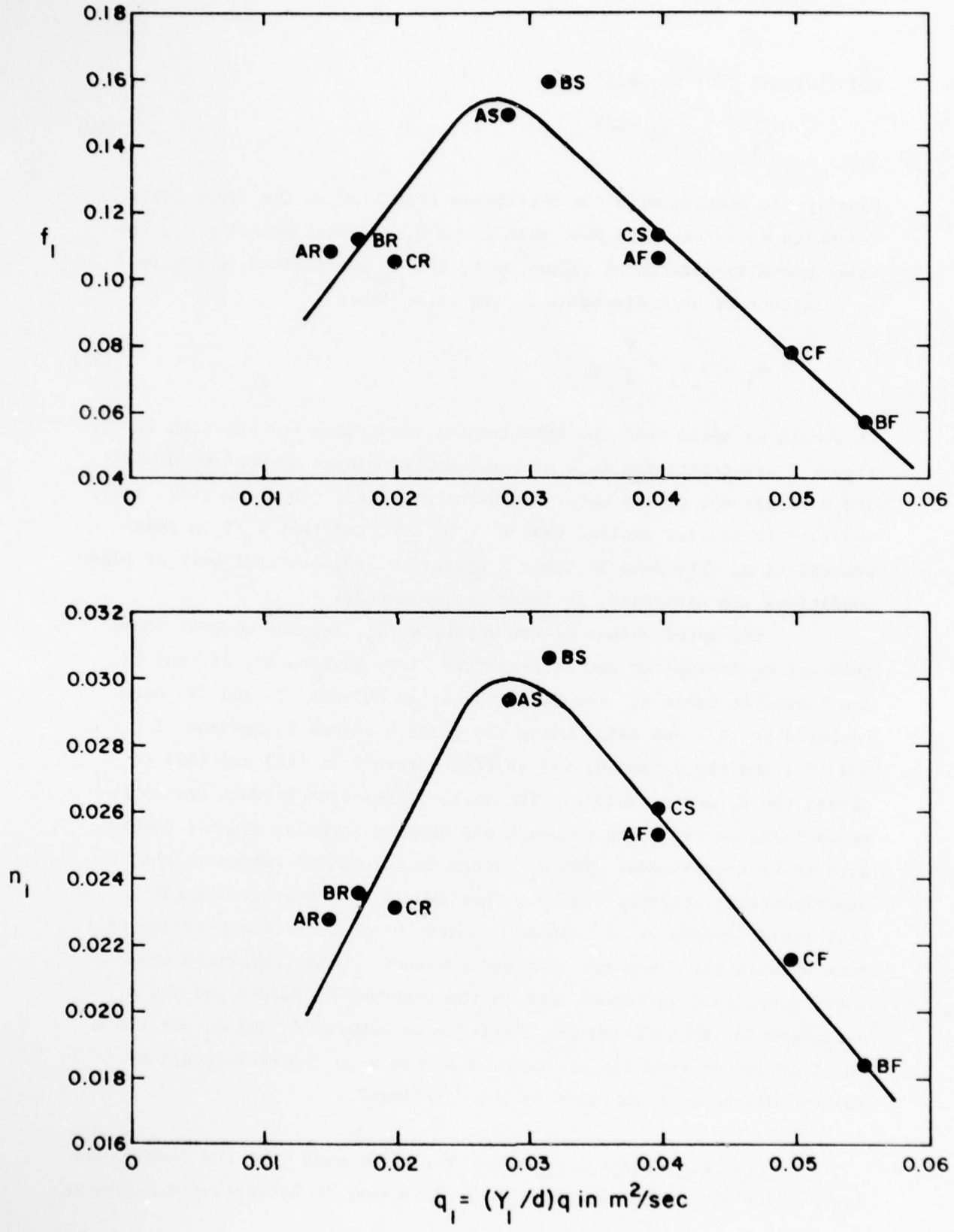

Figure 7. Variation of bed friction factors with unit discharge in lower layer.

Table 4. ESTIMATED DEPTHS FOR EQUIVALENT ICE-COVERED FLOWS

Run	q	S	Observed			Computed by Darcy-Weisbach formula		Computed by Manning formula	
	m^2/sec		d_F m	d_I m	d_I/d_F	$\hat{d}_I$ m	$\hat{d}_I/d_F$	$\hat{d}_I$ m	$\hat{d}_I/d_F$
(1)	(2)	(3)	(4)	(5)	(6)	(7)	(8)	(9)	(10)
AF	0.0397	0.00180	0.106	-	-	-	-	-	-
AS				0.118	1.11	0.126	1.19	0.127	1.20
AR				0.121	1.14	0.141	1.33	0.140	1.32
BF	0.0552	0.00208	0.102	-	-	-	-	-	-
BS				0.122	1.20	0.132	1.29	0.130	1.27
BR				0.148	1.45	0.184	1.80	0.185	1.81
CF	0.0497	0.00198	0.107	-	-	-	-	-	-
CS				0.133	1.24	0.131	1.22	0.130	1.21
CR				0.162	1.51	0.170	1.59	0.169	1.58

depth Y_1 and mean velocity U_1 is tested further, using modified forms of the Alam and Kennedy (1969) bed-form friction-factor chart.

Following Taylor and Brooks (1961), the Darcy-Weisbach friction factor for the bed is separated into two parts,

$$f_1 = f_1' + f_1'' \tag{52}$$

where f_1' is due to the roughness of the sand grains, and f_1'' is due to the form drag associated with the large-scale features of the bed forms. Values of the bed-form friction factor, f_1'', are determined by subtracting f_1' from f_1, where f_1' is evaluated by means of the Lovera and Kennedy (1969) flat bed friction factor diagram, where f_1' is represented as a function of the Reynolds' number, $\mathbb{R} = \bar{U}r_b/\nu$, and the relative roughness, r_b/D_{50}. The Alam and Kennedy bed-form friction-factor chart, which is based on river and flume data from many sources, consists of a set of empirical curves representing constant values of $\bar{U}/\sqrt{gD_{50}}$ on a graph of f_1'' vs r_b/D_{50}. For the purposes of the present investigation when using these charts, r_b, the hydraulic radius of the bed is replaced by U_1 for flows with simulated ice covers, and $Y_1 = d$ for free-surface flows. It is furthermore assumed that $U_1 = \bar{U}$. Also, no sidewall corrections are made insofar as $r_b/d > 0.90$ for all free-surface data included in the present analysis, and the need for corrections would be even less for data from experiments with simulated ice covers. Values of the flat-bed and bed-form friction factors and related quantities for the present experiments are listed in table 5. The rows with a run designation followed by a prime, e.g. AS', contain values of the various quantities computed for equivalent ice-covered flows with the $\hat{d}_I$ values in table 4.

Figures 8 and 9 show data from the present investigation, together with data from Annambhotla (1969) and Onishi et al. (1972) for free-surface flows in the same flume with the same bed material, superimposed on modified forms of the Alam and Kennedy bed-form friction-factor chart. The numbers next to the plotted points denote values of the third variable: $\bar{U}/\sqrt{gD_{50}}$ in figure 8, and Y_1/D_{50} in figure 9. The only

Table 5. FLAT-BED, AND BED-FORM FRICTION FACTORS AND RELATED QUANTITIES

Run	f_1	$R = \frac{\bar{U}Y_1}{\nu}$	Y_1/D_{50}	f_1'	$\frac{\bar{U}}{\sqrt{gD_{50}}}$	f_1''
(1)	(2)	(3)	(4)	(5)	(6)	(7)
AF	0.106	36,300	424	0.018	7.58	0.088
AS	0.149	26,100	378	0.020	6.09	0.129
AS'*	0.149	29,300	408	0.018	6.32	0.131
AR	0.108	15,000	218	0.025	5.54	0.083
AR'	0.119	18,000	454	0.024	5.70	0.095
BF	0.057	54,000	408	0.020	10.93	0.037
BS	0.159	30,900	390	0.019	6.48	0.140
BS'	0.099	43,900	424	0.019	8.44	0.080
BR	0.112	16,300	237	0.024	5.83	0.088
BR'	0.124	21,000	296	0.023	6.02	0.101
CF	0.077	43,600	428	0.018	9.37	0.059
CS	0.113	35,500	424	0.018	7.52	0.095
CR	0.105	17,700	259	0.024	6.20	0.081

* Primes following run designation identify rows corresponding to computed equivalent ice-covered flows based on $\hat{d}_I$ values in table 4.

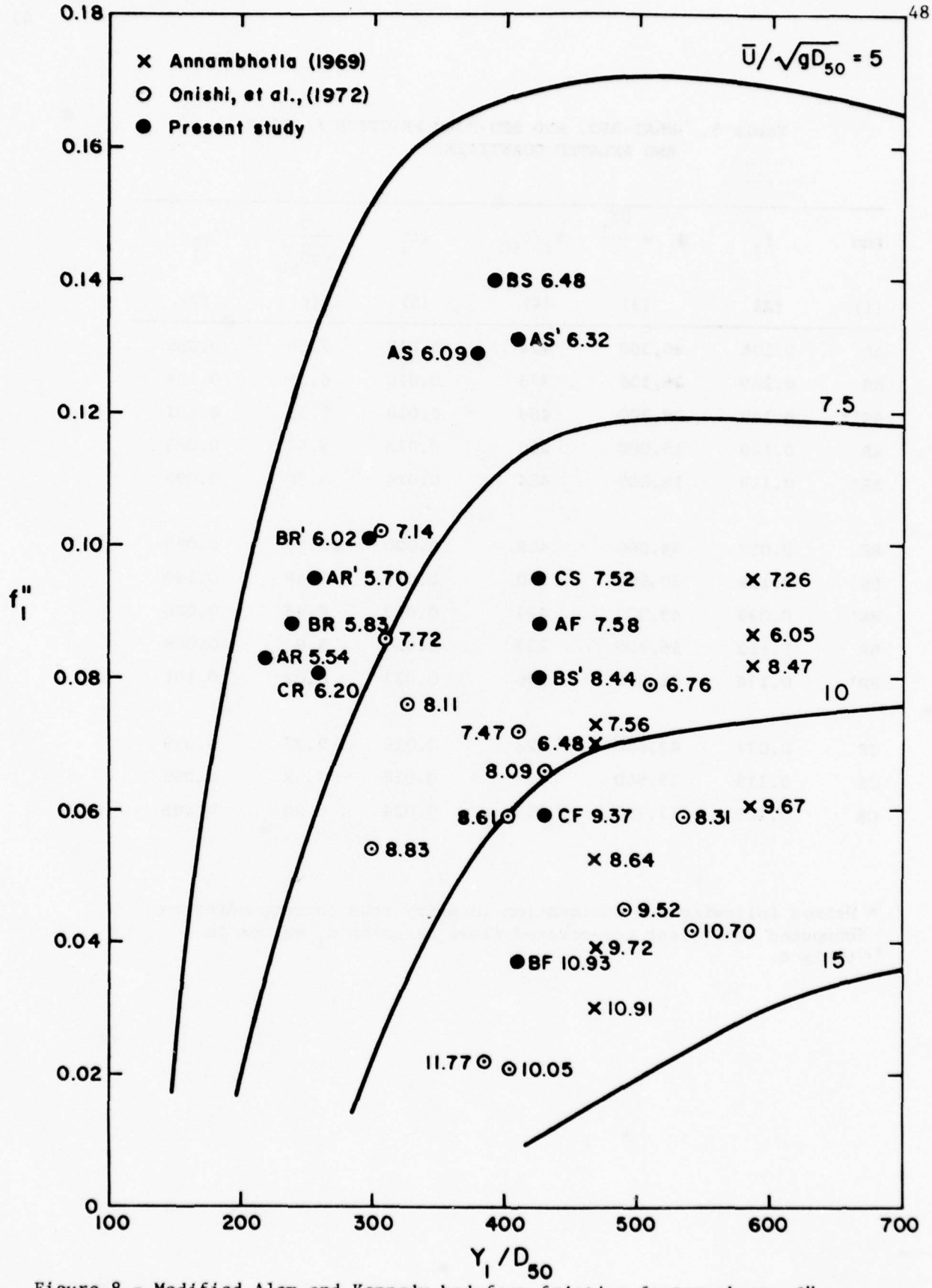

Figure 8.- Modified Alam and Kennedy bed-form friction factor chart; f_1'' vs. Y_1/D_{50} with $\bar{U}/\sqrt{gD_{50}}$ as third variable.

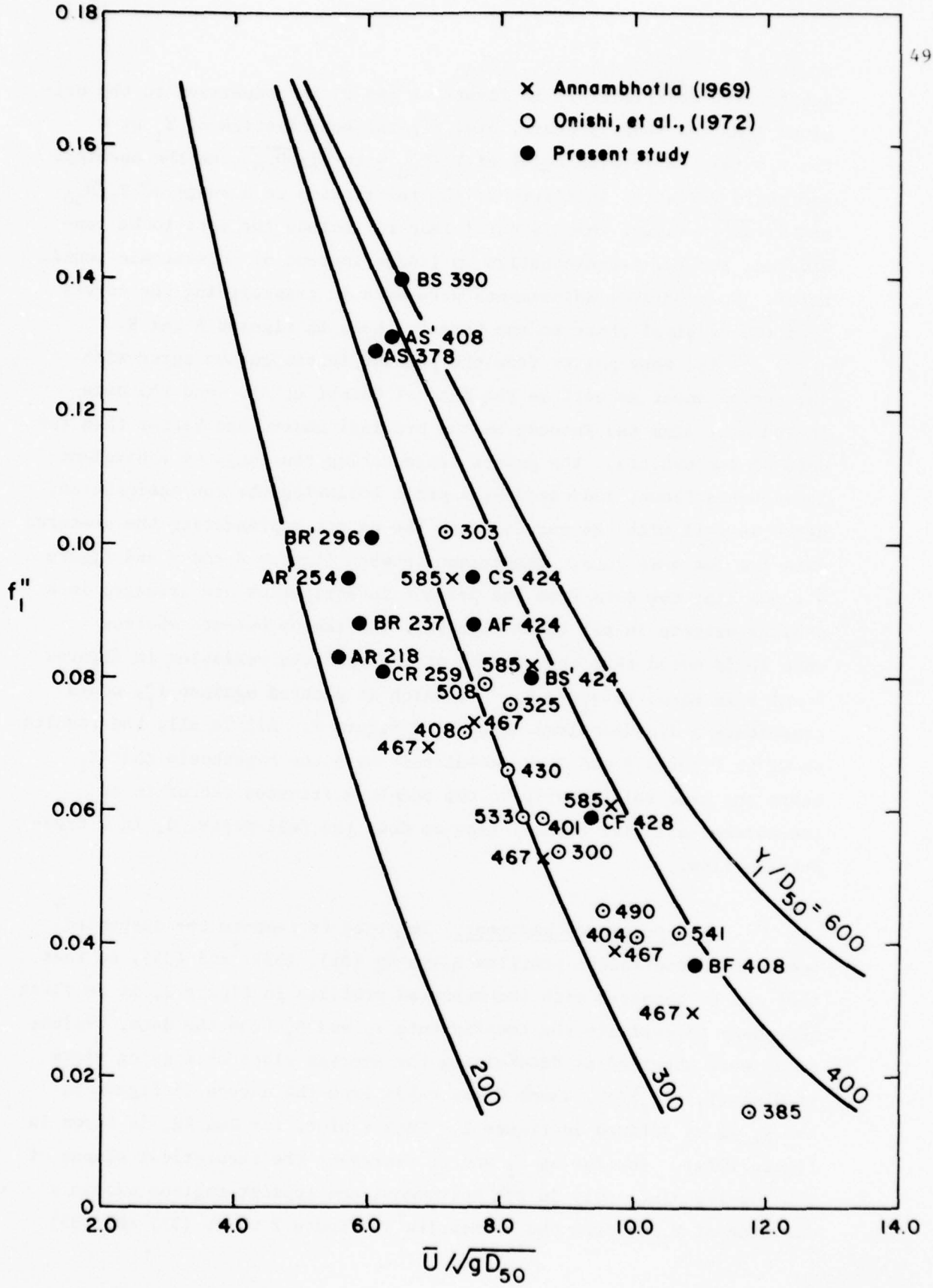

Figure 9.- Modified Alam and Kennedy bed-form friction factor chart; f_1'' vs. $\bar{U}/\sqrt{gD_{50}}$ with Y_1/D_{50} as third variable.

substantive modifications in figures 8 and 9, in comparison to the original Alam and Kennedy chart, are: (1) the substitution of Y_1 or d for r_b; (2) the interchanging of Y_1/D_{50} with $\bar{U}/\sqrt{gD_{50}}$ as the abscissa and third variables in figure 9; (3) restriction to a range of Y_1/D_{50} and $\bar{U}/\sqrt{gD_{50}}$ values that is sufficient to include the data to be considered; and (4) representation in linear instead of logarithmic coordinates. No numerical adjustments were made in transcribing the curves from the original chart to the formats shown in figures 8 and 9.

The data points from the present investigation agree with the curves about as well as the data of Onishi et al., and the data included by Alam and Kennedy on the original chart, and better than the data of Annambhotla. The points representing the computed equivalent ice-covered flows, indicated by a prime following the run designation, agree as well with the curves as do the points representing the measured data for the same runs. Comparison between figures 8 and 9 and figure 7 shows that the data from the present investigation are arranged in a similar pattern in all three figures. The reason becomes obvious when it is noted that the product of the abscissa variables in figures 8 and 9 is equal to $q_1/\sqrt{g}\ D_{50}^{3/2}$, which if plotted against f_1'', would constitute a dimensionless version of figure 7. All in all, the results shown in figures 8 and 9 are consistent with the hypothesis that Y_1 bears the same relationship to the bed-form friction factor in an ice-covered alluvial channel flow as does the full depth, d, in a free-surface flow.

F. Suspended Sediment. In order to compute the suspended sediment concentration profiles given by (31), (33), and (35), so that they can be compared with the measured profiles in figure 5, it is first necessary to evaluate the coefficients z_i and β_i from the data. Values of z_i were obtained by determining the average slope of log-log plots of C vs $(Y_i - y_i)/y_i$, where C was taken from the curves in figure 5, and y_i is as defined in figure 1. Such a plot, for Run BS, is shown in figure 10(a). Insofar as z_1 and z_2 represent the theoretical slopes of the log-log plots only in the bottommost and topmost regions within a distance of $Y_i/2d$ from the boundaries in figure 2 where (31) and (35)

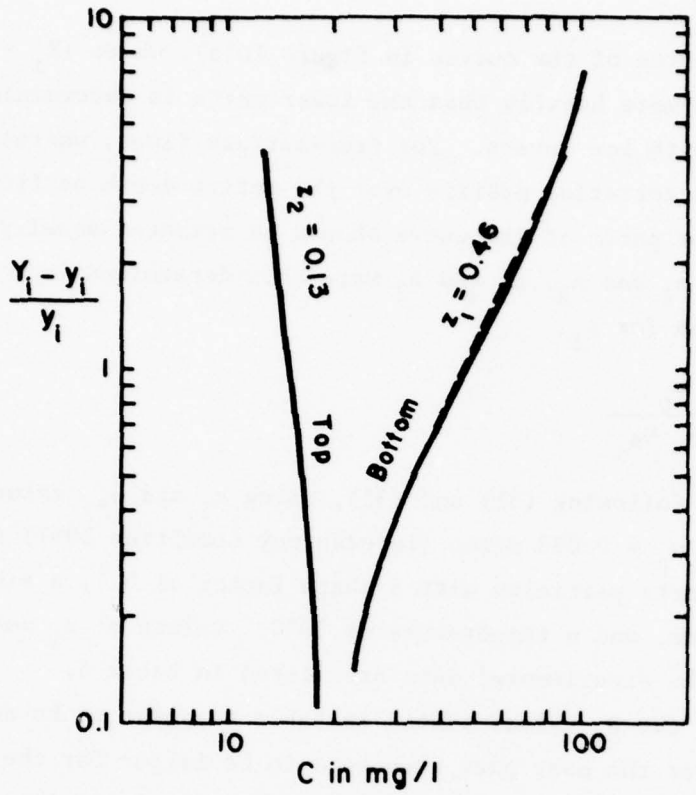

(a) Log-log profile

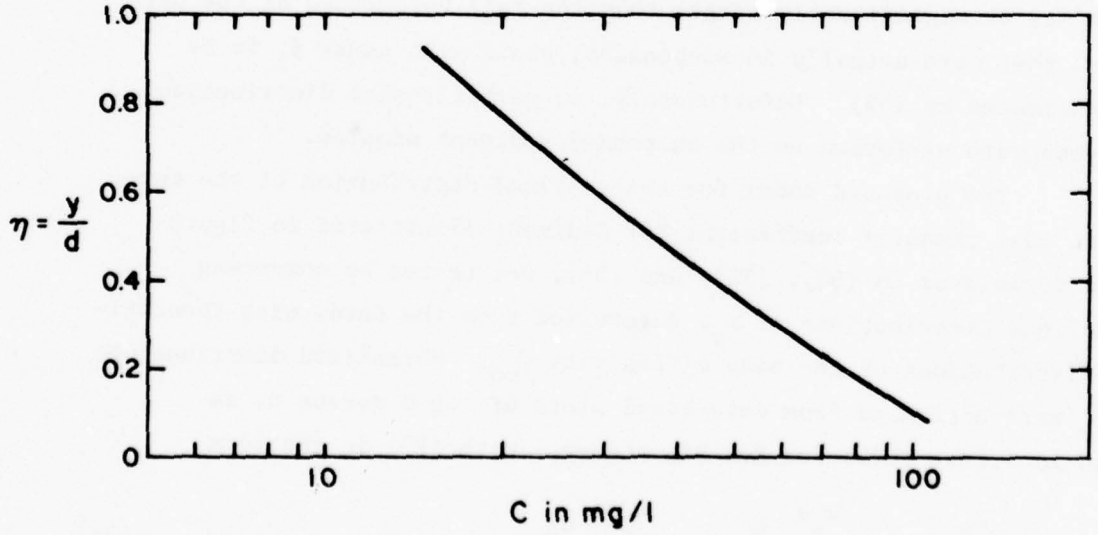

(b) Semi-log profile

Figure 10.- Log-log and semi-log concentration profiles for Run BS.

apply, the upper parts of the curves in figure 10(a), where $(Y_i - y_i)/y_i > 1$, should be weighted more heavily than the lower parts in determining z_i values for flows with ice covers. For free-surface flows, wherein (31) represents the concentration profile over the entire depth of flow, the lower and upper parts of the curve should be weighted equally. Having determined z_1 and z_2, β_1 and β_2 were then determined from the definition equation for z_i,

$$z_i = \frac{w_p}{\beta_i \kappa_i u_{*_i}} \tag{53}$$

given immediately following (31) and (35), using κ_i and u_{*i} values from table 2, and $w_p = 0.033$ m/sec (Interagency Committee 1957) for naturally worn quartz particles with a shape factor of 0.7, a sieve diameter of 0.25 mm, and a temperature of 20°C. Values of z_i and β_i determined from the experimental data are listed in table 6.

Most of the β_i values listed in table 6 appear to be unreasonably large. For the most part they tend to be larger for the A than for the B series, and for the upper than for the lower layer, —— situations wherein the quantity of suspended sediment in the samples tended to be smaller and probably less accurately determined. Use of fall velocities corresponding to the median diameter of the bed material, which may be significantly larger than the fall velocities of the particles that were actually in suspension, could also cause β_i to be overestimated by (53). Unfortunately, no particle-size distribution analyses were performed on the suspended sediment samples.

The proposed model for the vertical distribution of the turbulent mass transfer coefficient for sediment illustrated in figure 2 and formulated in (30), (32), and (34), was tested by comparing normalized distributions of ε_s, determined from the data, with theoretical distributions of the eddy diffusivity ε_{mo}. Normalized distributions of ε_s were estimated from data-based plots of log C versus η, as shown in figure 10(b) for Run BS, together with (27) in the form

$$\frac{\varepsilon_s}{\beta_i \overline{\varepsilon_{mo}}} = -\frac{w_p d}{\beta_i \bar{\varepsilon}_{mo}} \frac{C}{\frac{dC}{d\eta}} = -\frac{w_p d}{\beta_i \bar{\varepsilon}_{mo}} \frac{d\eta}{d\ln C} \tag{54}$$

Table 6. QUANTITIES ASSOCIATED WITH SUSPENDED SEDIMENT CONCENTRATION PROFILES

Run	i	z_i	β_i	$\bar{\varepsilon}_{mo}$ m^2/sec	$\frac{\bar{\varepsilon}_s}{\beta_i \bar{\varepsilon}_{mo}}$ [1]	$\frac{\bar{\varepsilon}_s}{\bar{\varepsilon}_{mo}}$ [2]
(1)	(2)	(3)	(4)	(5)	(6)	(7)
AF	1	0.47	3.6	0.000322	1.54	3.60
AS	1	0.23	5.6	0.000306	1.09	5.92
	2	0.31	14			
AR	1	0.28	6.6	0.000247	1.23	9.51
	2	0.14	8.3			
BF	1	0.90	1.7	0.000412	1.17	1.70
BS	1	0.46	3.4	0.000262	1.29	4.96
	2	0.13	25			
BR	1	0.86	1.9	0.000299	1.32	2.54
	2	0.60	2.2			

[1] from figure 11

[2] from (36) and (56)

approximated by

$$\frac{\varepsilon_s}{\beta_i \bar{\varepsilon}_{mo}} \approx - 0.4343 \frac{w_p d}{\beta_i \bar{\varepsilon}_{mo}} \Delta\eta_{\substack{1 \text{ log cycle} \\ \text{of C}}} \tag{55}$$

In (55) $\bar{\varepsilon}_{mo}$ is the depth-averaged eddy diffusivity, obtained by averaging (13) over $d = Y_1 + Y_2$ to get

$$\bar{\varepsilon}_{mo} = \frac{d}{6} \left[\kappa_1 u_{*_1} \left(\frac{Y_1}{d}\right)^2 + \kappa_2 u_{*_2} \left(\frac{Y_2}{6}\right)^2\right] \tag{56}$$

and $\Delta\eta_{\substack{1 \text{ log cycle} \\ \text{of C}}}$ is the change in η corresponding to the change in one log cycle of C of the tangent to the log C versus η curve at the value of η for which the local value of $\varepsilon_s/\beta_i\bar{\varepsilon}_{mo}$ is being determined.

Vertical distributions of $\varepsilon_s/\beta_i\bar{\varepsilon}_{mo}$ estimated in the above manner for each run are shown as the solid curves in figure 11, where they are compared with distributions of $\varepsilon_i/\bar{\varepsilon}_{mo}$, computed according to (13), represented by the dashed curves. The results in figure 11 are somewhat inconclusive, mainly because the local values of ε_s obtained by graphical differentiation are so sensitive to small differences in the way the curves like those in figure 10(b) are drawn. Considering this, the $\varepsilon_s/\beta_i\bar{\varepsilon}_{mo}$ distribution curves for Runs AS, AR, BF and BS, are reasonably consistent with the proposed model. Values of $\bar{\varepsilon}_s/\beta_i\bar{\varepsilon}_{mo}$, which is equal to the ratio of the area under the solid curves to the area under the dashed curves, are listed in column 6 of table 6. Values of $\bar{\varepsilon}_s/\bar{\varepsilon}_{mo}$ computed from (36) and (56) are listed in column 7 .

Figure 12 shows suspended sediment concentration profiles computed by (31), (33), and (35), compared with the average of the concentrations measured at the centerline and the right and left quarter points. The agreement in all cases is quite good. It follows from the extreme sensivity of the distribution of ε_s to small changes in concentration profiles, referred to in connection with figure 11, that computed concentration profiles are relatively insensitive to quite large variations in the distribution, if not the magnitude, of ε_s.

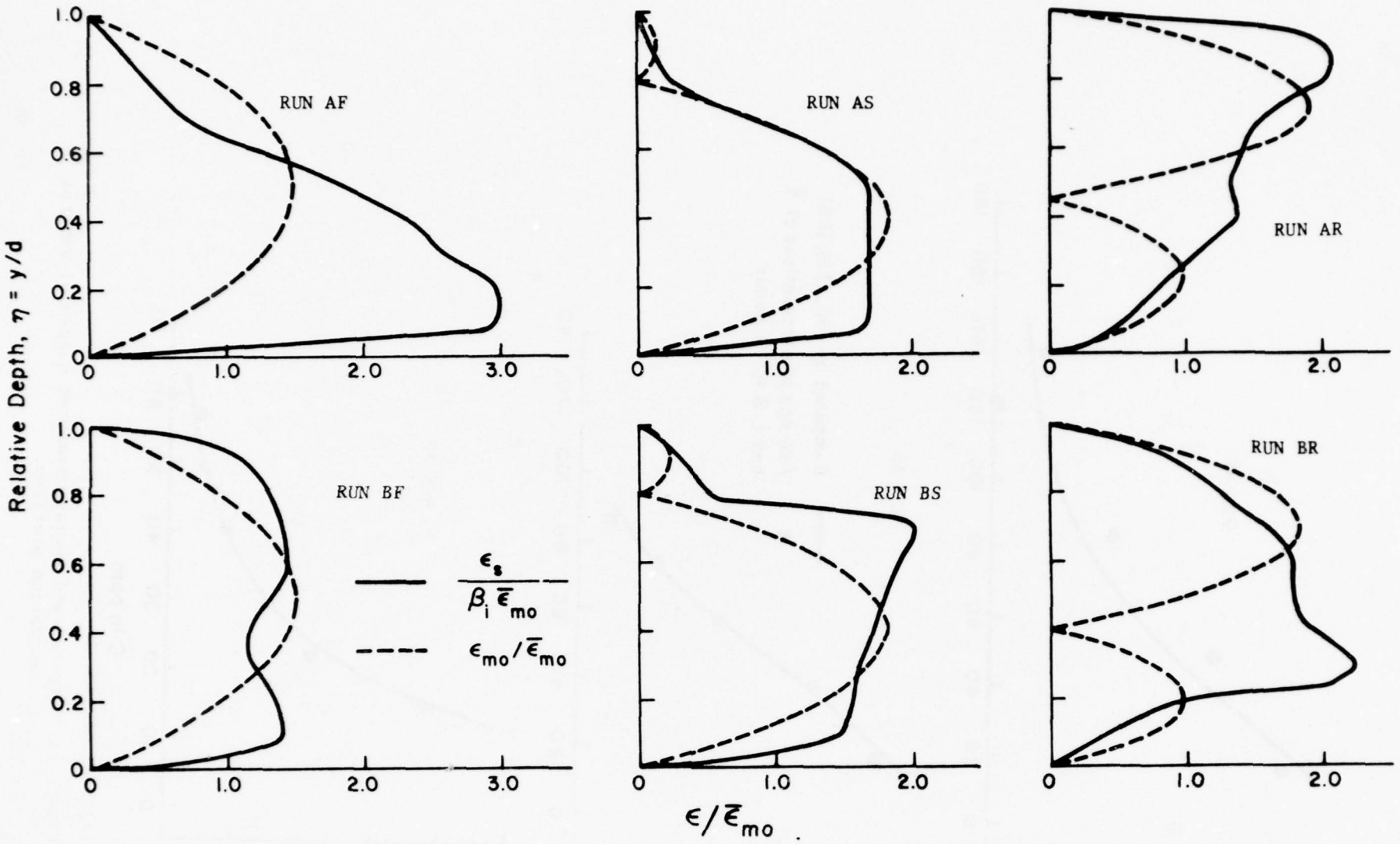

Figure 11. Vertical distributions of turbulent mass transfer coefficient for suspended sediment, and eddy diffusivity.

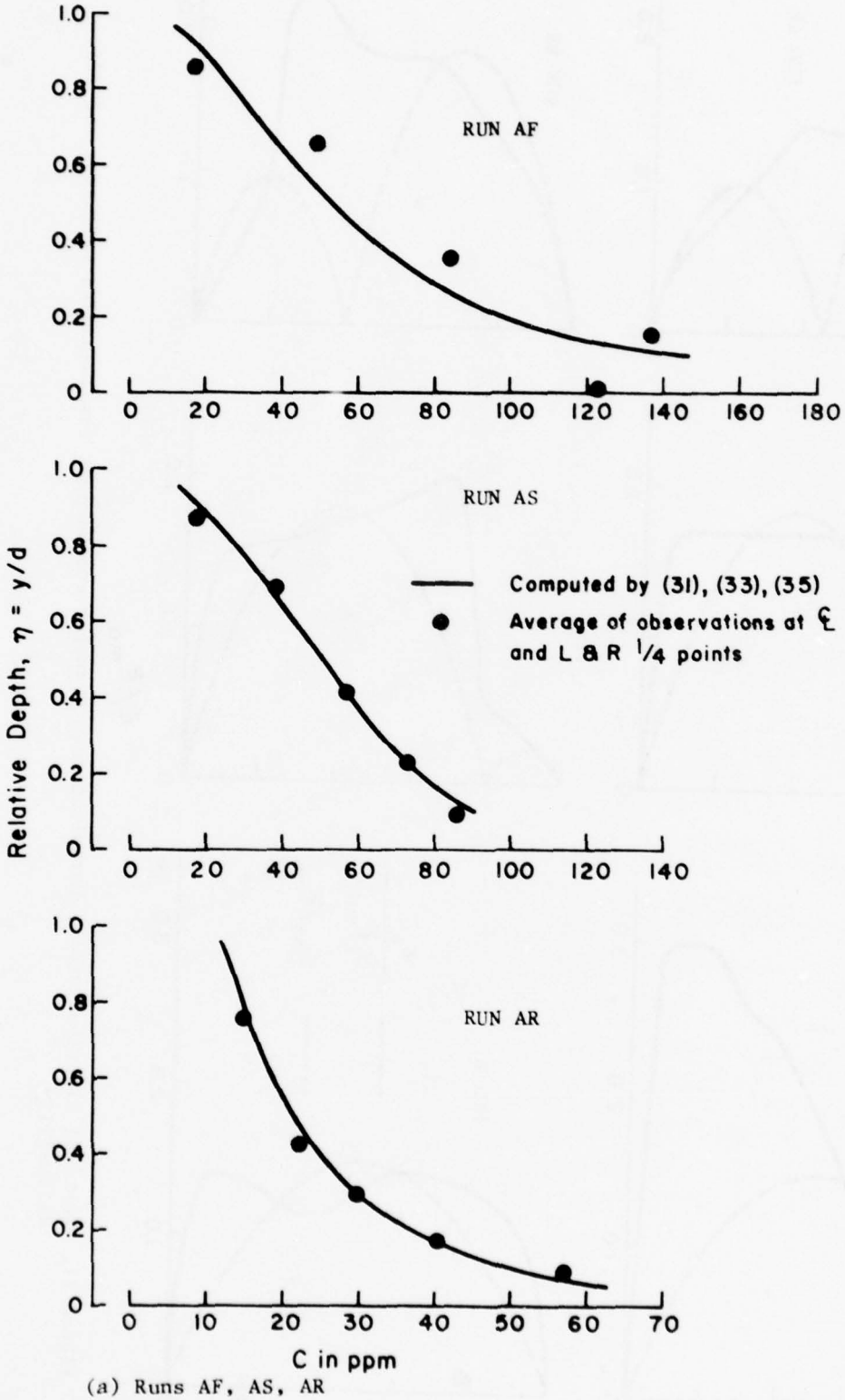

(a) Runs AF, AS, AR

Figure 12. Computed and average measured suspended sediment concentration profiles.

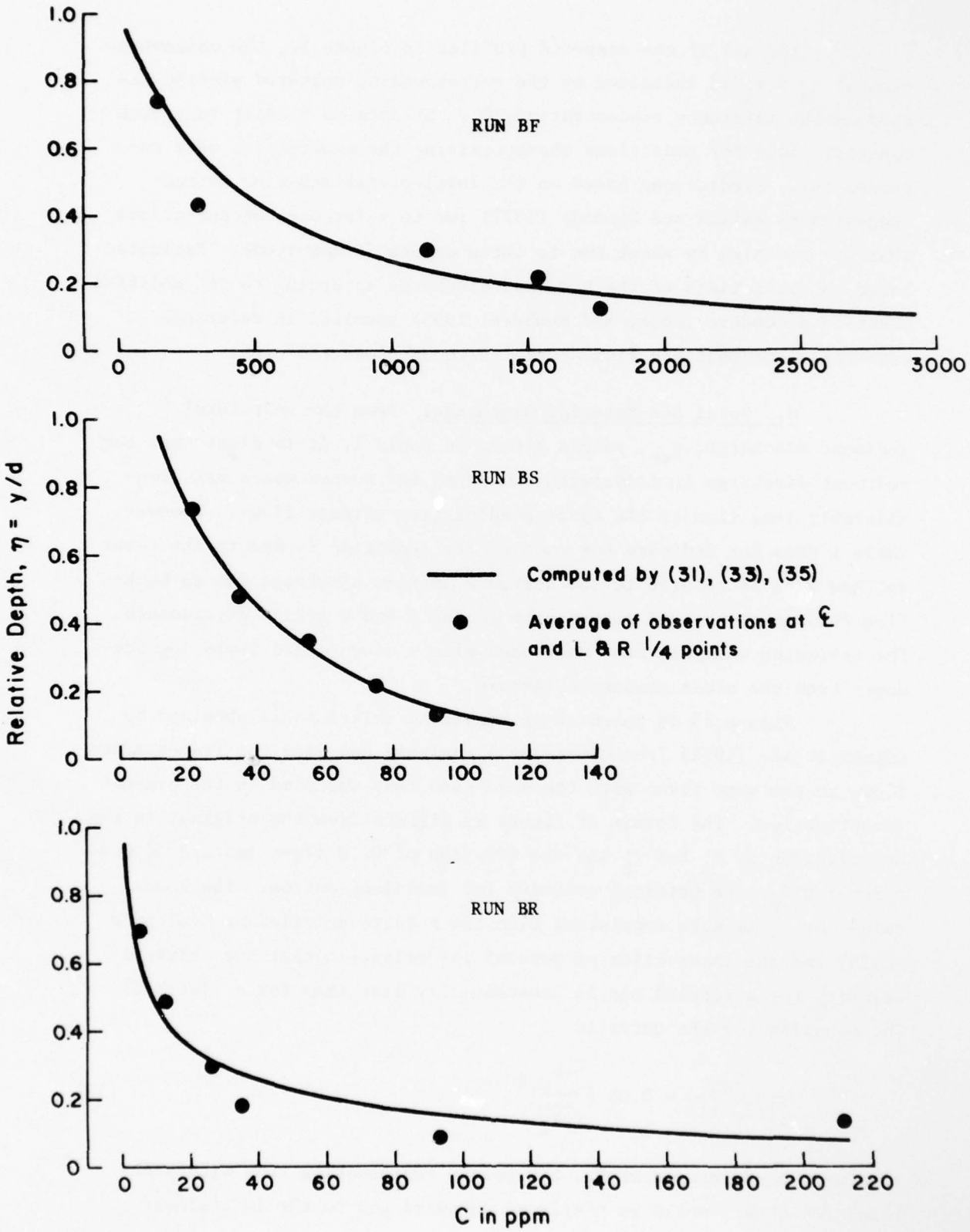

(b) Runs BF, BS, BC

Figure 12. (continued).

For all of the computed profiles in figure 12, the concentration at $\eta_a \approx Y_1/2d$ indicated by the corresponding measured profile was used as the reference concentration, C_a. Efforts to predict reference concentrations for conditions characterizing the experiments were unsuccessful. Predictions based on the level-of-maximum-flux method suggested by Willis and Kennedy (1977) led to reference concentrations that are too high by about two to three orders of magnitude. Estimates based on predictions of the bed-load discharge according to the modified Einstein procedure (Colby and Hembree, 1955) resulted in reference concentrations that are from about 1.5 to 30 times too high.

G. Total Bed-Material Discharge. From the unit total sediment discharge, q_{st}, values listed in table 1, it is clear that the sediment discharge in flows with simulated ice covers was always considerably less than in the corresponding free surface flows. However, table 1 does not indicate how much of the reduction is due to the cover and how much is related to the decrease in flow discharge due to backflow through the second return pipe in the A and B series experiments. The following analysis was undertaken with a view toward isolating ice-cover from the other causative factors.

Figure 13 is based on an empirical relationship obtained by Onishi et al. (1972) from dimensional analysis and data for free-surface flows in the same flume with the same sand that was used in the present investigation. The format of figure 13 differs from the original in the substitution of Y_1 for r_b and the adoption of 0.18 m/sec instead of 0.24 m/sec for U_c, the critical velocity for incipient motion. The lower value for U_c is more consistent with the results compiled by Hjulström (1935) and the observation of several investigators that the critical velocity for a rippled bed is substantially less than for a flat bed. The equation for the curve is

$$\frac{\hat{q}_{st}}{g^{1/2} Y_1^{3/2}} = 0.03 \left[\frac{\bar{U}-U_c}{\sqrt{gY_1}}\right]^4 \qquad (57)$$

If d were used instead of Y_1, the points representing runs with simulated ice covers would be displaced downward and to the left almost

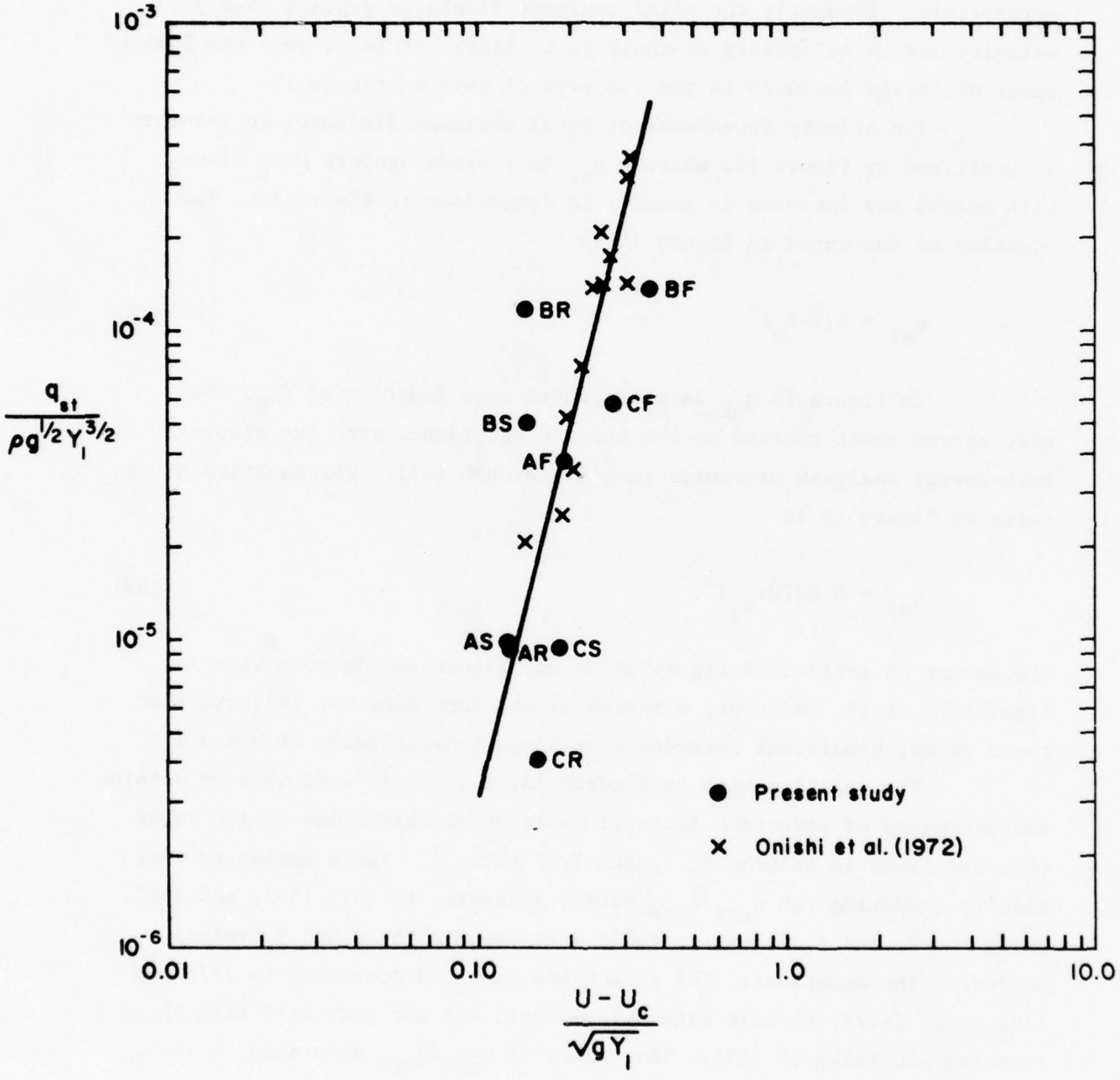

Figure 13. Variation of dimensionless unit total sediment discharge with effective Froude number.

parallel to the curve, so it makes little difference whether Y_1 or d is used. As in the original plot presented by Onishi et al., inclusion of Y_1/D_{50} or d/D_{50} as a third variable does not improve the relationship perceptibly. Evidently the total sediment discharge depends mainly on velocity and is relatively insensitive to depth, at least over the limited range of depths included in the two sets of data in figure 13.

The primary dependence of total sediment discharge on velocity is confirmed by figure 14, wherein q_{st} is plotted against $\bar{U}-U_c$ alone, with hardly any increase in scatter in comparison to figure 13. The equation of the curve in figure 14 is

$$\hat{q}_{st} = 2(\bar{U}-U_c)^4 \tag{58}$$

In figure 15 q_{st} is represented as a function of $\bar{U}\tau_0$, the unit stream power exerted on the bed, in accordance with the simple work-energy analysis presented in (41) through (43). The equation of the curve in figure 15 is

$$\hat{q}_{st} = 0.02[\bar{U}\tau_{0_1}]^4. \tag{59}$$

The amount of scatter in figure 15 is not significantly more than in figures 13 or 14. However, a review of the data does not indicate that there is any consistent dependency on slope independently of $\bar{U}$ and Y_1.

The relationships in figures 13, 14, and 15 were used to obtain the estimates of reduction in total sediment discharge due to ice cover that are shown in columns 5, 6, and 7 of table 7. These estimates were made by computing the $\hat{q}_{stI}/\hat{q}_{stF}$ ratios according to (57) (58), and (59), using the $\hat{d}_I$ and d_F values in table 4 to compute the $\bar{U}$ and Y_1 values needed in the equations. The reductions computed according to (57) and (58) agree fairly closely with one another, but not very well with those computed according to (59). The values of $\hat{q}_{stI}/\hat{q}_{stF}$ according to (59), after introducing continuity, reduce to $(Y_1/d)^4$. The ratios according to (57) and (58) depend on $\hat{d}_I/d_F$ and U_c in addition to Y_1/d. Insofar as they agree more closely with the measured values of q_{stI}/q_{stF} for Runs CS and CR in column (8), the only ones for which there were equivalent

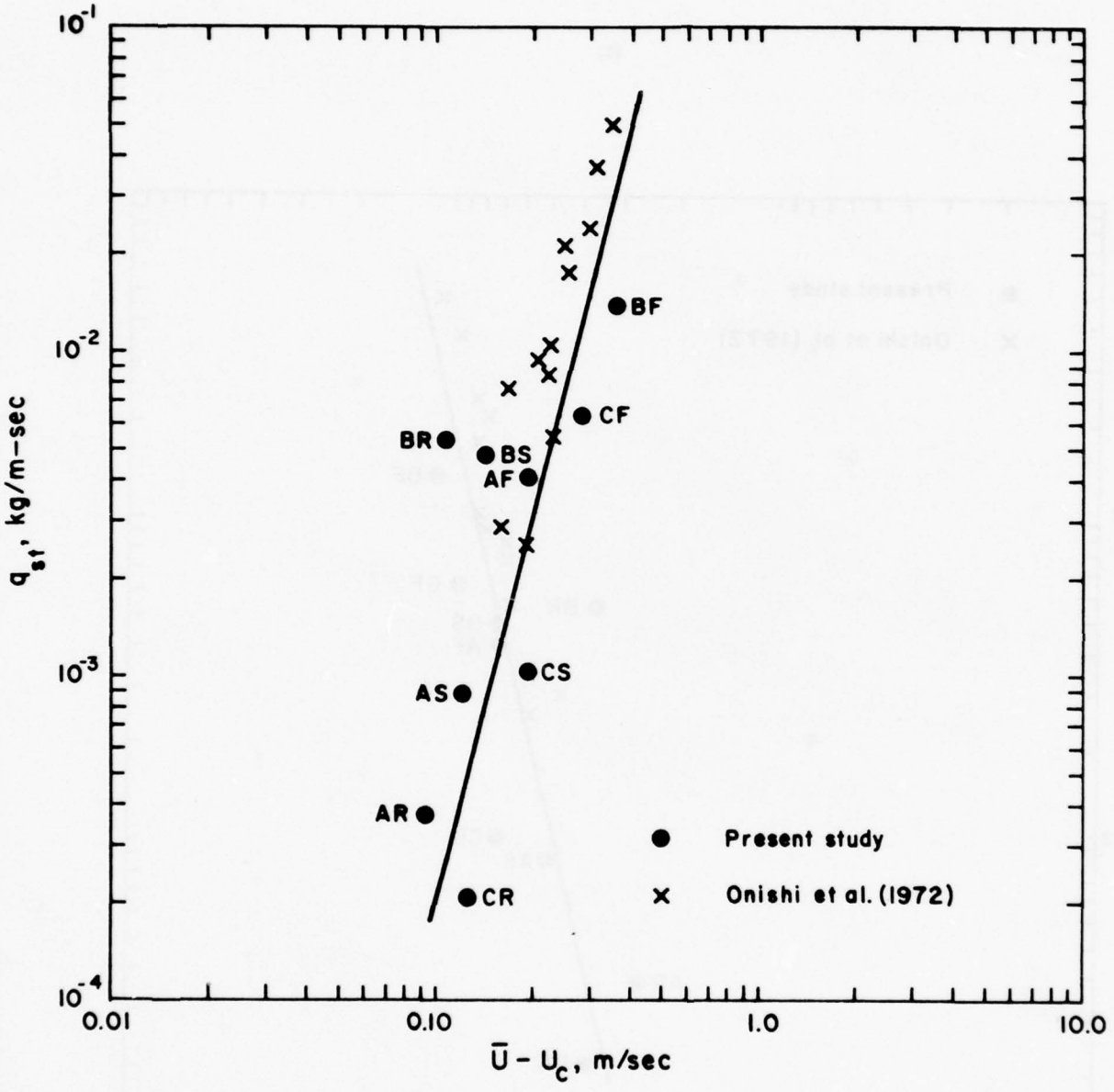

Figure 14.- Variation of unit total sediment discharge with effective velocity.

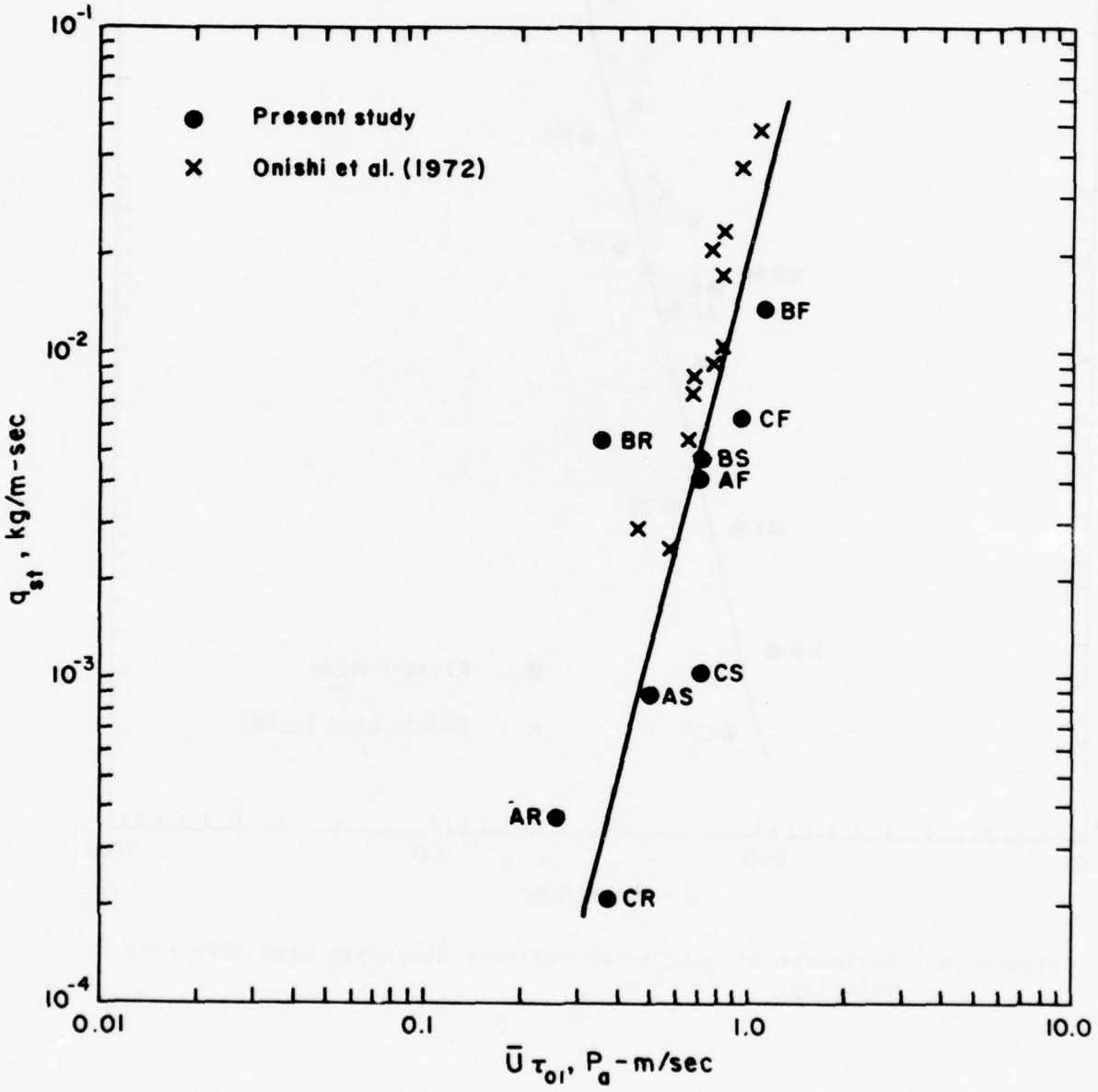

Figure 15.- Variation of unit total sediment discharge with unit stream power exerted on bed.

Table 7. ESTIMATES OF REDUCTION IN UNIT TOTAL SEDIMENT DISCHARGE FOR EQUIVALENT ICE-COVERED FLOWS

Run	q	S	q_{stF}	Estimates of $\hat{q}_{stI}/\hat{q}_{stF}$			Measured
	m^2/sec		kg/m-sec	Eq. (57)	Eq. (58)	Eq. (59)	q_{stI}/q_{stF}
(1)	(2)	(3)	(4)	(5)	(6)	(7)	(8)
AF	0.0397	0.00180	0.0409				
AS				0.221	0.216	0.410	-
AR				0.0968	0.0749	0.0410	-
BF	0.0552	0.00208	0.0139				
BS				0.186	0.189	0.410	-
BR				0.0134	0.0114	0.0256	-
CF	0.0497	0.00198	0.00631				
CS				0.244	0.241	0.410	0.160
CR				0.0304	0.0242	0.0256	0.0330

ice-covered and free-surface flows, the estimates based on (57) and (58) are to be preferred. From these, it is concluded that the total sediment discharge in an ice-covered channel may be reduced to less than one quarter of that in an equivalent free surface flow if the cover is smooth, and to well under ten percent if the cover is rough.

H. Bed Profiles. Quantitative measures of the bed-form characteristics were obtained from a statistical analysis of the zero-crossing distances and amplitudes of the digitized longitudinal bed profiles. The analysis adopted herein is essentially as described by Annambhotla (1969).

Longitudinal profiles taken along the centerline and plotted by the Incremental Plotter at the University Computer Center are shown in figures 16. The two sets of profiles for the A and B series of runs were taken respectively before and after the velocity and suspended sediment profiles. Insofar as the profiles appeared to indicate a reasonably stationary stochastic process, they were not passed through a filter to attenuate the low frequency components as was done with Annambhotla's Missouri River bed profiles.

A definition sketch for the zero-crossing distances and amplitudes analysis of a bed profile is shown in figure 17. A zero-crossing is defined as a point where the bed profile crosses the line defining the mean bed level in a cartesian coordinate system that is tilted at the flume slope, S. In figure 17 this line is coincident with the x-axis. The zero-crossing distance is then defined as the longitudinal distance between successive zero-crossings. A bed-form length, L, is the sum of two successive zero crossings. The positive and nagative amplitudes, a^+ and a^-, are defined as the maximum positive and negative displacements of the bed from the mean level between two successive upward (or downward) zero crossings. The height, H, of a bed form is the sum of the magnitudes of a pair of adjacent positive and negative amplitudes.

Mean values, unbiased standard deviations, and unbiased skewness coefficients were computed for H, L, and a^+, and $|a^-|$ from each bed profile. For a set of N discrete values $Z_1, Z_2, \ldots, Z_n$, in this case

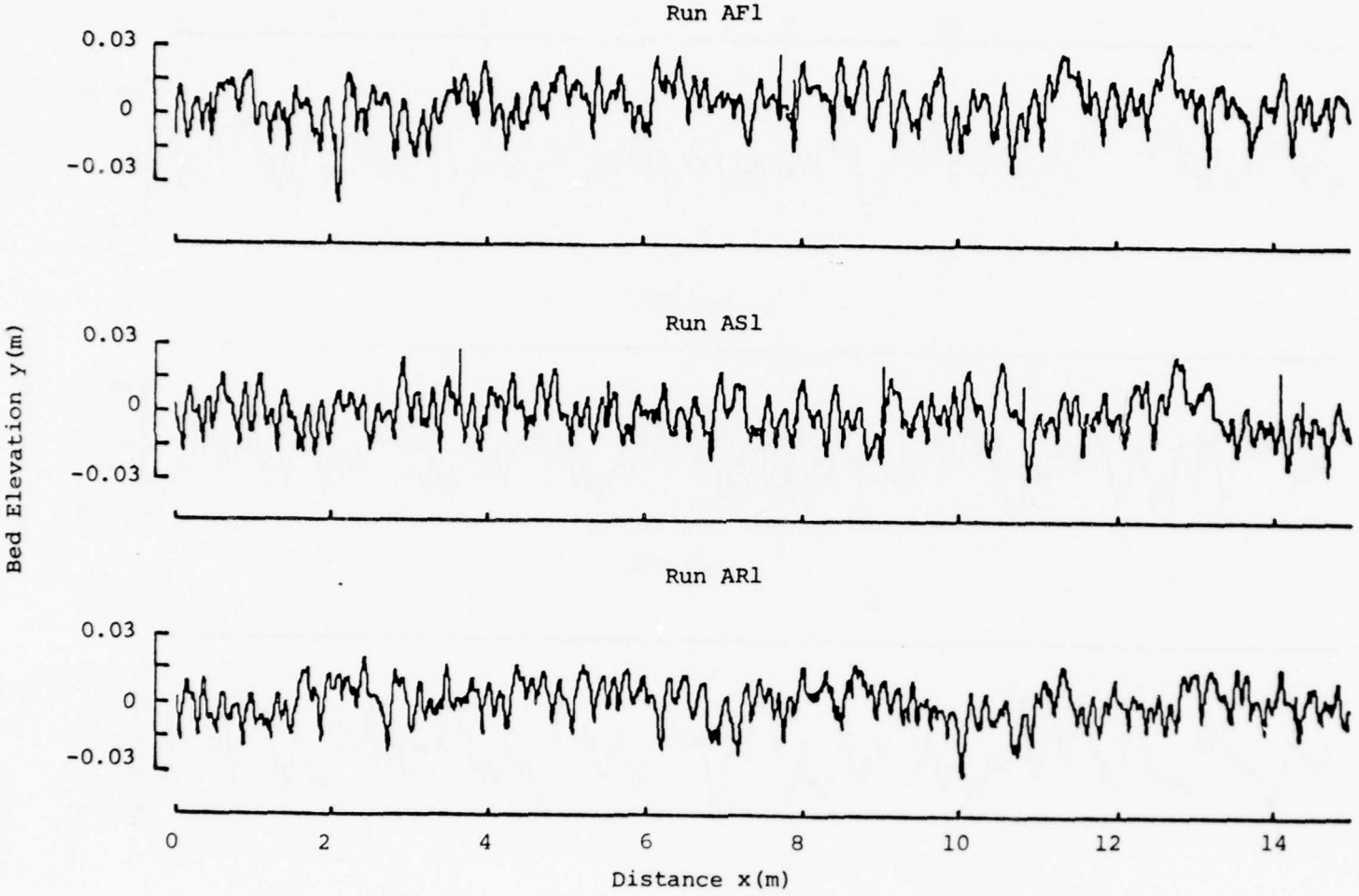

(a) Runs AF1, AF2 and AR1

Figure 16. Longitudinal bed profiles.

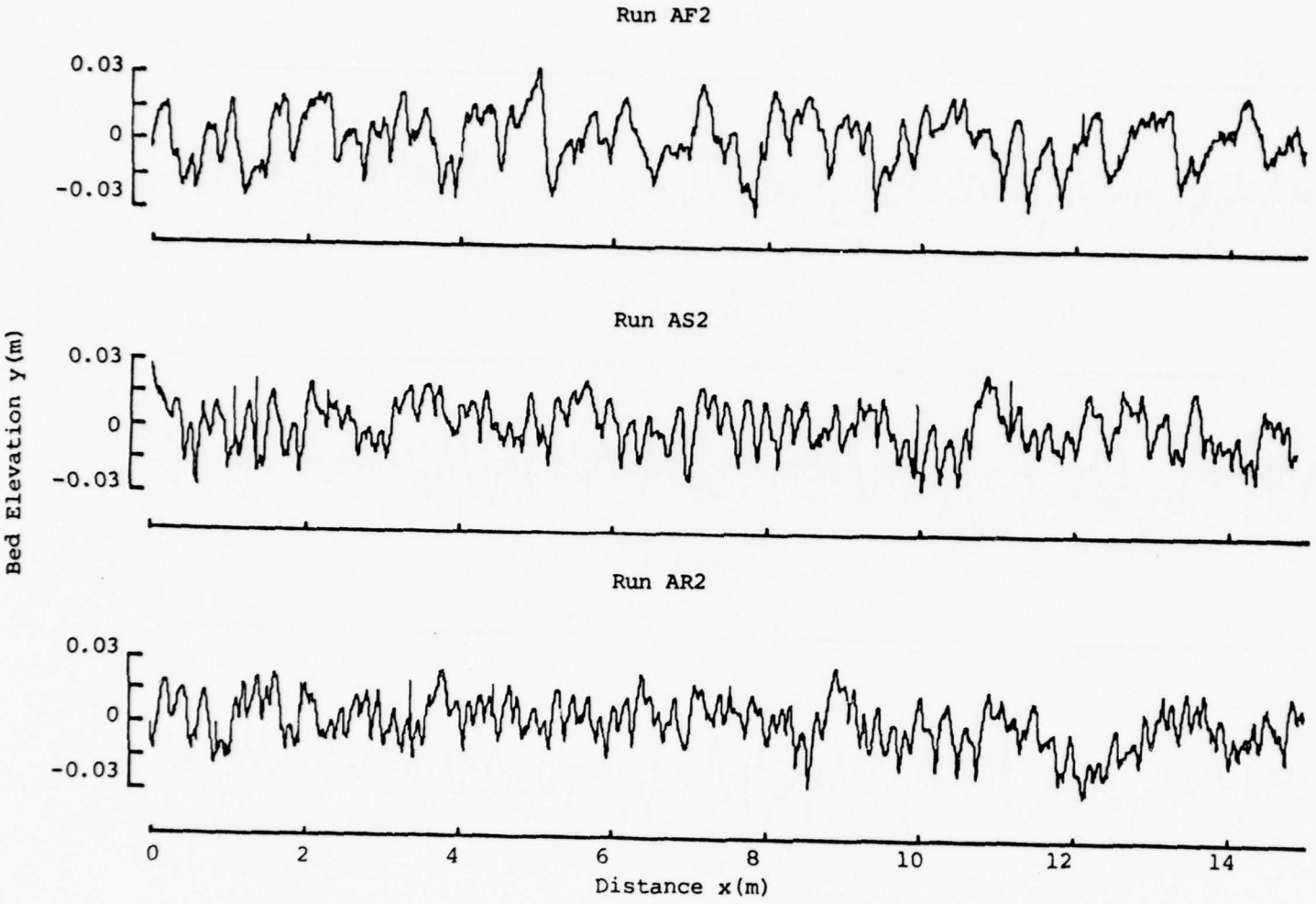

(b) Runs AF2, AS2 and AR2

Figure 16. (continued).

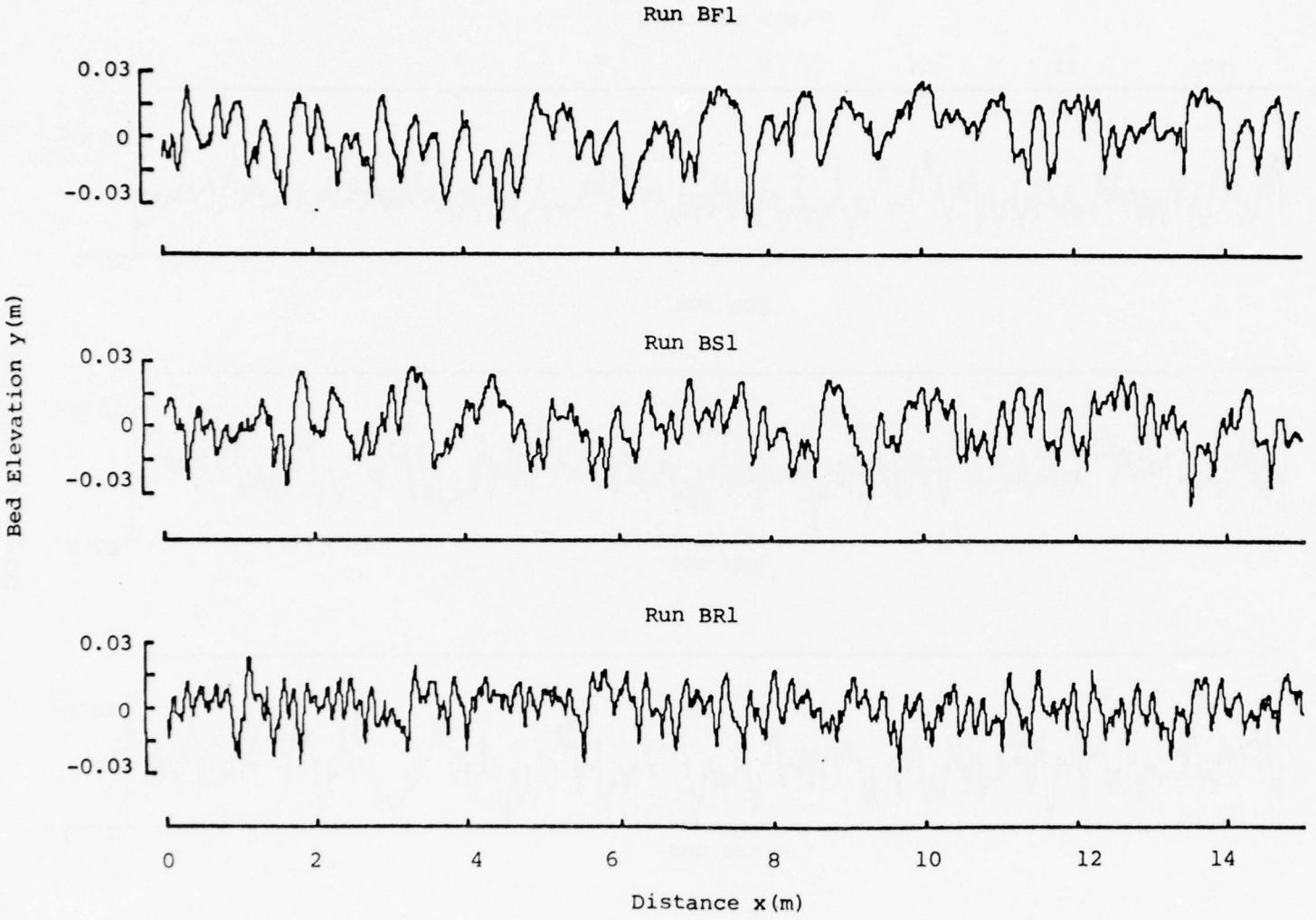

(c) Runs BF1, BF2 and BR1

Figure 16. (continued).

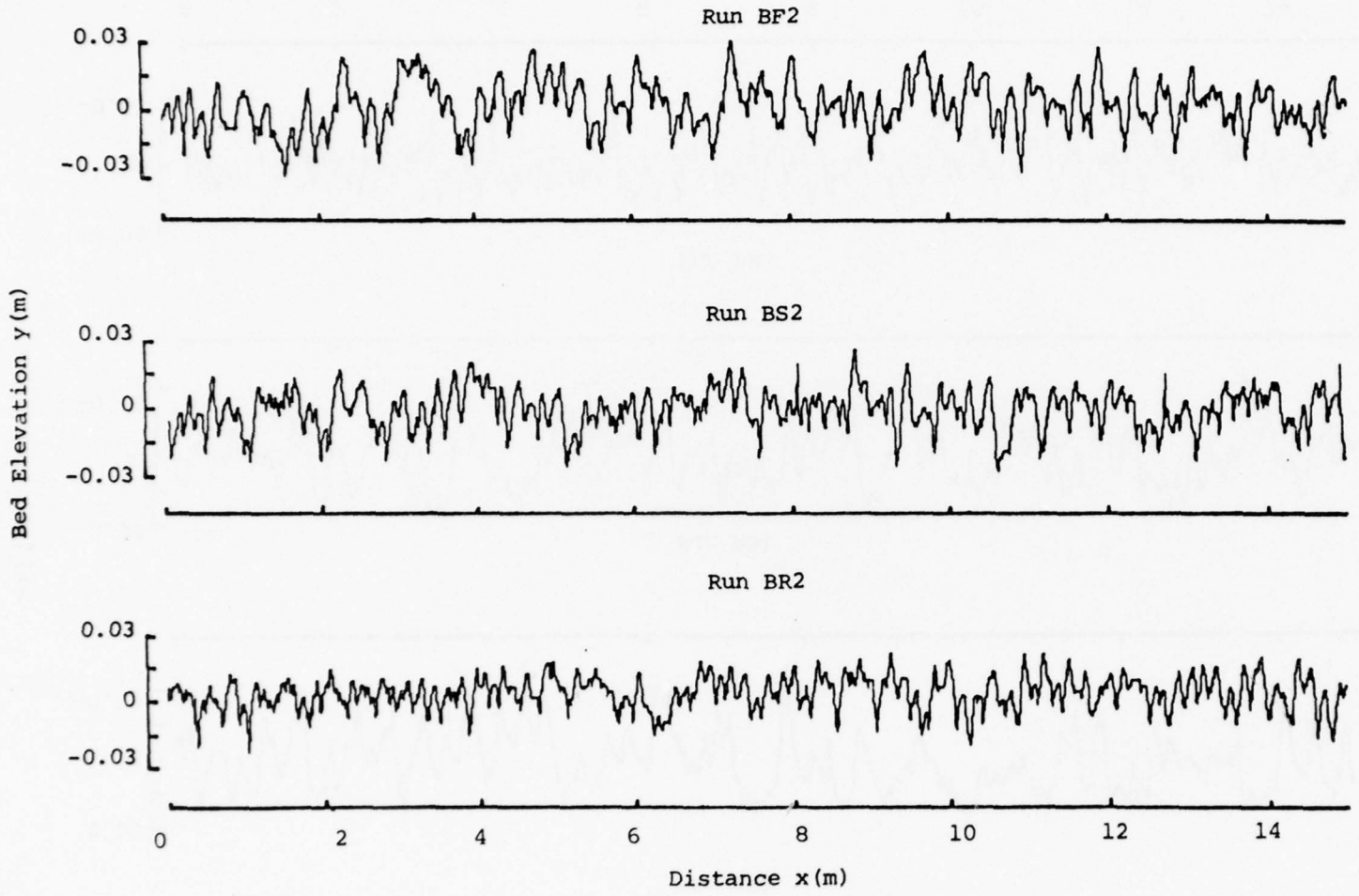

(d) Runs BF2, BS2 and BR2

Figure 16. (continued).

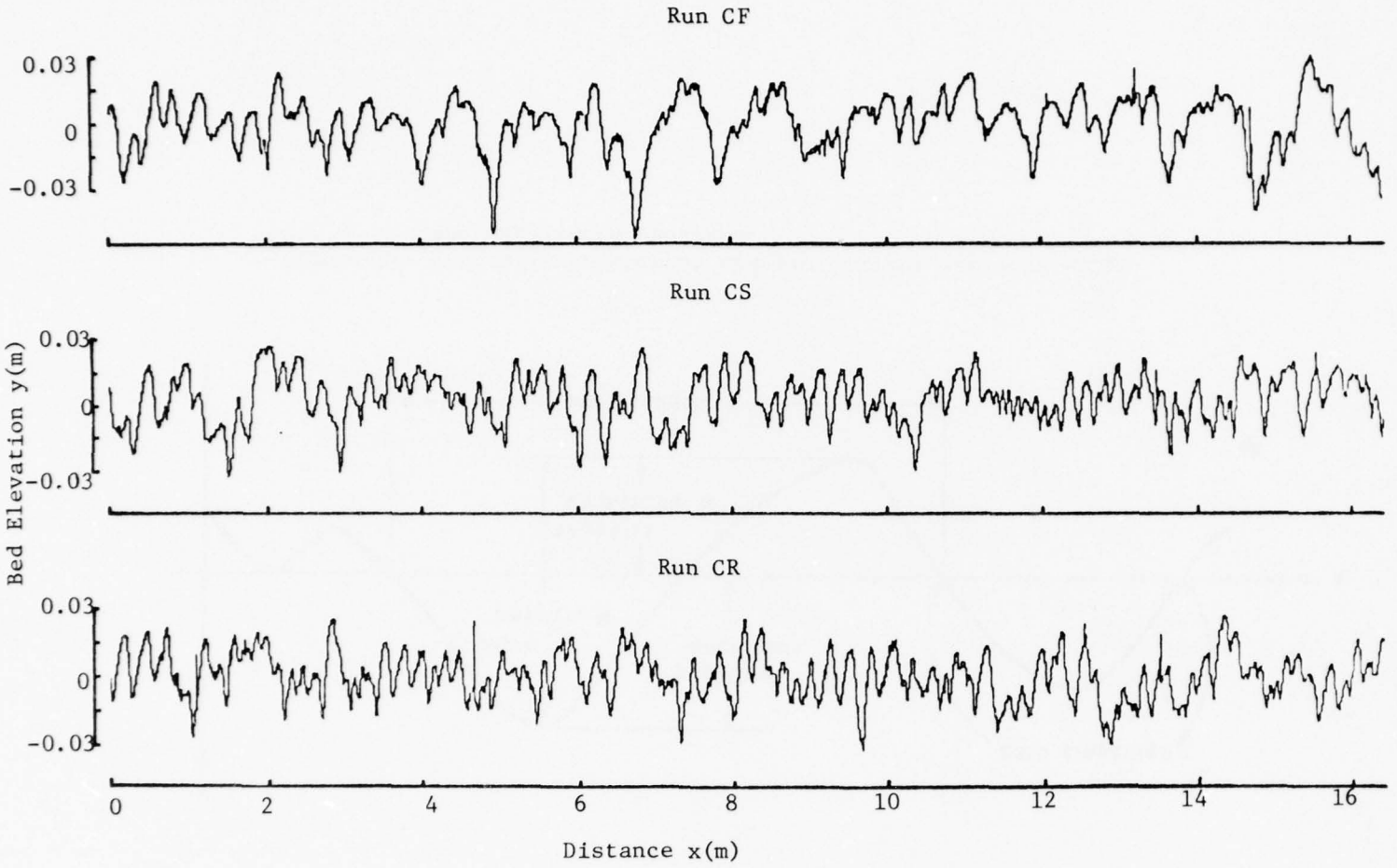

(e) Runs CF, CS and CR

Figure 16. (continued).

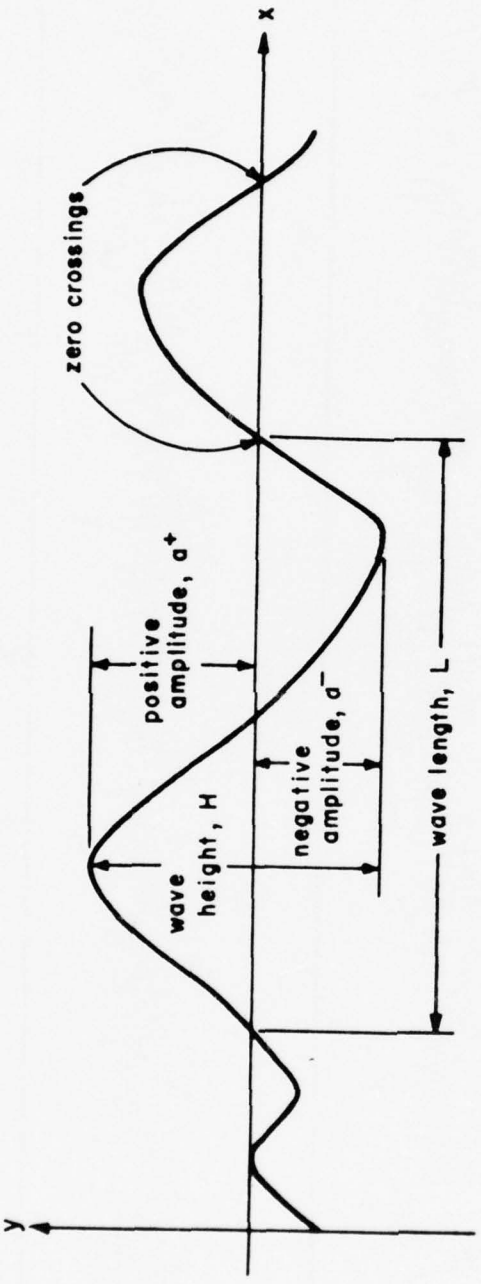

Figure 17. Definition sketch of bed-profile for zero-crossings and amplitudes analysis.

representing any one of the above four bed-form characteristics, the mean, μ, is computed by

$$\mu = \frac{1}{N} \sum_{j=1}^{N} Z_j \tag{60}$$

the unbiased standard deviation, σ, by

$$\sigma = \left[\frac{m_2}{N-1}\right]^{1/2} \tag{61}$$

and the unbiased skewness coefficient, θ, by

$$\theta = \frac{N^2}{(N-1)(N-2)} \frac{m_3}{m_2^{2/3}} \tag{62}$$

where m_2 and m_3 are the second and third central moments defined respectively by

$$m_2 = \frac{1}{N} \sum_{j=1}^{N} (Z_j - \mu)^2 \tag{63}$$

and

$$m_3 = \frac{1}{N} \sum_{j=1}^{N} (Z_j - \mu)^3 \tag{64}$$

The results are listed in table 8, where values of the coefficient of variation, σ/μ, are listed instead of the standard deviation. For the A and B series of runs, the values listed are the averages obtained from 6 profiles, one each taken along the centerline and the sailing lines one quarter of the flume width to the right and left, before and after the velocity and suspended sediment concentration profiles were obtained. Comparison of the results for the individual profiles indicates no consistent significant differences between those for the center, left, and right sailing lines. Therefore profiles were taken only along the centerline in the C series. Means, standard deviations, and skewness coefficients of H, L, a^+, and $|a^-|$ for each profile obtained in the A and B series are tabulated by Song (1978).

Table 8. STATISTICAL MEASURES OF BED-FORM CHARACTERISTICS

Run	Statistical Measure	Bed-form characteristics			
		Wave height H	Wave length L	Positive amplitude a^+	Negative amplitude $\|a^-\|$
(1)	(2)	(3)	(4)	(5)	(6)
AF	Mean, (m)	0.0185	0.216	0.0086	0.0100
	Coeff. of Var.	0.541	0.627	0.79	0.82
	Skewness	0.12	0.72	0.67	0.71
AS	Mean, (m)	0.0184	0.206	0.0086	0.0098
	Coeff. of Var.	0.565	0.681	0.79	0.74
	Skewness	0.32	1.42	0.76	0.63
AR	Mean, (m)	0.0159	0.200	0.0073	0.0086
	Coeff. of Var.	0.547	0.680	0.78	0.80
	Skewness	0.21	1.04	0.62	0.75
BF	Mean, (m)	0.0198	0.312	0.0088	0.0110
	Coeff. of Var.	0.677	0.839	0.84	0.92
	Skewness	0.42	1.25	0.67	0.85
BS	Mean, (m)	0.0201	0.272	0.0094	0.0107
	Coeff. of Var.	0.562	0.715	0.74	0.81
	Skewness	0.19	1.23	0.54	0.58
BR	Mean, (m)	0.0176	0.208	0.0085	0.0092
	Coeff. of Var.	0.574	0.708	0.76	0.80
	Skewness	0.21	1.39	0.55	0.75
CF	Mean, (m)	0.0221	0.388	0.0097	0.0124
	Coeff. of Var.	0.747	0.750	0.84	1.10
	Skewness	0.74	0.73	0.65	1.22
CS	Mean, (m)	0.0208	0.272	0.0095	0.0113
	Coeff. of Var.	0.587	0.729	0.74	0.83
	Skewness	0.22	1.12	0.36	0.87
CR	Mean, (m)	0.0189	0.218	0.0091	0.0098
	Coeff. of Var.	0.577	0.726	0.84	0.84
	Skewness	0.16	1.26	0.64	0.81

The following trends can be seen from the results in table 8. Going from the free-surface (F) to the smooth-cover (S) condition, the mean L, the coefficients of variation for H, a^+, and $|a^-|$, and the skewness coefficient for $|a^-|$ all tend to decrease; and the mean H, a^+, and $|a^-|$, and the coefficient of variation for L all stay about the same (i.e. change by less than about 10 percent). Going from the smooth-cover to the rough-cover condition, the mean H, $|a^-|$, and L all tend to decrease; and the coefficients of variation for H, $|a^-|$, and L all stay about the same. The overall effect of the simulated ice cover appears to be toward a reduction and uniformity of the ripple sizes. Because the flows with and without simulated ice covers were equivalent only in the C series of runs, the tendencies described above were considered to be trends only if they occurred in the C series and in at least one of either the A or B series. Whatever effect the covers may have had on the skewness coefficients appears to have been inconsistent except for the effect on $|a^-|$ as noted above. However, it is noteworthy that all skewness coefficients are positive, indicating a greater preponderance of smaller as opposed to larger ripples. In addition there is a consistent tendency for the skewness coefficients for the different bed-form characteristics to increase in the following order: H, a^+, $|a^-|$, L.

Percentage-distribution histograms for H, L, a^+, and $|a^-|$ for one centerline bed profile from Runs CF, CS, and CR are shown in figure 18. No attempt was made to fit them by the probability density functions corresponding to any probability law. They are included to add visual reinforcement to the results summarized in table 8. Similar histograms for the A and B series of runs are shown in Song (1978).

The relationship between the bed-form friction factor f_1'' and the relative roughness $Y_1\bar{L}/\bar{H}^2$ based on the mean ripple height and length is shown in figure 19. Experimental results from the present investigation are compared there with data for free-surface flows obtained in the same flume and with the same sand by Annambhotla (1969), and with the equation

$$\frac{1}{\sqrt{f_1''}} = 3.3 \log \frac{Y_1\bar{L}}{\bar{H}^2} - 2.3 \qquad (65)$$

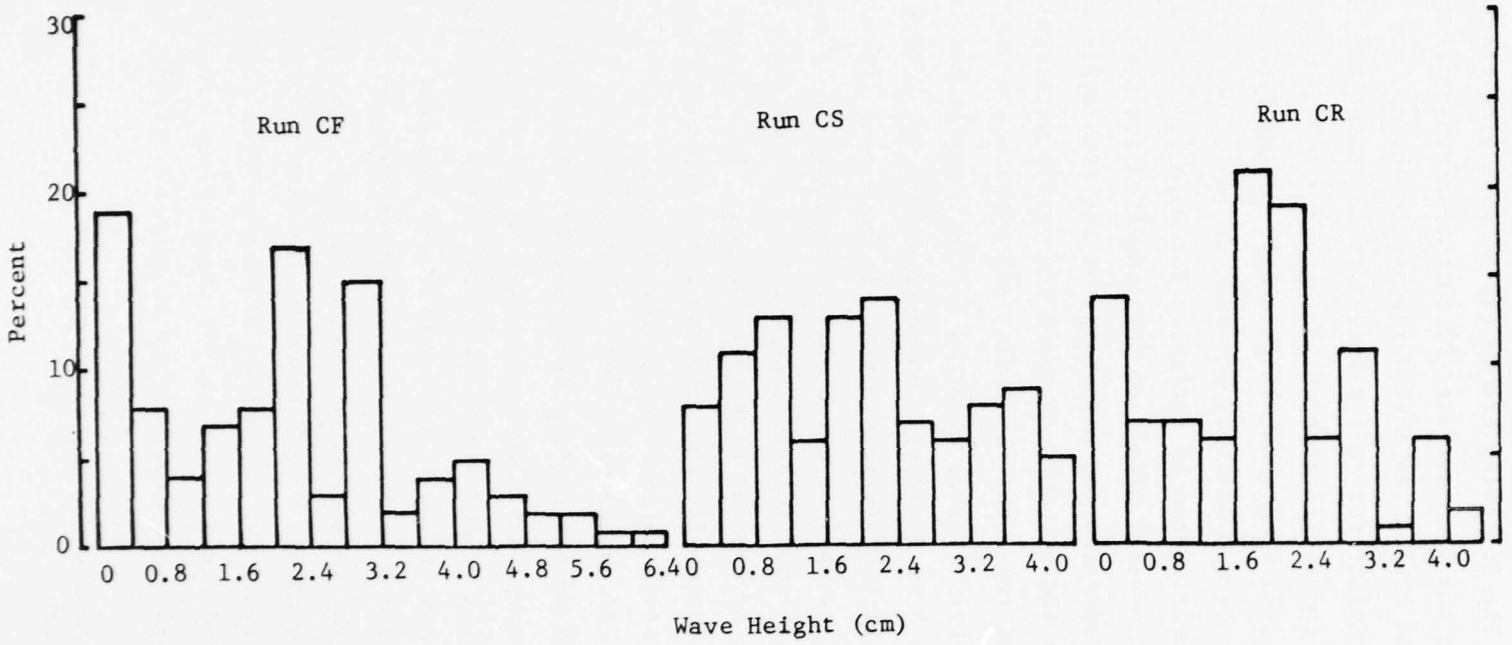

(a) Wave height distributions

Figure 18. Percentage distribution histograms for bed-form characteristics, Runs CF, CS and CR.

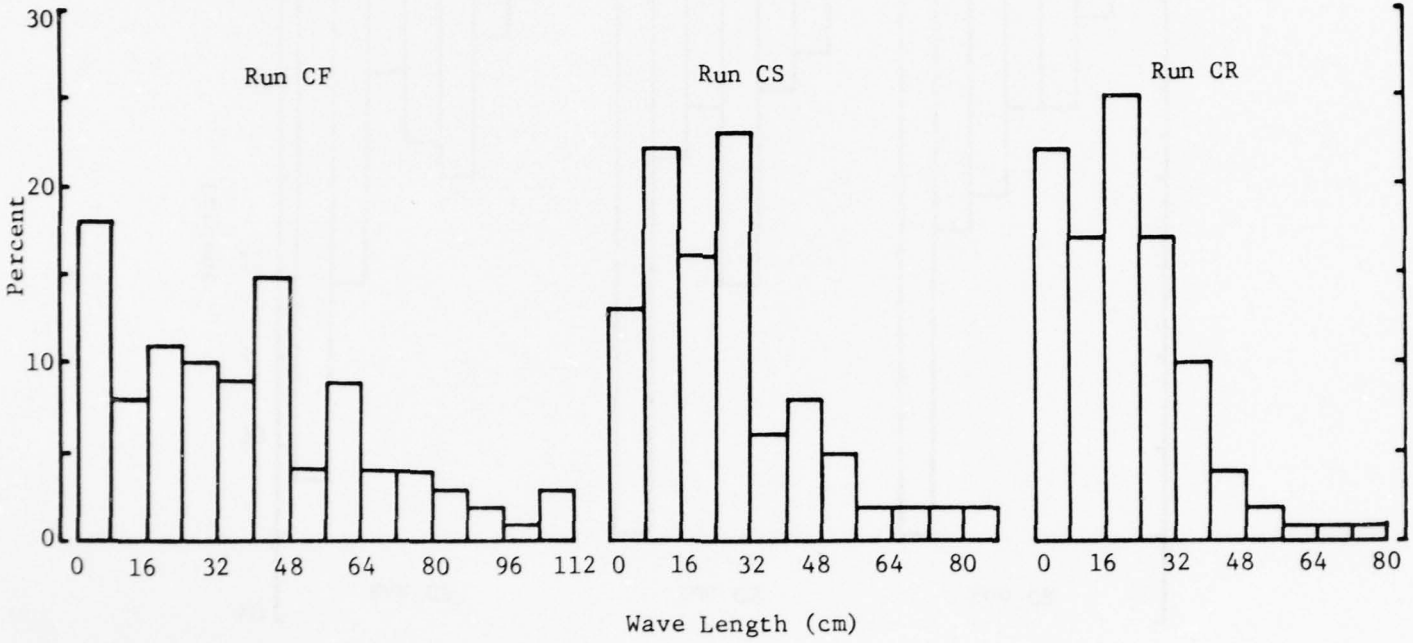

(b) Wave length distributions

Figure 18. (continued).

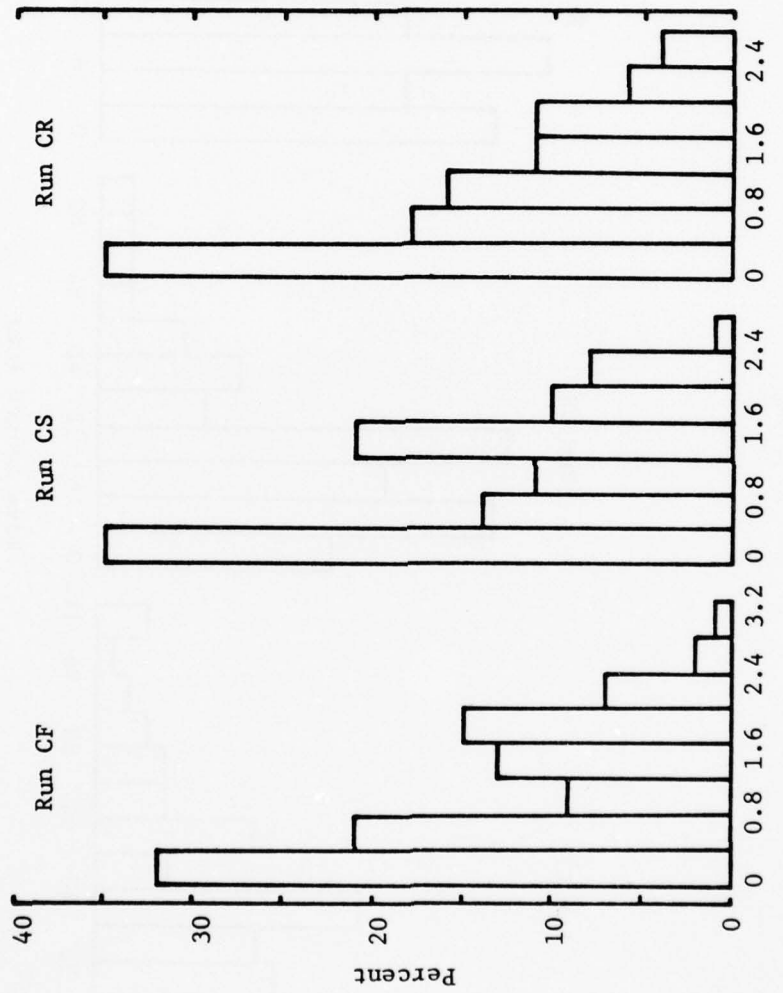

(c) Positive amplitude distributions

Figure 18. (continued).

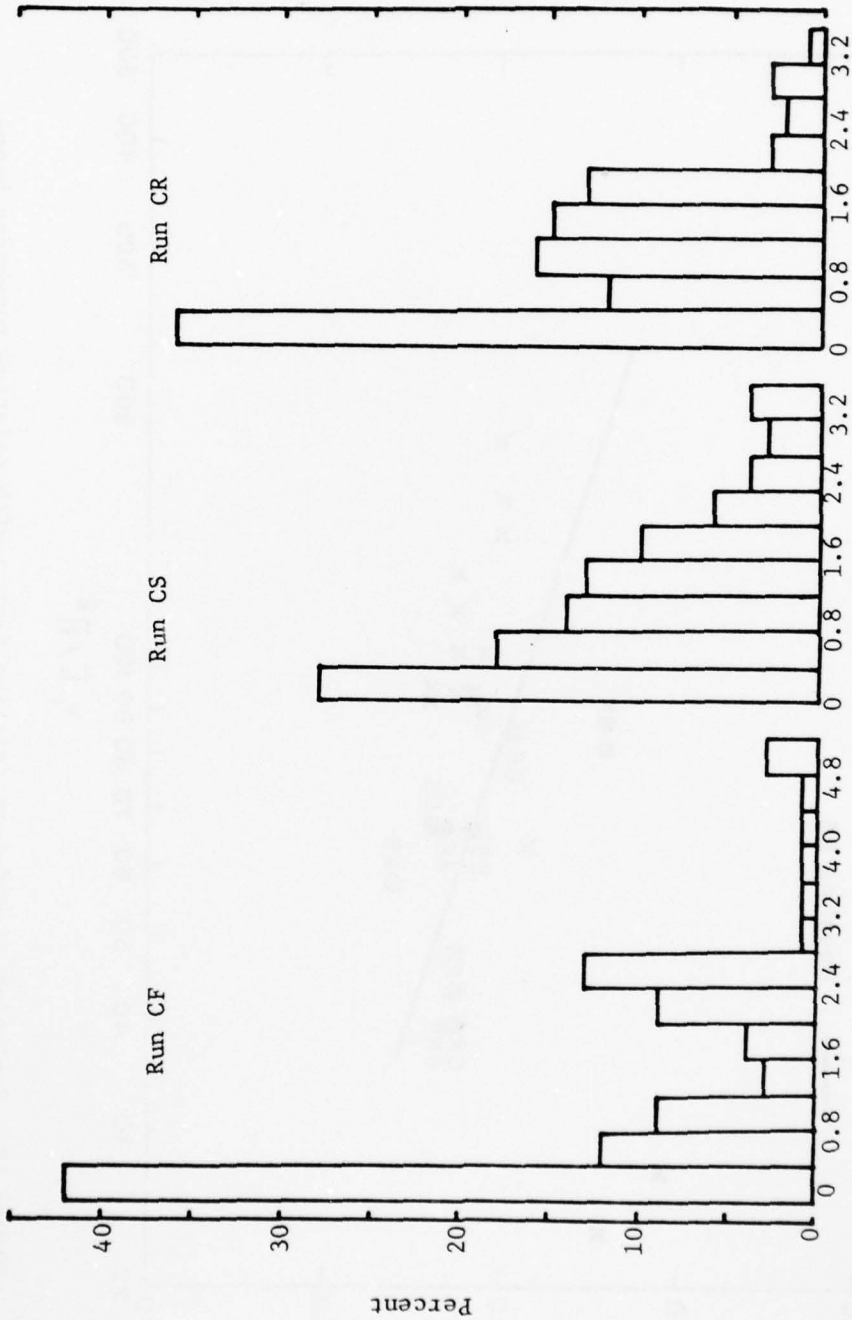

(d) Negative amplitude distributions

Figure 18. (continued).

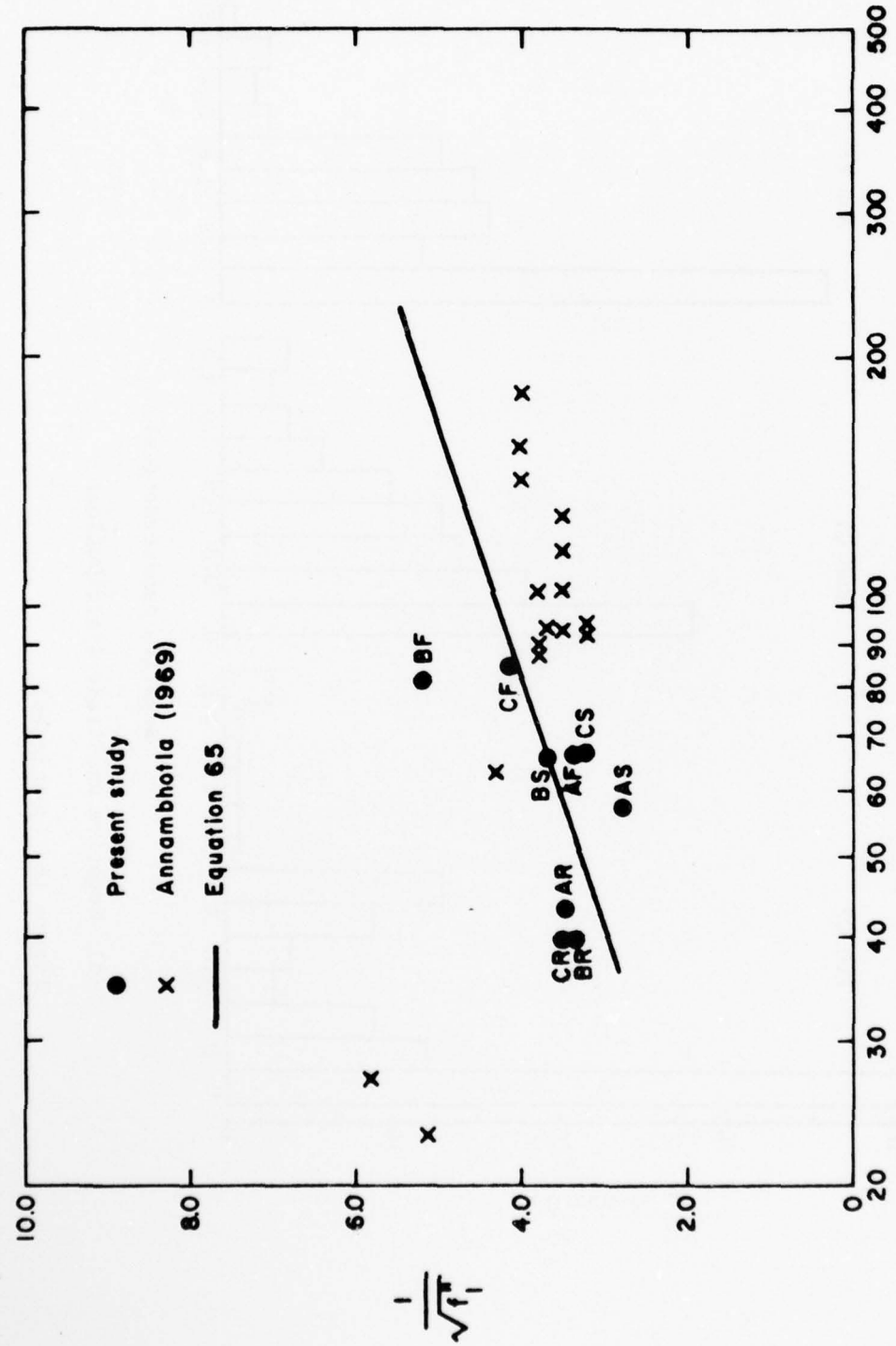

Figure 19. Variation of bed-form friction factor with relative roughness based on mean ripple dimensions.

Equation 65 is a slightly modified form of Vanoni and Hwang's (1967) logarithmic bed-form friction factor relation

$$\frac{1}{\sqrt{f''}} = 3.5 \log \frac{r_b}{e\bar{H}} - 2.3 \qquad (66)$$

where e is the areal concentration of ripples on the bed. The changes are: the approximation of e by $\bar{H}/\bar{L}$; decreasing the value of the numerical coefficient from 3.5 to 3.3; and the substitution of Y_1 for r_b. Vanoni and Hwang found that the equation with the first two modifications provided a rough fit to the data from several investigations wherein no direct measurements to determine e had been obtained. The third modification is introduced herein as another test of the hypothesis that the flow in the lower layer of an ice-covered channel is like a free-surface flow with depth equal to Y_1. Except for the two points of Annabhotla's that are far to the left of the others, the degree of scatter in figure 19 does not much exceed that in Vanoni and Hwang's original relationship. It is therefore concluded that Y_1 is about as good a characteristic flow dimension to use in defining the relative roughness of the bed of an ice-covered flow, as is d or r_b for a free-surface flow.

IV. SUMMARY, CONCLUSIONS, AND RECOMMENDATIONS

A. Summary. When an ice cover forms, flow processes in alluvial channels assume an additional degree of complexity. The immediate effect of the ice cover is to approximately double the wetted perimeter of the channel, which radically alters the distributions of boundary and internal shear stresses, and of velocity. These alterations in turn give rise to several additional changes which usually include an increase in depth, a reduction in velocity and sediment transport, and a change in the bed configuration and consequently the hydraulic roughness of the bed. The extent of these changes evidently depend in large measure on the hydraulic roughness of the underside of the ice cover relative to the roughness of the bed. However, the roughness of

the bed depends on the bed configuration which in turn is free to adjust to the new shear stress distribution, creating an internal feedback loop.

The main objective of this investigation was to obtain basic information on how ice covers affect the sediment transport characteristics of alluvial streams with a view toward formulating recommendations that would help the U.S. Geological Survey to improve field sampling and data collection procedures for ice-covered alluvial channels. To this end, a series of experiments was performed in a laboratory flume wherein detailed comparisons were made between the characteristics of alluvial-channel flow processes occurring under simulated ice covers, and those occurring in equivalent free surface flows. In particular, the experimental investigation addressed the effects of smooth and rough ice covers on the following characteristics of the flows: (1) depth versus discharge and friction-factor relationships; (2) velocity distribution; (3) suspended sediment concentration profiles and discharge; (4) total bed-material discharge; and (5) characteristics of bed forms and their relationship to bed friction factors. The experiments were restricted to flows with a 0.25 mm sand bed in the ripple regime.

B. Conclusions. The results of the experiments combined with basic principles from mechanics and hydraulics gives rise to the following conclusions:

1. The flow in an ice-covered channel is divided by a plane of zero shear stress, i.e., locus of maximum velocity, into a lower and an upper layer. Since the shear stress at the bed of an ice-covered channel is the same as the shear stress at the bed of a free-surface flow with the same depth and average velocity as the lower layer of the ice-covered flow, it follows that features of the flow which depend mainly on the bed shear stress and the mean velocity should also be essentially the same. To the extent that this is true, it should be possible to use relationships developed for free-surface flows in alluvial channels for predicting certain features of flows in ice-covered alluvial channels.

2. The Karman-Prandtl logarithmic velocity defect law, commonly used for free-surface flows, was found to apply reasonably well to both the lower and upper layers of flows with simulated ice covers. The vertical distance from the lower or upper boundary to the locus of maximum velocity is simply substituted for the depth. However, values of the von Karman κ may differ from those in free-surface flows. Another significant feature of the velocity distribution observed in the experiments is that the mean velocities in the lower and upper layers are nearly equal to each other and to the overall mean velocity.
3. The relative thicknesses of the lower and upper layers, which depend mainly on the roughnesses of the lower and upper boundaries relative to each other, were found tc depend primarily on the roughness of the underside of the simulated ice cover and to be relatively independent of unit discharge over the range of experimental conditions, implying that the bed roughness, given a particular ice cover, may also be relatively independent of unit discharge.
4. The total depth of flow in a channel with a given unit discharge and slope was found to be significantly increased by the addition of a simulated ice cover. The amount of increase, relative to the depth for a free-surface flow condition, was determined to be from 20 to 30 percent for a smooth cover and from 30 to 80 percent for a rough cover.
5. The Alam-Lovera-Kennedy bed-form friction factor relationships developed for free-surface, alluvial-channel flows, were found to apply equally well to ice-covered, alluvial-channel flows when the thickness of the lower layer in an ice-covered flow is substituted for the full depth of a corresponding free-surface flow having the same mean velocity and slope.
6. Solutions of the Schmidt-O'Brien equation, with turbulent mass transfer coefficients for suspended sediment based on Bouissinesq eddy diffusivities computed for the shear-stress

distribution in an ice-covered flow, were found to be qualitatively compatible with the measured suspended sediment concentration profiles. However, good quantitative agreement between computed and measured profiles in most cases could only be obtained by utilizing unreasonably large values of the ratio of sediment-to-momentum diffusivity (and/or small values of sediment settling velocity) in the computations. Overall, the results of the suspended sediment concentration measurements were not sufficiently consistent to reach any significant conclusions concerning the effect of an ice cover on the vertical distribution of suspended sediment.

7. The total bed-material discharge of a flow was found to be greatly reduced by the addition of a simulated ice cover. Relative to total sediment discharges in free-surface flows with the same unit discharge, slope, and bed-material characteristics, total sediment discharges were determined to be on the order of 20 percent for flows with a smooth cover, and 5 percent for flows with a rough cover.
8. The overall effect on bed configuration of adding a simulated ice cover was a tendency toward a significant reduction in ripple sizes, with the mean length decreasing somewhat more than the mean height, accompanied by a less pronounced tendency for the ripples to become more uniform in size. A rough cover tended to produce greater reduction in ripple sizes than a smooth cover, but the uniformity of ripple sizes was about the same for smooth and rough covers.
9. The thickness of the lower layer was found to be about as good a characteristic flow dimension to use in defining the relative roughness of the bed of an ice-covered flow, as is the depth or hydraulic radius for a free-surface flow.

C. Recommendations. With reference to possible modifications in the field sampling and data collection procedures of the U.S. Geological Survey for ice-covered alluvial channels, the results of this investigation suggest the following:

1. Insofar as the thickness of the lower layer of the flow was found to be an important parameter for flows with an ice cover, it is recommended that velocity measurements in the field be obtained at enough additional points in selected-verticals to define the locus of maximum velocity (i.e. zero shear stress) at cross sections where current-meter discharge measurements are obtained.
2. Any information on bed configuration, even if only visual (e.g. whether bed appears to be flat, or covered by dunes or ripples) would be useful in interpreting data, as would be descriptions of the roughness of the underside of the ice cover.
3. Insofar as the evidence indicates that sediment discharge is substantially reduced by ice cover, less frequent sediment discharge measurements when an ice cover exists would appear to be justified for most sampling stations. However, to learn more about sediment transport phenomena in ice-covered streams, fewer sets of more detailed and complete measurements are recommended.

REFERENCES

ALAM, A.M.Z. & KENNEDY, J.F. 1969 Friction factors for flow in sand bed channels. Journal of the Hydraulics Division, ASCE, Vol. 95, No. HY6, Proc. Paper 6900, pp. 1973-1992.

ASHTON, G.D. & KENNEDY, J.F. 1972 Ripples on undersideof river ice covers. Journal of the Hydraulics Division, ASCE, Vol. 98, No. HY9, Proc. Paper 9191, pp. 1603-1624.

ANNAMBHOTLA, V.S.S. 1969 Statistical properties of bed forms in alluvial channels in relation to flow resistance. Ph.D. dissertation, The University of Iowa.

CAREY, K.L. 1966 Observed configuration and computed roughness of the underside of river ice, St. Croix River, Wisconsin. U.S. Geological Survey Professional Paper 550-B, pp. B192-B198.

COLBY, B.R. & HEMBREE, C.H. 1955 Computations of total sediment discharge, Niobrara River near Cody, Nebraska. U.S. Geological Survey Water-Supply Paper 1357.

EINSTEIN, H.A. 1950 The bed load function for sediment transportation in open channels. Technical Bulletin 1026, U.S.D.A., Soil Conservation Service.

GRIGG, N.S. 1970 Motion of single particles in alluvial channels. Journal of the Hydraulics Division, ASCE, Vol. 96, No. HY12, Proc. Paper 7770, pp. 2501-2518.

HANCU, S. 1967 Modelarea Hidraulica in Curenti de aer sub presiune, Editura Academiei Republicii Socialiste Romania.

HJULSTRÖM, F. 1935 Studies of the morphological activity of rivers as illustrated by the River Fyris. Bulletin, Geological Institute of Upsala, Vol. XXV.

INTERAGENCY COMMITTEE 1957 Some fundamentals of particle size analysis, a study of methods used in measurement and analysis of sediment loads in streams. Report No. 12. Subcommittee on Sedimentation, Interagency Committee on Water Resources, St. Anthony Falls Hydraulic Laboratory, University of Minnesota.

ISMAIL, H.M. 1952 Turbulent transfer mechanism and suspended sediment in closed channels. Transactions, ASCE, Vol. 117, Paper No. 2500, pp. 409-446.

JAIN, S.C. 1971 Evolution of sand wave spectra. Ph.D. dissertation, The University of Iowa.

JOBSON, H.E. & SAYRE, W.W. 1970 Vertical transfer in open channel flow. Journal of the Hydraulics Division, ASCE, Vol. 96, No. HY3, Proc. Paper 7148, pp. 703-724.

LARSEN, P.A. 1969 Head losses caused by an ice cover on open channels. Journal of the Boston Society of Civil Engineers. Vol. 56, No. 1, pp. 45-67.

LOVERA, F. & KENNEDY, J.F. 1969 Friction factors for flat-bed flows in sand channels. Journal of the Hydraulics Division, ASCE, Vol. 95, No. HY4, Proc. Paper 6678, pp. 1227-1234.

ONISHI, Y., JAIN S.C. & KENNEDY, J.F. 1972 Effects of meandering on sediment discharges and friction factors of alluvial streams. IIHR Report No. 141, Iowa Institute of Hydraulic Research, The University of Iowa.

SHEN, H.T. & HARDEN, T.O. 1978 The effect of ice cover on vertical transfer in stream channels. Water Resources Bulletin, AWRA, Vol. 14, No. 6, pp. 1429-1439.

SIMONS, D.B. & RICHARDSON, E.V. 1966 Resistance to flow in alluvial channels. U.S. Geological Survey Professional Paper 422J.

SONG, G.B. 1978 Sediment transport and bed forms under ice covers. M.S. thesis, The University of Iowa.

SQUARER, D. 1968 An analysis of relationships between flow conditions and statistical measures of bed configurations in straight and curved alluvial channels. Ph.D. dissertation, The University of Iowa.

TAYLOR, R.H. & BROOKS, N.H. 1962 discussion of - Resistance to flow in alluvial channels. Transactions, ASCE, Vol. 127, Part I, pp. 982-992.

TYWONIUK, N. & FOWLER, J.L. 1972 Winter measurements of suspended sediments. The Role of Snow and Ice in Hydrology, Proc. Banff Symposia, UNESCO - WMO - IAHS, Vol. 1, pp. 814-827.

UZUNER, M.S. 1975 The composite roughness of ice covered streams. Journal of Hydraulic Research, IAHR, Vol. 13, No. 1, pp. 79-102.

VANONI, V.A. 1974 Factors determining bed forms of alluvial streams. Journal of the Hydraulics Division, ASCE, Vol. 100, No. HY3, Proc. Paper 10396, pp. 363-377.

VANONI, V.A. & HWANG, L-S 1967 Relation between bed forms and friction in streams. Journal of the Hydraulics Division, ASCE, Vol. 93, No. HY3, Proc. Paper 5242, pp. 121-144.

WILLIS, J.C. & KENNEDY, J.F. 1977 Sediment discharge of alluvial streams calculated from bed-form statistics. IIHR Report No. 202, Iowa Institute of Hydraulic Research, The University of Iowa.

AD-A066 991 IOWA INST OF HYDRAULIC RESEARCH IOWA CITY F/G 8/12
EFFECTS OF ICE COVERS ON ALLUVIAL CHANNEL FLOW AND SEDIMENT TRA--ETC(U)
FEB 79 W W SAYRE, G B SONG

UNCLASSIFIED IIHR-218 NL

2 OF 2
AD A066991

END
DATE FILMED
6-79
DDC

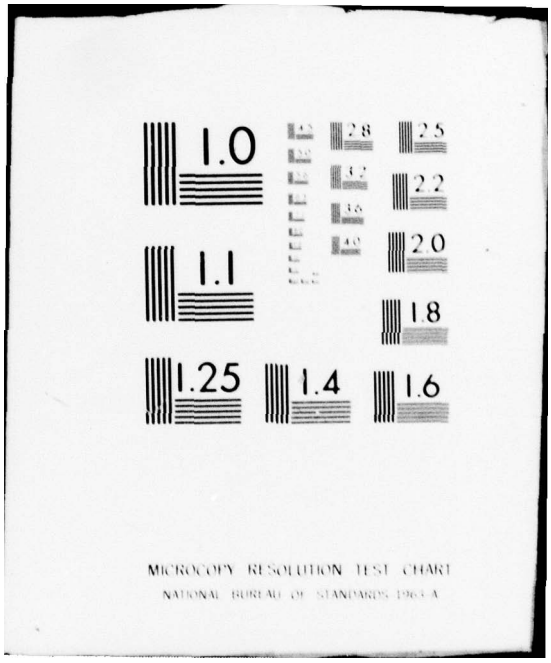
1.0
1.1
1.25
1.4
1.6
2.8
2.5
2.2
2.0
1.8
MICROCOPY RESOLUTION TEST CHART
NATIONAL BUREAU OF STANDARDS 1963-A

APPENDIX A

PROGRAM AND AGENDA FOR USGS-IIHR WORKSHOP ON MEASUREMENT OF SUSPENDED SEDIMENT TRANSPORT IN ICE-COVERED ALLUVIAL STREAMS, NOVEMBER 25, 1975

U S G S - I I H R W O R K S H O P

ON MEASUREMENT OF SUSPENDED SEDIMENT TRANSPORT IN ICE-COVERED ALLUVIAL STREAMS,

NOVEMBER 25, 1975

The Iowa Institute of Hydraulic Research (IIHR) was commissioned by the USGS to review and evaluate the aspects of the USGS data collection and interpretation program that relate to the measurement of suspended-sediment transport in ice-covered alluvial channels. In conjunction with this project a one-day workshop was held at The University of Iowa, Iowa City, on Tuesday, November 25, 1975.

Purpose. The main purpose of the workshop is to exchange information, identify problems and possible solutions thereto, and formulate goals on matters relating to sampling techniques and equipment, data analysis and interpretation, and design of data collection programs. The workshop will serve the dual purpose of providing IIHR project personnel with sources of information concerning USGS field experience in ice-covered alluvial streams, and providing USGS personnel with information and insights resulting from IIHR investigations of ice regimes and the mechanics of flow in ice-covered channels.

List of Participants

John Ficke, USGS, Reston, Virginia
Steve Hindall, USGS, Madison, Wisconsin
Carl Nordin, USGS, Denver, Colorado
John Skinner, USGS, Minneapolis, Minnesota
Jack Kennedy, IIHR, University of Iowa
Bill Sayre, IIHR, University of Iowa
Ed Slattery, IIHR, University of Iowa
George Ashton, CRREL, Hanover, New Hampshire

Agenda. The meeting will be loosely structured to allow for free interchange and spontaneity. A tentative list of the topics to be covered follows:

1. Sediment transport in ice-covered alluvial streams within context of USGS water measurement and sampling program.

USGS-IIHR WORKSHOP

ON MEASUREMENT OF SUSPENDED SEDIMENT TRANSPORT
IN ICE-COVERED ALLUVIAL STREAMS,

NOVEMBER 25, 1975

page 2

2. Measurement of suspended sediment transport in ice-covered channels.
   a. equipment and procedural problems due to ice cover and/or freezing conditions.
   b. presentation of typical sets of data that illustrate the effects of ice covers on sediment concentration and velocity distribution data.
   c. design of sampling program, location of sampling verticals and/or points, frequency of sampling.
   d. analysis and interpretation of data.

3. Measurement of supporting data such as discharge, slope, bed configuration, bed load transport, ice ripples, ice texture. How much of this kind of supporting data is needed to satisfy USGS objectives?

4. Mechanics of flow in ice-covered channels.
   a. ice regimes--formation, evolution, and breakup of ice covers.
   b. resistance to flow, distribution of velocity and suspended sediment under different ice regimes.
   c. speculations on interactions involving ice cover, bed configuration, and bed and suspended load transport.

5. Tour of IIHR laboratories with emphasis on ice and sediment transport facilities.

Assignments. Everyone will no doubt have something to contribute on each agenda item. However, the following assignments are being made to ensure that all bases are covered and to give each participant a clearer concept of his role and the particular contributions he is expected to make.

Ficke:

1. Introductory comments relating to item 1 on agenda.
2. Contribute perspective to items 2c, 2d and 3 from viewpoint of total program objectives.

Hindall:

1. Contribute benefit of field experience in measuring sediment transport and related phenomena in ice-covered channels, and experience in analyzing and interpreting the data. Should be prepared to make a 20- to 30-minute oral presentation with slides, photographs, graphs, tables, etc. on items 2a and 2b of agenda, to get the discussion started.

USGS-IIHR WORKSHOP

ON MEASUREMENT OF SUSPENDED SEDIMENT TRANSPORT
IN ICE-COVERED ALLUVIAL STREAMS,

NOVEMBER 25, 1975

page 3

2. Contribute perspective to items 2c, 2d and 3 from viewpoint of field investigator.

Ashton:

1. Oral presentation with slides (30 minutes) covering spectrum of ice-related phenomena in rivers.
2. Contribute broad perspective on river-ice phenomena.

Nordin:

1. Resource person on relationships to other USGS alluvial channel investigations.
2. Contribute perspective to all items.

Skinner:

1. Resource person on sampling equipment and instrumentation.

Kennedy and Sayre:

1. Oral presentations to initiate discussion on item 4 of the agenda.
2. Contribute perspective on items 2c, 2d and 3 from the academic viewpoint.

Slattery:

1. Audiovisual equipment. Transparency, opaque and slide projectors. Tape recorder.
2. Contribute perspective from the viewpoint of the graduate research assistant who's going to be doing much of the work on this project.

Travel and Accommodations. The most convenient way to reach Iowa City is by air to Cedar Rapids. Iowa City is about 20 miles from the Cedar Rapids Airport. Reservations for the entire group have been made for the nights of November 24 and 25 and the Iowa House in the Iowa Memorial Union, located on the University campus. Direct transportation between the Airport and the Iowa House is provided by Iowa Limousine Service, Inc. for all incoming and outgoing flights, so it is not necessary to rent cars at the Airport.

Social Activities. All of the workshop participants are invited to dinner on the evening of Monday, November 24, at one of the well known Amana Colony restaurants, as guests of the Iowa Institute of Hydraulic Research. We will meet in the lobby of the Iowa House from where transportation will

USGS-IIHR WORKSHOP

ON MEASUREMENT OF SUSPENDED SEDIMENT TRANSPORT
IN ICE-COVERED ALLUVIAL STREAMS,

NOVEMBER 25, 1975

page 4

be provided, at 7:00 p.m. Please note when making travel reservations.

Time and Place of Workshop. 8:00 a.m., Tuesday, November 25, in Michigan State Room, third floor of Iowa Memorial Union.

Information. For additional information, if needed, call either Bill Sayre (319-353-3082) or Jack Kennedy (319-353-4679).

APPENDIX B

FIELD TRIP TO UPPER IOWA RIVER NEAR DORCHESTER, IOWA ON JANUARY 20, 1976

FIELD TRIP TO UPPER IOWA RIVER NEAR DORCHESTER, IOWA
JANUARY 20, 1976

Personnel: Bill Matthes and Dick Downs, USGS,
Iowa District Office, performed measurements.

Bill Sayre and Ed Slattery, IIHR,
accompanied as observers and assisted in measurements.

I. Purpose

A. Observe discharge and sediment measurement techniques for ice-covered streams.
B. Become familiar with measurement and sampling equipment.

II. Description of Gaging Station

A. Located at Route 76 bridge
B. Gage house contains stage recorder consisting of bubble gage, digital punched-tape recorder, and strip-chart recorder for backup.
C. Manual plumb bob for measuring stage, attached to wire rope and reel assembly mounted on bridge railing.

III. Selection and Preparation of Cross Section

A. Cross Section located in straight reach approximately 200 ft upstream bridge where streamlines parallel to each other and to banks, and composition of bed considered to be typical.
B. Probe for weak spots across section with ice chisel. Stretch tagline across river and fix, perpendicular to shore.
C. Locate positions of sampling verticals. Drill holes with power auger along tagline at about 2-ft intervals above channel where water flowing, and at about 4- to 7-ft intervals in shallow areas where ice reaches to bottom of channel.

IV. Depth Soundings

A. Measure total depth from top of ice to bottom of channel at each hole with ice rod, similar to surveyor's rod.
B. Measure thickness of ice, using steel angle attached to ice rod to find underside of ice cover.
C. Subtract ice thickness from total depth to get water depth.

V. Velocity Measurements

A. Velocities measured with vane-type current meter attached to bottom of rod supported from above by tripod assembly resting on ice.
B. Velocities measured at 0.6 depth from underside of ice where water depth equal to or less than 2.5 ft, and at 0.2 and 0.8 depth where depth greater than 2.5 ft.
C. Beeps counted for at least 40 seconds.

D. Velocities measured at 0.6 depth multiplied by empirical correction factor of 0.92 to get mean velocity, to account for effect of ice cover on velocity distribution.

VI. Suspended Sediment Sampling

A. Samples obtained at about 8 verticals using a US DH-48 hand sampler mounted to a rod.
B. Depth-integrated samples obtained. Except at deepest sampling locations, two locations sampled with one bottle.
C. Very little suspended sediment in samples.

VII. Bed-Material Sampling

A. Piston-type core sampler used to obtain bed-material samples at same verticals where suspended sediment samples obtained.
B. Samples placed in labeled plastic frozen-food containers.
C. Samples appeared to be well-graded with significant quantity of coarse sand.

VIII. Bed-Load Sampling.

A. Helley-Smith bed-load sampler used for measuring bed load at same sampling locations where suspended sediment and bed-material samples obtained.
B. Sampling holes in ice had to be enlarged with chain saw before sampler could be lowered into water.
C. Sampler lowered to bed in vertical position, left on bed in horizontal position pointing upstream for 30 seconds, and raised to surface in vertical position.
D. Sample transferred from collector to labeled container.

IX. Ice and Bed Features

A. Blocks of ice, about 4 ft x 1 ft, were cut with chain saw and turned over.
B. Observed ripple-like features with well-defined ridge-like crests on undersurface of ice.
C. Water clear enough to see bed through holes. Bed mostly flat. Ripple crests visible where bed composed of fine sand.

X. Comments and Criticisms.

A. V-D. Correction factor of 0.92 to account for ice-cover effect on velocity distribution seems very arbitrary. Shape of velocity profile depends on roughness of ice cover relative to roughness of bed, which can vary considerably.
B. VII-A. Much of bed-material sample lost while raising piston sampler. More difficult to recover sample without losing some than under free-surface conditions because small hole in ice restricts freedom of motion in raising sampler.

C. VIII-C. 30 seconds seems to be a very short sampling period for bed-load samples, particularly under ice-cover conditions when bed load expected to be low.

D. VIII-C. 3-inch square entrance section of Helley-Smith sampler tended to get choked with ice. Shouldn't affect results if occurring only while sampler being retrieved. However it is not clear that no ice was entering sampler and affecting entrance conditions during lowering and 30-second measurement period on bed.

Figure B1. Looking upstream toward sampling cross section.

Figure B2. Velocity measurement.

Figure B3. Suspended-sediment sampling.

Figure B4. Preparing to lower Helley-Smith bed-load sampler.

BIBLIOGRAPHIC DATA SHEET	1. Report No. IIHR #218	2.	3. Recipient's Accession No.
4. Title and Subtitle Effects of ice covers on alluvial channel flow and sediment transport processes			5. Report Date Feb 1979 6.
7. Author(s) W.W. Sayre & G.B. Song			8. Performing Organization Rept. No.
9. Performing Organization Name and Address Institute of Hydraulic Research The University of Iowa Iowa City, IA 52242			10. Project/Task/Work Unit No. 11. Contract/Grant No.
12. Sponsoring Organization Name and Address U.S. Geological Survey Water Resources Division			13. Type of Report & Period Covered 14.

15. Supplementary Notes

16. Abstracts

Ice covers cause a number of changes in alluvial channel flows by approximately doubling the wetted perimeter and thereby producing a redistribution of the boundary and internal shear stresses. A series of flume experiments was conducted to investigate the effects of simulated ice covers on various characteristics of alluvial channel flows. In comparison to free-surface flows with the same unit discharge and energy slope, flows with simulated ice covers were found to have substantially larger depths and lower average velocities. Due mainly to the lower velocities sediment discharges were found to be sharply reduced. Flow in an ice-covered channel is divided by a plane of zero shear stress into a lower and an upper layer. To the extent that the shear stress and velocity distributions in the lower layer are the same as in a free surface flow with the same mean velocity, and depth equal to the thickness of the lower layer, relationships developed for flows in alluvial channels with a free surface can be used for predicting several features of flows in ice-covered alluvial channels.

17. Key Words and Document Analysis. 17a. Descriptors

ice cover, alluvial channel flow, sediment transport processes

17b. Identifiers/Open-Ended Terms

17c. COSATI Field/Group

18. Availability Statement	19. Security Class (This Report)	21. No. of Pages
unlimited	UNCLASSIFIED	102
	20. Security Class (This Page) UNCLASSIFIED	22. Price

INSTRUCTIONS FOR COMPLETING FORM NTIS-35 (Bibliographic Data Sheet based on COSATI Guidelines to Format Standards for Scientific and Technical Reports Prepared by or for the Federal Government, PB-180 600).

1. **Report Number.** Each individually bound report shall carry a unique alphanumeric designation selected by the performing organization or provided by the sponsoring organization. Use uppercase letters and Arabic numerals only. Examples FASEB-NS-73-87 and FAA-RD-73-09.

2. Leave blank.

3. **Recipient's Accession Number.** Reserved for use by each report recipient.

4. **Title and Subtitle.** Title should indicate clearly and briefly the subject coverage of the report, subordinate subtitle to the main title. When a report is prepared in more than one volume, repeat the primary title, add volume number and include subtitle for the specific volume.

5. **Report Date.** Each report shall carry a date indicating at least month and year. Indicate the basis on which it was selected (e.g., date of issue, date of approval, date of preparation, date published).

6. **Performing Organization Code.** Leave blank.

7. **Author(s).** Give name(s) in conventional order (e.g., John R. Doe, or J.Robert Doe). List author's affiliation if it differs from the performing organization.

8. **Performing Organization Report Number.** Insert if performing organization wishes to assign this number.

9. **Performing Organization Name and Mailing Address.** Give name, street, city, state, and zip code. List no more than two levels of an organizational hierarchy. Display the name of the organization exactly as it should appear in Government indexes such as Government Reports Index (GRI).

10. **Project/Task/Work Unit Number.** Use the project, task and work unit numbers under which the report was prepared.

11. **Contract/Grant Number.** Insert contract or grant number under which report was prepared.

12. **Sponsoring Agency Name and Mailing Address.** Include zip code. Cite main sponsors.

13. **Type of Report and Period Covered.** State interim, final, etc., and, if applicable, inclusive dates.

14. **Sponsoring Agency Code.** Leave blank.

15. **Supplementary Notes.** Enter information not included elsewhere but useful, such as: Prepared in cooperation with . . . Translation of . . . Presented at conference of . . . To be published in . . . Supersedes . . . Supplements . . . Cite availability of related parts, volumes, phases, etc. with report number.

16. **Abstract.** Include a brief (200 words or less) factual summary of the most significant information contained in the report. If the report contains a significant bibliography or literature survey, mention it here.

17. **Key Words and Document Analysis. (a). Descriptors.** Select from the Thesaurus of Engineering and Scientific Terms the proper authorized terms that identify the major concept of the research and are sufficiently specific and precise to be used as index entries for cataloging.
(b). Identifiers and Open-Ended Terms. Use identifiers for project names, code names, equipment designators, etc. Use open-ended terms written in descriptor form for those subjects for which no descriptor exists.
(c). COSATI Field/Group. Field and Group assignments are to be taken from the 1964 COSATI Subject Category List. Since the majority of documents are multidisciplinary in nature, the primary Field/Group assignment(s) will be the specific discipline, area of human endeavor, or type of physical object. The application(s) will be cross-referenced with secondary Field/Group assignments that will follow the primary posting(s).

18. **Distribution Statement.** Denote public releasability, for example "Release unlimited", or limitation for reasons other than security. Cite any availability to the public, other than NTIS, with address, order number and price, if known.

19 & 20. **Security Classification.** Do not submit classified reports to the National Technical Information Service.

21. **Number of Pages.** Insert the total number of pages, including introductory pages, but excluding distribution list, if any.

22. **NTIS Price.** Leave blank.